DEVELOPMENT AND CONTROL OF AN UNDERACTUATED TWO-WHEELED MOBILE ROBOT

GUO ZHAO QIN

(B.S.(Hons.), HUST)

A THESIS SUBMITTED

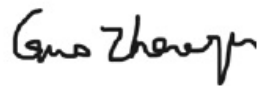**FOR THE DEGREE OF DOCTOR OF PHILOSOPHY**

NUS GRADUATE SCHOOL FOR INTEGRATIVE SCIENCES

AND ENGINEERING

NATIONAL UNIVERSITY OF SINGAPORE

2012

Declaration

I hereby declare that the thesis is my original work
and it has been written by me in its entirety. I have
duly acknowledged all the sources of information
which have been used in the thesis.
This thesis has also not been submitted for any
degree in any university previously.

Guo Zhao Qin
04 March 2013

Acknowledgments

Finally, I would like to express my deepest gratitude to my family members for their unconditional love and support during all these years. This thesis is dedicated to them.

Contents

Summary

The two-wheeled mobile robot (2WMR), which consists of two wheels in parallel and an inverse pendulum, is inherently unstable. In this thesis, the control objective is to use only one actuator to perform position or velocity control of the wheels while balance the pendulum. This type of system is defined as an underactuated system, with fewer actuators than the number of independent variables to be controlled. For control of underactuated systems, many of the conventional control designs for fully actuated systems are not applicable. In addition, various uncertainties such as the joint and the ground frictions, the varying slope angle of the ground, etc., exist in the 2WMR system, which makes the control difficulty arise, especially when the uncertain part has unmatched components that are not in the control range space. To sum up, the 2WMR system is a nonlinear, unstable and underactuated system with uncertainties, thus the control system design is challenging and robustness should be one of the main concerns in the design.

In this thesis, five different control schemes are proposed for control of the underactuated 2WM-R, which are also applicable to similar underactuated mechanical systems.

First, a linear controller based on linear matrix inequality (LMI) method is studied. The design of linear controller for nonlinear system is often based on a linearized model around the desired equilibrium, i.e., the nonlinear terms and uncertainties are just ignored in the control design. In this work, the nonlinear terms and uncertainties are taken into consideration in the linear controller design. The LMI approach is employed to obtain the feedback gains for the linear controller. Lyapunov method is applied to investigate the stability region of the 2WRM system under the linear control. The Lyapunov function and the feedback gains are obtained concurrently, which can reveal a fairly accurate stability region.

Second, an SMC with a linear sliding surface is studied. The SMC law is derived by using

Lyapunov theory, which guarantees the finite reaching time of the sliding surface and leads to a

sliding manifold with all the matched uncertainties rejected. To stabilize the sliding manifold, the

controller parameters should be chosen appropriately. By transforming the sliding mode design

into a nominal linear controller design for control of a nominal 2WMR system, the controller

parameters are easier to be determined. Furthermore, the proposed SMC can incorporate various

linear control design methods and thus leads to a stable sliding manifold, which inherits the same

properties as that of the aforementioned nominal system under the linear control.

Third, an integral sliding mode control is designed. The sliding mode exists from the very

beginning, therefore the system is more robust against perturbations than the other SMC systems

with reaching phase. The ISMC has an extra degree of freedom in control when sliding mode

is achieved. We utilize this extra degree of freedom to implement a linear nominal controller,

which is found adequate in stabilizing the sliding manifold. The implemented ISMC, with an

integral sliding surface and a switching term, is able to completely nullify the influence from the

matched uncertainties. The linear nominal controller is designed to stabilize the sliding manifold

that is subject to unmatched uncertainties.

Next, a Takagi-Sugeno type fuzzy logic controller is proposed. The FLC design is based on both

human experience and information of the 2WMR dynamic model. The FLC structure including

the fuzzy labels, membership functions, and inference is chosen based on heuristic knowledge

about the 2WMR. The output parameters of the FLC are determined by comparing the output

of the FLC with a linear controller at certain operating points, which avoids the difficulty and

tediousness in manual tuning. The new FLC outperforms a linear controller because it provides

varying feedback gains, which are adapted to the current states of the 2WRM. Compared with

FLCs designed in other existing works, the proposed FLC has fewer fuzzy rules and parameters

to be determined, which implies a simpler and more realizable design for real implementation. The proposed FLC is successfully implemented on the real-time platform and shows effectiveness.

To the end, a synthesized FLC is developed without incorporating any model-based controller, and hence an accurate mathematic model is not required. The synthesized design consists of three phases: determination of the FLC structure through heuristic knowledge about the 2WMR; quantitative determination of the output parameters for stabilization of the 2WMR; and tuning of the FLC output parameters using iterative learning tuning (ILT). The main idea behind the proposed methodology is to maximize the utilization of all the information available, which is achieved by combining partially model-based and partially model-free designs, and hence improve the FLC performance.

List of Tables

List of Figures

Chapter 1

Introduction

1.1 Backgrounds and Motivations

Systems that have fewer control inputs than the degrees of freedom (DOF) to be controlled are defined as underactuated systems. Control of underactuated systems is a popular research topic due to its wide range of applications in robotics, underwater vehicles, aerospace vehicles, etc. [2,21,23,45]. From practical concerns such as cost reduction or weight reduction, many systems are designed to be underactuated. Some systems become underactuated when actuator failure occurs. As benchmark examples of nonlinear and underactuated systems, the cart-pendulum is often used to demonstrate and verify the effectiveness of control algorithms.

In recent years, the control of 2WMR or two-wheeled inverted pendulum (2WIP) has attracted attentions from both researchers and engineers. However, most of the published works are based on theocratical analysis and results are obtained by simulations, only few have implemented the proposed control schemes on real time platforms. The well known commercial product, two-wheeled SEGWAY, is a popular personal transporter. For research and education purposes, prototypes and products of two-wheeled mobile vehicle or robot have been designed in universities and research institutes [1, 12–14, 26, 28, 47, 64, 65, 68, 71]. The 2WMR usually consists of two actuated wheels in parallel and an unactuated inverse pendulum. The control objective of

the 2WMR is to perform position or velocity control of the wheels while stabilize the pendulum around the upright position that is an unstable equilibrium point.

Due to the difference in system configuration, underactuated 2WMRs can be classified into the class without input coupling where the actuator is mounted on the wheel (class A), and the class with input coupling where the actuator is mounted on the pendulum or chassis (class B). The class A is more complex in mechanical construction but easier in controller design owing to the absence of input coupling between the wheel and pendulum. In contrast, the class B is easier in mechanical construction but more challenging in controller design due to the input coupling between the wheel and the pendulum. Current research works mostly focus on studying underactuated systems without input coupling, however, the proposed methods have limited applications.
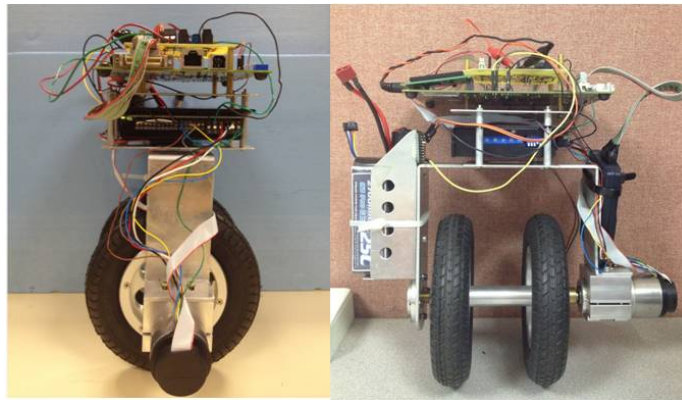
Figure 1.1: Prototype of the two-wheeled mobile robot.

This thesis is devoted to the development and control of a 2WMR with input coupling. A prototype of 2WMR is built in our lab as shown in Fig. 1.1. The lower part of the 2WMR consists of two wheels in parallel. The upper part of the 2WMR is a designed steel-frame, where all the electrical components are fixed. The frame can be regarded as an inverted pendulum. The motor shaft coupler is fixed at the center of the wheel and the motor housing is rigidly connected to the pendulum, thus the torque generated by the motor directly acts on both the wheels and the

pendulum with the same size but opposite directions, which results in the input coupling of the 2WMR system.

The control of inverted pendulum and similar underactuated mechanical systems is a rather challenging problem even no uncertainties are considered existing in the systems, thus, the problem has attracted much attention from researchers whose interest are in the field of control theory. In plenty of theoretical works, stabilizing algorithms based on Lyapunov theory, passivity, feedback linearization, etc., are developed for underactuated mechanical systems [20,24,25,31,32,50,67]. The effectiveness of the proposed controllers are verified through simulations. However, these controllers may not function well on real-life underactuated mechanical systems. First, the controller design and stability prove are based on the accurate mathematical models, however, there exists model mismatch between the nominal mathematical models and the real-life plants. Second, some of the control algorithms are too complicated to implement. By realizing the fact that uncertainties could affect system performance or even devastate system stability, researchers are motivated to explore robust control designs for underactuated systems [3,29,37,48,49,57,61,81].

Linear controller is widely used in industrial applications due to its easiness in algorithm computing and parameter tuning. In [26, 47, 64, 65, 68], full-state feedback linear controller is implemented on the 2WMRs. In [47, 68], the feedback gains for the linear controller are obtained through linear quadratic regulator (LQR) method and further manually tuned during experimental testings. In [26], pole-placement method is used to obtain the feedback gains for the linear controller. In [64, 65], the feedback gains for the linear controller are tuned manually.

For control of nonlinear system, the design of a linear controller is often based on a linearized model of the nonlinear system around the desired equilibrium point. Therefore, the linear controller may become ineffective when the system states are away from the desired equilibrium

point or when the system is in presence of uncertainties. Nevertheless, it would be meaningful to explore the stability region of the nonlinear and uncertain system when it is under the linear control. Generally, linear controller with larger feedback gains provides better robustness. However, implementation of linear controller with high feedback gains requires the system sampling frequency to be high enough, which implies the need of high-performance hardware components, such as the sensors and the control board. Furthermore, considering that the motor capacity is limited, linear controller with large feedback gains could result in control signal saturation when system states are away from the desired equilibrium, which would devastate the effectiveness of the controller. The limited robustness of the linear controller motives researchers to explore nonlinear robust control methods for underactuated systems.

As one of the well known robust control techniques, sliding mode control method is often employed for controlling systems with uncertainties and has been successfully applied to many practical systems, including underactuated systems [3, 29, 36, 48, 49, 57, 61, 81]. The SMC was originally proposed in the early 1950s and developed since then [72–75, 82–84, 86, 87]. In SMC design, first a sliding surface is specified, on which system generates desired trajectory. Next, a discontinues control law is derived to make the system trajectory reach the sliding surface in a finite time and maintain on the surface afterwards. The main advantages of the SMC are: (1) SMC is applicable to systems with various type of uncertainties, as long as the upper bounds of the uncertainties are known, in other words, the SMC design requires less information of the uncertainties in comparison with classical control techniques. (2) In the ideal sliding mode, all uncertainties which are in the control range space, namely, matched uncertainties, are nullified.

In standard SMC design for full actuated system, it is straightforward to conclude the convergence of the system states when system is in the sliding mode. However, for underactuated system, the standard SMC design and stability analysis are not applicable because the system

has fewer inputs than the independent variables to be controlled. As a result, a nonlinear sliding manifold or in general an internal dynamics must be stabilized by the proper selection of the sliding surface coefficients. In [3, 29, 48, 49], coupled sliding mode control laws along with a linear coupled sliding surface are proposed for controlling of the underactuated system, where the coupled linear sliding surface is designed by incorporating multiple independent state variables into a scalar sliding surface. The single actuator can thus be used to manipulate the scalar sliding surface. Conclusions regarding the convergence of the states, however, can not be drawn directly from the convergence of the sliding surface due to the presence of the sliding manifold or the internal dynamics, thus the stability of the sliding motion governed by the sliding manifold should be further investigated, namely, the sliding surface design is required. In [29, 48, 49], stable sliding manifolds are obtained with appropriately selected sliding surface coefficients. In [3], a stabilizing control law is assumed existing.

Other types of SMC for controlling underactuated systems have been discussed in [36, 57, 61, 81]. In [81], a SMC design based on the cascade normal form [45] is proposed, and the validity holds under certain assumptions. However, the 2WMR studied in our work does not meet these assumptions. Second-order SMC designs for underactuated systems are discussed in [36, 57, 61]. The drawback of the second-order SMC is that its design requires the derivative of the sliding surface, hence the derivative signals of all system states, to be available, which is generally difficult if the system is with model uncertainties. In [36], the second-order SMC is designed for system without any uncertainties. In [57, 61], the second-order SMC design and system stability analysis are based on the assumption that all state derivatives are available.

Design of optimal SMC algorithms has attracted particular interests recently [6–8, 41, 43, 46, 52, 77]. In a typical SMC design, stability is the only concern in the switching surface design. The optimal SMC design aims at achieving both robust and optimal control, thus shows

the superiority in practical applications. However, no results about optimal SMC design for underactuated system have been shown in the existing works. Thus it would be meaningful and interesting to explore optimal or suboptimal SMC designs for underactuated systems.

Another good alternative for handling system with uncertainties is the fuzzy logic technique. One major feature of a fuzzy system is its capability of processing vague information in a logic manner. A fuzzy system is essentially a knowledge based system, which uses fuzzy sets and fuzzy rules to describe the relationships between the inputs and the outputs. The fuzzy sets use linguistic variables, rather than quantitative variables, to represent imprecise concepts, thus the design provides a user-friendly interface. The fuzzy rules, which describe the operation of fuzzy sets in the form of approximate reasoning, function as a decision maker with powerful reasoning capabilities, thus the designers' knowledge can be incorporated directly in the design. In the control area, fuzzy systems have been widely used for system modeling and control [27, 38, 39, 70].

The application of the fuzzy logic technique in controller design, known as fuzzy logic control (FLC), has been widely employed for controlling systems with uncertainties. FLC offers a nonlinear controller with robustness for systems with parametric and functional uncertainties, as well as disturbances [5, 38, 42, 70]. The FLC design provides flexibility in structure design and parameter selection, thus it can be easily incorporated with other control methods, such as adaptive control [38, 44], genetic algorithms [42], learning control [16], linear LQR control [69], and H_2 and H_∞ control [17]. FLC design based on human experience and experts' knowledge is generally model-free, which is complementary to model-based control design. However, for systems with complicated dynamic behaviors, such as underactuated mechanical systems, the human knowledge could be not enough to accomplish the FLC design, which motivates researchers to synthesize model based control methods in the FLC design.

Another important application of the fuzzy system is system modeling. Fuzzy systems are theoretically capable of uniformly approximating any continuous real function to any degree of accuracy, i.e., any nonlinear system can be represented by a fuzzy system. Based on the obtained fuzzy model, control algorithms can be further designed. The use of fuzzy approximations avoids the need to derive the mathematical model of the system to be controlled. However, to generate an approximated mathematical model with enough accuracy, the fuzzy system needs to use a large number of fuzzy rules, which is not desirable in real implementations.

Application of model-free FLC design for real platforms could be problematic considering the large number of fuzzy rules and controller parameters to be determined and the limited heuristic knowledge for complex dynamics for systems such as underactuated systems. It is motivated to synergize a model-free design with heuristic knowledge and a model-based design with an available plant model, so that all information relevant to the system can be fully utilized in FLC design. Most importantly, to make the developed control algorithms be simple and easy to apply, the number of fuzzy rules and parameters to be determined should be minimized.

A major difficulty in the design and implementation of nonlinear controllers, such as SMC and FLC, is the determination and tuning of the controller parameters. To make the nonlinear control algorithms be simple and easy to implement, it is motivated to find systematic methods for choosing and tuning controller parameters.

1.2 Statement of Contributions

This thesis focuses on linear and nonlinear controllers design for an underactuated 2WMR with input coupling. The developed methods can also be extend to a class of underactuated system with or without input coupling. Real-time implementation of the proposed controllers are also addressed. In this section, the contributions of this thesis are briefly summarized as

below:

1. In Chapter 2, development and modeling of an underactuated 2WMR prototype with input coupling is presented. Essentially, the developed 2WMR can be regarded as a 2-D unicycle system with the lateral stability guaranteed. The mathematic model of the 2WMR is derived and internal dynamic analysis is presented. Design of reference signals are discussed for 2WMR under different control objectives and different travel circumstances.

2. In Chapter 3, a linear state-feedback controller, simple and realizable, is found adequate in stabilizing the nonlinear 2WMR system in a wide range around the equilibrium. However, it is extremely difficult to verify the effectiveness of such a linear state feedback for systems in the presence of nonlinearity and uncertainties. A main contribution of this part of work is to explore the design issue and effectiveness of the linear controller for the underactuated 2WMR. Two alternative methods are introduced to obtain the feedback gains for the linear controller, one is based on LQR to achieve a optimal design and the other is based on Linear Matrix Inequality (LMI) approach to achieve a robust design. Lyapunov method is employed to analyze the stability region of the closed-loop 2WMR system when linear controller is applied.

3. In Chapter 4, a sliding mode controller (SMC) is proposed. When designing the SMC for the 2WMR, various uncertainties are taken into consideration, including matched uncertainties such as the joint friction, and unmatched uncertainties such as the ground friction, payload variation, or road slope. The SMC proposed is capable of handling system uncertainties and applicable to general underactuated systems with or without input coupling. For sliding surface design, the selection of the sliding surface coefficients is in general a sophisticated design issue because those coefficients are non-affine in the sliding

manifold. In this work, the sliding surface design is transformed into a linear controller design, which is simple and systematic. By virtue of the systematic design, various linear control techniques, such as linear quadratic regulator (LQR) or linear matrix inequality (LMI), can be incorporated in the sliding surface design to achieve optimality or robustness for the sliding manifold. The effectiveness of the SMC is verified through intensive simulations and experimental testings.

4. In Chapter 5, a novel implementation of an integral sliding mode controller (ISMC) on the 2WMR is presented. It is the first time that integral sliding mode control method is successfully applied to a real-time platform of 2WMR and several critical issues are addressed. Similarly as in Chapter 4, when designing the ISMC for the 2WMR, various uncertainties are taken into consideration, including matched uncertainties such as the joint friction, and unmatched uncertainties such as the ground friction, payload variation, or road slope. ISMC is suitable for control of the underactuated 2WMR because ISMC provides an extra degree of freedom in control when sliding mode is achieved. We utilize this extra degree of freedom to implement a linear nominal controller, which is found adequate in stabilizing the sliding manifold in a wide range around the equilibrium. The implemented ISMC, with an integral sliding surface and a switching term, is able to completely nullify the influence from the matched uncertainties. The implemented linear nominal controller, which is a linear quadratic controller (LQR), is stabilizing the sliding manifold that is subject to unmatched uncertainties. The effectiveness of ISMC is verified through intensive simulation and experiment results.

5. Chapter 6 presents a novel implementation of a Takagi-Sugeno (T-S) type fuzzy logic controller (FLC) on the 2WMR. The novelties of this chapter lie in three aspects. First, the FLC is a synthesized design which utilizes both heuristics knowledge and model infor-

mation of the 2WMR system. The FLC structure including the fuzzy labels, membership

functions, and inference is chosen based on heuristic knowledge about the 2WMR. The

output parameters of the FLC are determined by comparing the output of the FLC with a

linear controller at certain operating points, which avoids the difficulty and tediousness in

manual tuning. The linear controller is designed based on a linearized model of the 2WMR

system. Second, the proposed FLC is a simple and realizable design for real implementa-

tion. Only two fuzzy labels are adopted for each fuzzy variable. Sixteen fuzzy rules are

used with eight output parameters and four range parameters for the membership functions

to be determined. Third, the proposed FLC is successfully implemented on the real-time

2WMR for regulation and setpoint control tasks. Satisfactory responses are achieved not

only when the 2WMR travels on a flat surface but also on an inclined surface. Through

comprehensive experimental-based investigations, the effectiveness of the proposed FLC

is validated, and the FLC shows superior performance than the existing methods.

6. In Chapter 7, we propose synthesized design of a FLC for control of the underactuated

2WMR. The synthesized design consists of three phases. First, the FLC structure including

the number of rules, membership functions, inference and parametric relations, are chosen

based on heuristic knowledge about the 2WMR. Second, on the basis of a linearized model

and linear feedback, the FLC output parameters are determined quantitatively for stabiliza-

tion of the 2WMR. Third, the FLC output parameters are tuned using an iterative learning

tuning (ILT) algorithm, which minimizes an objective function that specifies the desired

2WMR performance. The rationale for the synthesized FLC design is full utilization of

the available information, which is achieved by combining model-based and model-free

designs, and hence improves the FLC performance. We minimize the number of FLC

rules and fuzzy labels. Six rules are used for regulation or setpoint tasks, whereas ten rules

are used with extra integral control to eliminate steady-state errors induced by system uncertainties and disturbances. Only two fuzzy labels are adopted for each fuzzy variable. The ILT process consists of two phases, exploration for stabilization and exploitation for better performance. The effectiveness of the proposed FLC is validated using intensive simulations and comparisons.

1.3   Thesis Outline

The thesis is organized as follows.

In Chapter 2, the detailed description of the 2WMR system is presented, including the hardware architecture and system dynamic model. Control objective for the 2WMR and references design are given.

In Chapter 3, a linear controller is proposed and two alternative methods are introduced to obtain the feedback gains for the linear controller. The effectiveness of the linear controller is investigated through simulations and experiment testings.

In Chapter 4, an SMC with a linear sliding surface is proposed and successfully implemented on the 2WMR platform.

In Chapter 5, an SMC with an integral-type sliding surface, i.e., an ISMC, is proposed and successfully implemented on the 2WMR platform.

In Chapter 6, a Takagi-Sugeno type FLC is proposed and successfully implemented on the 2WMR platform.

In Chapter 7, synthesized design of an FLC for velocity control of the 2WMR is presented.

In Chapter 8, the work of this thesis is summarized and recommendations are made on possible directions of the future research.

Chapter 2

Hardware Development and Problem Formulation

2.1 Introduction

In this chapter, hardware description of the 2WMR platform is presented in Section 2.2. Section 2.3 focuses on the modeling and analysis of the 2WMR dynamic model. It is shown that the internal dynamic of the 2WMR system is inherently unstable, which is consistent with the nature of the inverse pendulum. In Section 2.4, design of reference signals is discussed for 2WMR under different control objectives and different travel circumstances.

2.2 Hardware Description of the 2WMR Platform

Fig.2.1 shows the overview of the hardware system and Fig.2.2 shows the main electrical components used for building the 2WMR.

The inertia measurement unit (IMU) combo board v1 (Sparks Fun Electronics) is used to measure the pendulum tilting angular and the pendulum angular velocity, which is equipped with an accelerometer (ADXL320) with a range of $+/-5$ g and a rate gyro (ADXRS613) capable of measuring up to $+/-150°/s$. The IMU sensor produces analogue output signals between
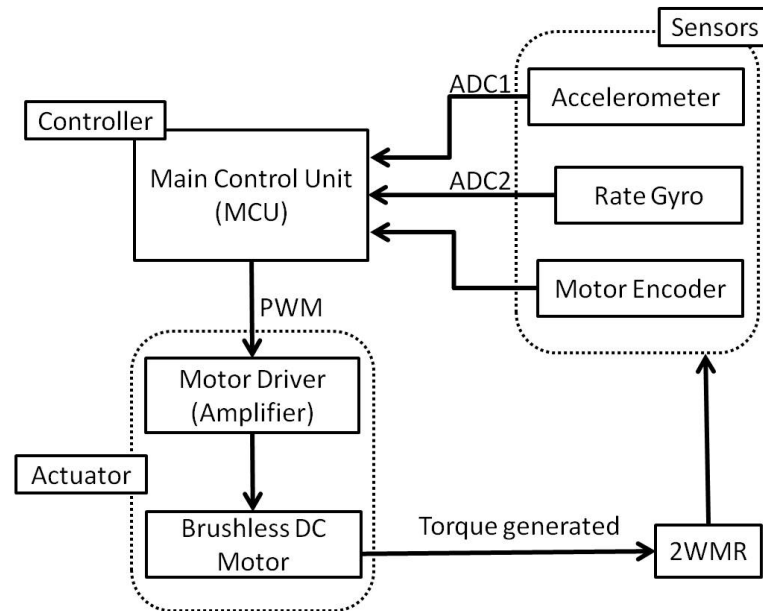
Figure 2.1: System overview for the 2WMR.
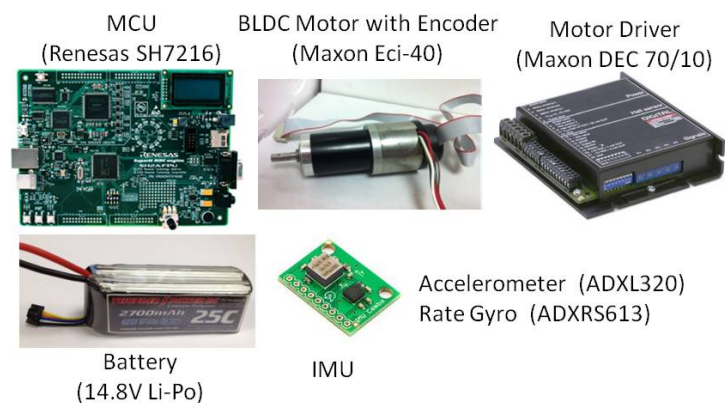
Figure 2.2: Main electrical components for the 2WMR.

0 V to 5 V, hence, the analogue-to-digital conversion (ADC) is needed to generate digital signals that the main control unit (MCU) can process. In addition, the combo board also has a built-in low-pass filter (LPF) for both the accelerometer and rate gyro with cut-off frequency of 500 Hz and 40 Hz, respectively.

The brushless DC motor (Maxon Eci-40), which acts as the only actuator, generates the required torque to drive the wheels while balance the pendulum. The brushless DC motor is controlled by a four quadrant motor driver (Maxon DEC 70/10), which could also be regarded as an amplifier. The motor driver works under the mode of torque control, and the torque constant of the motor is 16.9 m·Nm/A. A gear box is mounted to the motor, which has a gear reduction ratio of 132 : 1 with gear efficiency of 80%.

To obtain the position and velocity information of the wheels, a three-channel magnetic encoder is fixed on the motor. The encoder has a resolution of 500 counts per turn (CPT). By coupling the encoder and reduction gear with the motor, the resultant resolution is equivalent of (500×132) CPT.

The MCU (Renesas micro-controller SH7216) is used to process the data measured by the sensors, compute the control signal according to the designed control algorithm and generate a PWM signal for the motor driver. Renesas SH7216-FPU is a 32-bit micro-controller, which is capable of operating with a maximum frequency of 200 mHz and has a floating-point unit (FPU), 1 mb of ROM and 128 kb of RAM. The MCU used meets the requirement for computation with maintaining a sufficiently high sampling frequency, which is 100 Hz in the implementation. The MCU can be programmed with C and C++ language.

The battery (14.8 V, 2700 mAh Li-Po) is fed to two voltage regulators to produce constant 12 V for the motor driver and 5 V for the micro-controller and the IMU.

2.3   Modeling and Analysis of the 2WMR System

2.3.1   Modeling of the 2WMR
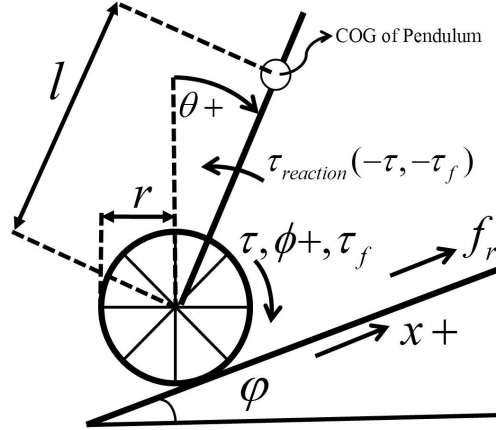
Figure 2.3: Model of the 2WMR.

Fig. 2.3 shows the model of the 2WMR. The wheel motion is defined along the surface. The wheels displacement and velocity are denoted by x and $\dot{x}$ respectively, with rightward as positive direction. ϕ is the angular rotation of the wheels with clockwise as positive direction, we have $\phi = x/r$, where r is the radius of the wheel. θ is the tilting angle of the pendulum with the upright position as zero point and clockwise rotation as positive direction. $\dot{\theta}$ is angular velocity of the pendulum. φ is the slope angle of the inclined road, for traveling on flat surface, $\varphi=0$. f_r is the friction between the wheels and the ground. τ is the torque generated by the motor and acting on the wheels with clockwise rotation as positive direction, which is also the control input u to the system. Note that the motor driving the wheel is directly mounted on the pendulum, there is a reaction torques $-\tau$ applied to the pendulum. τ_f is the joint friction, which also acts on both the wheel and the pendulum as τ_f and $-\tau_f$ respectively. Other system parameters are as:

$m_w = 1.551\ kg$: the mass of the wheels;

$m_p = 1.6\ kg$: the mass of the pendulum;

$I_w = 0.005\ kg \times m^2$: the rotation inertia of the wheels;

$I_p = 0.027 \ kg \times m^2$: the rotation inertia of the pendulum;

$r = 0.08 \ m$: the radius of the wheel;

$l = 0.13 \ m$: the distance between Center of Gravity (COG) of the pendulum and the center of the wheel;

$g = 9.81 \ m/s^2$: the acceleration of gravity.

Lagrangian mechanics method is used to derive the mathematical model of the 2WMR system (refer to Appendix A.1), which leads to a second-order nonlinear model given by

$$a\ddot{x} + b\ddot{\theta} - m_p l \sin(\theta + \varphi)\dot{\theta}^2 + \sin\varphi(m_p + m_w)g = \frac{1}{r}(\tau + \tau_f - rf_r), \qquad (2.1)$$

$$b\ddot{x} + c\ddot{\theta} - m_p lg \sin\theta = -\tau - \tau_f, \qquad (2.2)$$

where $a = m_w + m_p + \frac{I_w}{r^2}$, $b = m_p l \cos(x_3 + \varphi)$ and $c = I_p + m_p l^2$.

For 2WMR with input coupling, the control input τ exists in both the wheel and the pendulum motion equations (2.1)(2.2). While for 2WMR without input coupling, τ only exists in motion equation of the wheel subsystem (2.1).

Four state variables are defined to describe the 2WMR system, the position and velocity of the wheels, the tilting angular and angular velocity of the pendulum, as $\mathbf{x} = [x_1, x_2, x_3, x_4]^T = [x, \dot{x}, \theta, \dot{\theta}]^T$. The state-space model of the 2WMR is

$$\begin{bmatrix} \dot{x}_1 \\ \dot{x}_2 \\ \dot{x}_3 \\ \dot{x}_4 \end{bmatrix} = \begin{bmatrix} x_2 \\ f_1(\mathbf{x}) \\ x_4 \\ f_2(\mathbf{x}) \end{bmatrix} + \begin{bmatrix} 0 \\ g_1(\mathbf{x}) \\ 0 \\ g_2(\mathbf{x}) \end{bmatrix}(u + d_m) + \begin{bmatrix} 0 \\ d_{u1}(\mathbf{x}) \\ 0 \\ d_{u2}(\mathbf{x}) \end{bmatrix}$$

$$(2.3)$$

$$y = [x_1, x_3]^T,$$

where

$$
\begin{aligned}
f_1 &= \frac{m_p l}{ac - b^2}\left[cx_4{}^2 \sin(x_3 + \varphi) - bg\sin x_3\right] - \frac{c\,(m_p + m_w)\,g\sin\varphi}{ac - b^2}, \\
f_2 &= \frac{m_p l}{ac - b^2}\left[-bx_4{}^2 \sin(x_3 + \varphi) + ag\sin x_3\right] + \frac{b(m_p + m_w)g\sin\varphi}{ac - b^2}, \\
g_1 &= \frac{1}{r}\frac{c}{ac - b^2} + \frac{b}{ac - b^2}, \\
g_2 &= \frac{1}{r}\frac{-b}{ac - b^2} + \frac{-a}{ac - b^2}, \\
d_m &= \tau_f, \\
d_{u1} &= \frac{-c}{ac - b^2}f_r, \\
d_{u2} &= \frac{b}{ac - b^2}f_r,
\end{aligned}
$$

and $b = m_p l \cos(x_3 + \varphi)$.

2.3.2   Equilibrium Point Analysis

At the equilibrium point, the wheel acceleration is zero ($\ddot{x} = 0$), the pendulum angular veloc-
ity and acceleration are zero ($\dot{\theta} = 0$, $\ddot{\theta} = 0$), meanwhile the joint friction does not exist ($\tau_f = 0$),
the dynamic equations (2.1)(2.2) become

$$
\sin\varphi(m_p + m_w)g = \frac{1}{r}(\tau - rf_r), \tag{2.4}
$$

$$
-m_p l g \sin\theta = -\tau. \tag{2.5}
$$

From the above equations, the pendulum equilibrium point is

$$
\theta_e = \arcsin\frac{r\sin\varphi(m_p + m_w)g + rf_r}{m_p l g}. \tag{2.6}
$$

For the 2WMR with input coupling, when it is stabilized on a inclined surface ($\varphi \neq 0$) or
traveling at a constant velocity ($f_r \neq 0$), a torque, denoted as τ_s, should be provided to overcome
the effect of gravity or the ground friction, meanwhile, the reaction torque $-\tau_s$ acts on the pen-
dulum. The balance of the pendulum can be reached only when the total torque acting on the

pendulum is zero. Thus, the pendulum tilts rightward or leftward from the upright position such that the torque resulted from the gravity of the pendulum equals to the reaction torque $-\tau_s$ but with the opposite direction.

Remark 2.1 *For the 2WMR with input coupling, the equilibrium of the pendulum varies with respecting to the slope angle of the traveling surface and the ground friction, as shown in (2.6). For 2WMR system without input coupling, the equilibrium of the pendulum keeps at the upright position, i.e., $\theta_e = 0$, which is irrelevant to the traveling circumstance.*

The pendulum equilibrium position is essentially determined by the mechanical configuration of the 2WMR platform and is irrelevant to the controller applied or control tasks specified. For different applications of the 2WMR, different mechanical design should be adopted.

2.3.3 Internal Dynamic Analysis

In order to transform the state space model into a companion form, define new state variables $\mathbf{z} = [z_1, z_2, z_3, z_4]^T = [x_1, x_2, x_3, g_2 x_2 - g_1 x_4]^T$. The new state space model in Z coordinates is

$$
\begin{bmatrix} \dot{z}_1 \\ \dot{z}_2 \\ \dot{z}_3 \\ \dot{z}_4 \end{bmatrix} = \begin{bmatrix} z_2 \\ h_1(\mathbf{z}) \\ h_2(\mathbf{z}) \\ h_3(\mathbf{z}) \end{bmatrix} + \begin{bmatrix} 0 \\ g_1(\mathbf{z}) \\ 0 \\ 0 \end{bmatrix} u,
\tag{2.7}
$$

$$
y = [z_1, z_3].
$$

where

$$
h_1(\mathbf{z}) = \frac{c}{ac - b^2} m_p l h_2^2 \sin(z_3 + \varphi) - \frac{b m_p l g \sin z_3}{ac - b^2} - \frac{c(m_p + m_w) g \sin \varphi}{ac - b^2},
$$

$$
h_2(\mathbf{z}) = \frac{g_2(z_3) z_2 - z_4}{g_1(z_3)},
$$

$$
h_3(\mathbf{z}) = -\frac{m_p l \sin z_3}{ac - b^2} (h_2^2 + \frac{g}{r}) + \frac{(m_p + m_w) g \sin \varphi}{ac - b^2} - \frac{\partial g_1}{\partial z_3} h_2^2 + \frac{\partial g_2}{\partial z_3} h_2 z_2,
$$

and $g_1(z_3) = g_1(x_3)$, $g_2(z_3) = g_2(x_3)$, $b(z_3) = b(x_3)$, $c(z_3) = c(x_3)$.

From (2.7), we can see that z_1, z_2 is in companion form and (z_3, z_4) sub-dynamics is not related with the control input u directly. Thus z_3 and z_4 form an internal dynamics

$$\begin{bmatrix} \dot{z}_3 \\ \dot{z}_4 \end{bmatrix} = \begin{bmatrix} h_2(\mathbf{z}) \\ h_3(\mathbf{z}) \end{bmatrix}.$$

If the internal dynamics of the system is stable, the 2WMR can be controlled to follow up arbitrary trajectory by using feedback linearization. Due to the nonlinearity in the internal dynamics, it is not easy to derive stability conditions that are state dependent. Let $z_1 = z_2 = 0$, the zero dynamics is

$$\dot{z}_3 = -\frac{z_4}{g_1} \tag{2.8}$$

$$\dot{z}_4 = -\frac{m_p l \sin z_3}{ac - b^2} \left(\left(\frac{-z_4}{g_1} \right)^2 + \frac{g}{r} \right) + \frac{(m_p + m_w) g \sin \varphi}{ac - b^2} - \frac{\partial g_1}{\partial z_3} (\frac{-z_4}{g_1})^2 \tag{2.9}$$

Now we show the zero dynamics has an unstable equilibrium around $\theta = \dot{\theta} = 0$. Linearizing the zero dynamics around the equilibrium $z_3 = z_4 = 0$ in (2.8), (2.9) with $\sin z_3 = z_3$, $\cos z_3 = 1$, $z_4^2 = 0$, and assume the 2WMR travels on a flat surface ($\varphi = 0$), we have

$$\dot{z}_3 = -\frac{z_4}{g_1} \tag{2.10}$$

$$\dot{z}_4 = -\frac{m_p l g z_3}{r(ac - b^2)} \tag{2.11}$$

where g_1, a, b, c are all positive constants.

For system (2.10) (2.11),

$$(z_3, z_4) = (0, 0)$$

is the equilibrium point, but as

$$g_1 > 0,$$

$$\frac{m_p l g z_3}{r(ac - b^2)} > 0,$$

the system is inherently unstable at the equilibrium point, that is, the zero dynamics of the 2WMR system is unstable.

2.4 Control Objective and References Design

2.4.1 Control Objective

The control objective is to achieve position or velocity control of the wheels, while balance the pendulum at the unstable equilibrium ($\theta=\theta_e$, $\dot{\theta}=0$). The reference signal for the system state vector $\mathbf{x}$ is chosen as $\mathbf{r} = [x_r,\ v_r,\ \theta_r,\ 0]^T$ with $\dot{x}_r = v_r$. We obtain the error state vector as $\mathbf{e} = [e_1,\ e_2,\ e_3,\ e_4]^T = \mathbf{x} - \mathbf{r} = [x_1 - x_r,\ x_2 - v_r,\ x_3 - \theta_r,\ x_4]^T$. Now the control objective is to ensure the convergence of $\mathbf{e}$. The error dynamic model of the 2WMR is obtained as

$$\dot{\mathbf{e}} = \eta(\mathbf{e}) + \mathbf{g}(\mathbf{e})[u + d_m(\mathbf{e},t)] + \mathbf{d}_u(\mathbf{e},t), \tag{2.12}$$

where η is the system nonlinear term, d_m is the lumped matched uncertainties, $\mathbf{d}_u$ is the lumped unmatched uncertainties. We have

$$\eta(\mathbf{e}) = [e_2,\ \eta_1(\mathbf{e}),\ e_4,\ \eta_2(\mathbf{e})]^T,$$

$$\mathbf{g}(\mathbf{e}) = [0,\ g_1(\mathbf{e}),\ 0,\ g_2(\mathbf{e})]^T,$$

$$d_m(\mathbf{e},t) = \tau_f,$$

$$\mathbf{d}_u(\mathbf{e},t) = [0,\ d_{u1}(\mathbf{e},t),\ 0,\ d_{u2}(\mathbf{e},t)]^T,$$

where

$$\eta_1 = \frac{m_p l}{ac - b^2}\left[ce_4{}^2\sin(e_3 + \theta_r + \varphi) - bg\sin(e_3 + \theta_r)\right] - \frac{c(m_p + m_w)g\sin\varphi}{ac - b^2} - \dot{v}_r,$$

$$\eta_2 = \frac{m_p l}{ac - b^2}\left[-be_4{}^2\sin(e_3 + \theta_r + \varphi) + ag\sin(e_3 + \theta_r)\right] + \frac{b(m_p + m_w)g\sin\varphi}{ac - b^2},$$

$$g_1 = \frac{1}{r}\frac{c}{ac - b^2} + \frac{b}{ac - b^2},$$

$$g_2 = \frac{1}{r}\frac{-b}{ac - b^2} + \frac{-a}{ac - b^2},$$

$$d_{u1} = \frac{-c}{ac - b^2}f_r,$$

$$d_{u2} = \frac{b}{ac - b^2}f_r,$$

and $b = m_p l \cos(e_3 + \theta_r + \varphi)$.

In the following chapters, control system design and stability analysis are based on the dynamics model formulated in (2.12), which can also be used to describe general underactuated systems (refer to Appendix A.2). Thus, the controllers designed for the 2WMR system are extendable to general underactuated systems with or without input coupling.

2.4.2   Trajectory Planning for the Wheel

Without loss of generality, in this thesis, we consider regulation and setpoint control tasks for the 2WMR. For regulation task, the references for the wheel position and velocity are as $x_r = 0$ and $v_r = 0$, respectively. For setpoint control, the 2WMR is supposed to reach a desired position x_d and stop there. For classical setpoint control task, a step signal is used as the reference. However, in real implementation, using a step function as the desired trajectory for the 2WMR would generate a large initial control signal due to the large initial position error, which yields a strong impact to the 2WMR and leads to unstable motion. To avoid the undesired impact, we convert the setpoint task into trajectory tracking task. High-order polynomials are sometimes used for computing a smooth trajectory [47], however, in this work, we simply use a linear segment and two parabolic blends to construct a smooth trajectory for the 2WMR, which also yields a smooth reference signal for the wheel velocity. The reference inputs are computed by the following equations and shown in Fig. 2.4.

$$v_r(t) = \begin{cases} \dfrac{v_m}{t_1} t & 0 < t < t_1, \\ v_m & t_1 \leq t \leq t_2, \\ v_m - \dfrac{v_m}{t_3 - t_2}(t - t_2) & t_2 \leq t \leq t_3, \\ 0 & t_3 \leq t \leq t_s, \end{cases} \tag{2.13}$$

$$x_r(t + T_s) = \begin{cases} x_r(t) + v_r T_s & \text{if } x_r(t) < x_d \\ x_d & \text{if } x_r(t) \geq x_d \end{cases}, \tag{2.14}$$

where x_d is the desired setpoint, T_s is the sampling time.

The planned reference signals for the wheel position and velocity yield zero initial position and velocity errors, which are desirable in feedback control design. According to Fig. 2.4, the 2WMR is supposed to move forward consistently and reach the setpoint $x_d = 1.5$ m around $t = t_3 = 16$ s.
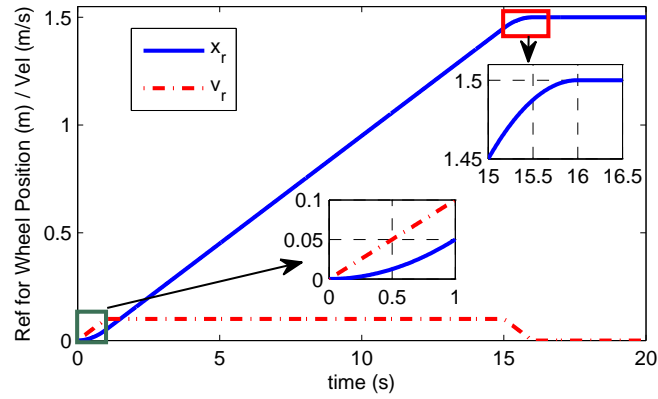
Figure 2.4: Reference signals for wheel velocity and position as described in (2.13)(2.14) with $t_1 = 1\ s$, $t_2 = 15\ s$, $t_3 = 16\ s$, $t_s = 20$, $v_m = 0.1\ m/s$, $x_d = 1.5\ m$.

2.4.3 Reference Position for the Pendulum

For regulation and setpoint control tasks, the 2WMR finally stops at the original position or the desired setpoint, and the ground friction disappears, i.e., $f_r = 0$. The pendulum equilibrium position (2.6) becomes

$$\theta_e = \arcsin \frac{r \sin \varphi (m_p + m_w)}{m_p l}.$$

To achieve a zero steady-state error for the pendulum angle, the reference position for the pendulum is chosen as $\theta_r = \theta_e$, that is

$$\theta_r = \arcsin \frac{r \sin \varphi (m_p + m_w)}{m_p l}. \tag{2.15}$$

The above θ_r is applicable only if the system parameters involved are known. For 2WMR travels on a flat surface, $\theta_r = 0$ since $\varphi = 0$.

2.5 Conclusion

In this chapter, the particular characteristics of the underactuated 2WMR system are investigated, according to which, references for both the wheel and the pendulum are designed.

Chapter 3

Design and Investigation of a Linear Controller

3.1 Introduction

Linear feedback controllers are by far the most widely adopted controllers in industry owing to their intuitiveness and relative simplicity. In fact, although linear controllers are relatively simple to use, they are able to provide a satisfactory performance in a wide range of process control tasks.

For control of the underactuated 2WMR, as the pendulum is inherent unstable, full state feedback control is indispensable. In linear feedback control design, the most important issue is how to choose the feedback gains. In [47, 62, 68], LQR method is adopted, which is based on a linearized model of the wheeled inverted pendulum. The linearized model is obtained by assuming the pendulum stays around the desired equilibrium point and no uncertainties exist in the system. The results shown in [62, 68] indicates that the linear controller can work when the pendulum stays in a limited region around the equilibrium, i,e., the linear controller may become ineffective when the pendulum is away from the desired equilibrium point or the system is in presence of uncertainties. Thus, robustness should be addressed in the controller design.

Furthermore, it would be meaningful to explore the stability region of the closed-loop 2WMR system when it is under linear control.

In this chapter, first, linear controller design based on LQR method is introduced and guidelines are provided on how to the select the weighting matrices Q and R. Second, a linear feedback controller based on LMI method is proposed to achieve a robust control, furthermore, Lyapunov method is employed to analyze the stability region of the closed-loop 2WMR system.

The chapter is organized as the following. In Section 3.2, the design of optimal linear controller based on LQR is presented. In Section 3.3, the robust linear controller based on LMI is proposed and stability region of the closed-loop system is discussed. In Section 3.4, simulation based studies are presented. Section 3.5 shows the implementation of the linear controller on the 2WMR. Conclusions are drawn in Section 3.6.

3.2   Optimal Linear Controller Based on LQR

The LQR design is based on a linearized dynamic model, which is obtained by linearizing the nonlinear error dynamic model (2.12) about the unstable equilibrium point. By assuming that $\sin e_3 \approx e_3$, $e_4{}^2 \approx 0$, $\cos e_3 \approx 1$, $f_r \approx 0$, $\tau_f \approx 0$, and φ is known, we have

$$
\begin{bmatrix} \dot{e}_1 \\ \dot{e}_2 \\ \dot{e}_3 \\ \dot{e}_4 \end{bmatrix} = \underbrace{\begin{bmatrix} 0 & 1 & 0 & 0 \\ 0 & 0 & \dfrac{-b_0 m_p l g \cos \theta_r}{ac - b_0{}^2} & 0 \\ 0 & 0 & 0 & 1 \\ 0 & 0 & \dfrac{a m_p l g \cos \theta_r}{ac - b_0{}^2} & 0 \end{bmatrix}}_{A_0} \begin{bmatrix} e_1 \\ e_2 \\ e_3 \\ e_4 \end{bmatrix} + \underbrace{\begin{bmatrix} 0 \\ g_{1,0} \\ 0 \\ g_{2,0} \end{bmatrix}}_{\mathbf{g}_0} (u + \eta_m), \qquad (3.1)
$$

where

$$
\eta_m = -r(m_p + m_w) g \sin \varphi,
$$

and

$$
\begin{aligned}
g_{1,0} &= \frac{c}{r(ac - b_0{}^2)} + \frac{b}{ac - b_0{}^2}, \\
g_{2,0} &= \frac{-b_0}{r(ac - b_0{}^2)} + \frac{-a}{ac - b_0{}^2},
\end{aligned}
$$

with $b_0 = m_p l \cos(\varphi + \theta_r)$ and θ_r is as (2.15).

The term η_m reflects the effect of the gravity when the 2WMR travels on an inclined surface. As we have discussed in Section 2.3.3, a constant torque τ_s should be provided to overcome the effect of the gravity. It can be seen that η_m is matched to the control input and can be compensated directly by letting $\tau_s = -\eta_m = r(m_p + m_w)g \sin\varphi$. Note that, in steady state, $r(m_p + m_w)g \sin\varphi = m_p l g \sin\theta_e$, thus, we also have $\tau_s = m_p l g \sin\theta_e$.

The control law is designed as:

$$
u = u_{lc} + \tau_s = u_{lc} - \eta_m, \tag{3.2}
$$

and

$$
u_{lc} = -k_1 e_1 - k_2 e_2 - k_3 e_3 - k_4 e_4 = -\mathbf{k}\mathbf{e},
$$

where $\mathbf{k} = [k_1,\ k_2,\ k_3,\ k_4]$.

The LQR design aims to minimize the following performance index

$$
J_{LQR} = \frac{1}{2}\int_0^\infty (\mathbf{e}^T Q\mathbf{e} + R u_{lc}{}^2)dt. \tag{3.3}
$$

with $Q \geq 0$ and $R > 0$.

The solution for the optimal control gain is as

$$
\mathbf{k} = R^{-1}\mathbf{g}_0{}^T P_1, \tag{3.4}
$$

where P_1 is the solution of the following Riccati equation

$$
P_1 A_0 + A_0{}^T P_1 - P_1 \mathbf{g}_0 R^{-1}\mathbf{g}_0{}^T P_1 + Q = 0.
$$

In this work, we choose the weighting matrix as $Q = diag\{q_1, q_2, q_3, q_4\}$, and R a scalar, where q_i and R are the weighting factors for e_i $(i = 1, 2, 3, 4)$ and u_{lc} respectively.

The relative values of q_i represent the relative weighting among e_i. If q_1 is bigger than q_2, there is higher penalty on error e_1 than e_2 and control tries to make smaller $e_1{}^2$ than $e_2{}^2$, and vice versa. For control of the 2WMR system, the main objective is the convergence of e_1 and e_3, thus it is nature to select q_1 and q_3 to be relatively larger than q_2 and q_4. Furthermore, considering that the balancing of the pendulum is more important than the tracking performance of the wheel, it is reasonable to select q_3 and q_4 to be relatively larger than q_1 and q_2, respectively.

The relative value of the weighting matrix Q and R expresses the relative importance of keeping **e** and u_{lc} near zero. If we place more importance on the convergence of **e**, then we can select Q to be relatively large to R, and so forth. Although we are interested in minimizing J_{LQR} in (3.3), the actual value of J_{LQR} is usually not of interest, which also means that we can set either Q or R to be fixed for the convenience of parameter tuning because it is their relative weight that is important. In this work, since Q is matrix and R is a scalar, it is better to fix Q and tune R to achieve desired performance. A smaller R results in a larger feedback gain and faster convergence of **e**, however, a larger magnitude of u_{lc}. Thus, the selection of R should achieve a compromise between these effects.

3.3   Robust Linear Controller Based on LMI

In this section, the linear controller design will be based on LMI and Lyapunov method. The obtained feedback gain is a robust solution.

For control of the 2WMR system, when the slope angle φ is known to the designer, the pendulum reference position θ_r is set as (2.15). Represent the nonlinear dynamic model (2.12)

in the following form

$$\dot{\mathbf{e}} = A(\mathbf{e})\mathbf{e} + \mathbf{g}(\mathbf{e})(u + \eta_m) + \phi(\mathbf{e}, t), \tag{3.5}$$

where

$$A(\mathbf{e}) = \begin{bmatrix} 0 & 1 & 0 & 0 \\ 0 & 0 & \dfrac{-bm_plg\cos\theta_r}{ac-b^2}\dfrac{\sin e_3}{e_3} & 0 \\ 0 & 0 & 0 & 1 \\ 0 & 0 & \dfrac{am_plg\cos\theta_r}{ac-b^2}\dfrac{\sin e_3}{e_3} & 0 \end{bmatrix}, \quad \mathbf{g}(\mathbf{e}) = \begin{bmatrix} 0 \\ g_1(\mathbf{e}) \\ 0 \\ g_2(\mathbf{e}) \end{bmatrix},$$

$$\phi(\mathbf{e}, t) = \begin{bmatrix} 0 \\ \dfrac{cm_ple_4{}^2\sin(e_3+\theta_r+\varphi)}{ac-b^2} - \dfrac{bm_plg(\cos e_3 - 1)\sin\theta_r}{ac-b^2} + g_1 d_m + d_{u1} \\ 0 \\ -\dfrac{bm_ple_4{}^2\sin(e_3+\theta_r+\varphi)}{ac-b^2} + \dfrac{am_plg(\cos e_3 - 1)\sin\theta_r}{ac-b^2} + g_2 d_m + d_{u2} \end{bmatrix}. \tag{3.6}$$

For control of the 2WMR system, when the slope angle φ is unknown to the designer, the

pendulum reference position θ_r is set as zero. The nonlinear dynamic model (2.12) becomes

$$\dot{\mathbf{e}} = A(\mathbf{e})\mathbf{e} + \mathbf{g}(\mathbf{e})u + \phi(\mathbf{e}, t) \tag{3.7}$$

with

$$\phi(\mathbf{e}, t) = \begin{bmatrix} 0 \\ \dfrac{cm_ple_4{}^2\sin(e_3+\varphi)}{ac-b^2} - \dfrac{c(m_p+m_w)g\sin\varphi}{ac-b^2} + g_1 d_m + d_{u1} \\ 0 \\ -\dfrac{bm_ple_4{}^2\sin(e_3+\varphi)}{ac-b^2} + \dfrac{b(m_p+m_w)g\sin\varphi}{ac-b^2} + g_2 d_m + d_{u2} \end{bmatrix}. \tag{3.8}$$

For (3.5), the control law is designed as (3.2), which is a linear controller plus a compensation

term. While for (3.7), a pure linear controller is used. By applying the proposed controllers, (3.5)

and (3.7) become as

$$\dot{\mathbf{e}} = A(\mathbf{e})\mathbf{e} + \mathbf{g}(\mathbf{e})(-\mathbf{k}\mathbf{e}) + \phi(\mathbf{e}, t)$$

with $\phi(\mathbf{e}, t)$ expressed in (3.6) and (3.8), respectively.

Let $\mathbf{k} = \mathbf{w}P$, the above equation becomes

$$\dot{\mathbf{e}} = A(\mathbf{e})\mathbf{e} - \mathbf{g}(\mathbf{e})\mathbf{w}P\mathbf{e} + \phi(\mathbf{e}, t). \tag{3.9}$$

Next, we express $A(\mathbf{e})$ and $\mathbf{g}(\mathbf{e})$ as $A_0 + \delta A(\mathbf{e})$ and $\mathbf{g}_0 + \delta \mathbf{g}(\mathbf{e})$, (3.9) becomes

$$\dot{\mathbf{e}} = (A_0 + \delta A)\mathbf{e} - (\mathbf{g}_0 + \delta g)\mathbf{w}P\mathbf{e} + \phi(\mathbf{e}, t), \tag{3.10}$$

and $\delta A = A(\mathbf{e}) - A_0$, $\delta \mathbf{g} = \mathbf{g}(\mathbf{e}) - \mathbf{g}_0$.

Define a Lyapunov function $V = \mathbf{e}^T P_2 \mathbf{e}$. Differentiating V with respect to t yields

$$
\begin{aligned}
\dot{V} &= \dot{\mathbf{e}}^T P_2 \mathbf{e} + \mathbf{e}^T P_2 \dot{\mathbf{e}} \\
&= [(A_0 + \delta A)\mathbf{e} - (\mathbf{g}_0 + \delta \mathbf{g})\mathbf{w}P_2\mathbf{e} + \phi]^T P_2 \mathbf{x} + \mathbf{e}^T P_2 [(A_0 + \delta A)\mathbf{e} - (\mathbf{g}_0 + \delta \mathbf{g})\mathbf{w}P_2\mathbf{e} + \phi].
\end{aligned}
$$

Next we discuss the determination of feedback gains and stability of the closed loop by classifying $\| \phi \|$ into three scenarios.

<u>Scenario 1.</u> $\|\phi\|$ is of equal or higher order in the state such that $\|\phi\| \to 0$, $\forall t \in \mathbb{R}^+$ as $\|\mathbf{e}\| \to 0$, i.e., ϕ is a vanishing term. Assume ϕ can be expressed as $D(\mathbf{e}, t)\mathbf{e}$, we have

$$\dot{V} = \mathbf{e}^T [(A_0 + \delta A + D - \mathbf{g}_0 \mathbf{w}P_2 - \delta \mathbf{g}\mathbf{w}P_2)^T P_2 + P_2(A_0 + \delta A + D - \mathbf{g}_0 \mathbf{w}P_2 - \delta \mathbf{g}\mathbf{w}P_2)]\mathbf{e}.$$

For $\dot{V} < 0$, we have the following sufficient condition

$$(A_0 + \delta A + D - \mathbf{g}_0 \mathbf{w}P_2 - \delta \mathbf{g}\mathbf{w}P_2)^T P_2 + P_2(A_0 + \delta A + D - \mathbf{g}_0 \mathbf{w}P_2 - \delta \mathbf{g}\mathbf{w}P_2) < 0. \tag{3.11}$$

Pre and post multiplying P_2^{-1}, and define $\bar{P}_2 = P_2^{-1}$, yields

$$\bar{P}_2 A_0{}^T + A_0 \bar{P}_2 - \mathbf{w}^T \mathbf{g}_0{}^T - \mathbf{g}_0 \mathbf{w} - \mathbf{w}^T \delta \mathbf{g}^T - \delta \mathbf{g}\mathbf{w} + \bar{P}_2(\delta A + D)^T + (\delta A + D)\bar{P}_2 < 0. \tag{3.12}$$

Using Young's inequality, we have

$$\bar{P}_2(\delta A + D)^T + (\delta A + D)\bar{P}_2 \le (\delta A + D)(\delta A + D)^T + \bar{P}_2{}^2$$

$$-\mathbf{w}^T \delta \mathbf{g}^T - \delta \mathbf{g}\mathbf{w} \le \delta \mathbf{g}\delta \mathbf{g}^T + W^T W \le \mu_1(\mathbf{e})I + \mathbf{w}^T \mathbf{w}$$

where $\mu_1(\mathbf{e})$ is the singular value of $\delta \mathbf{g}\delta \mathbf{g}^T$.

Define $\mu_2(\mathbf{e})$, $\mu_d(\mathbf{e}, t)$ the singular values of $\delta A \delta A^T$, $D^T D$ and assume μ_d is uniformly bounded

by $\mu_3(\mathbf{e},t)$, we have

$$(\delta A + D)(\delta A + D)^T = \delta A \delta A^T + DD^T + \delta A D^T + D\delta A^T \leq 2(\mu_2 + \mu_3)I$$

As a result, (3.12) becomes

$$\bar{P}_2 A_0{}^T + A_0 \bar{P}_2 - \mathbf{w}^T \mathbf{g}_0{}^T - \mathbf{g}_0 \mathbf{w} + \bar{P}_2{}^2 + (\mu_1 + 2\mu_2 + 2\mu_3)I + \mathbf{w}^T \mathbf{w} < 0. \qquad (3.13)$$

Define $\mu = \mu_1 + 2\mu_2 + 2\mu_3$, and we case the above inequality in LMI form as

$$\begin{cases} \max \mu \\[2mm] \begin{bmatrix} \mu I + \bar{P}_2 A_0{}^T + A_0 \bar{P}_2 - \mathbf{w}^T \mathbf{g}_0{}^T - \mathbf{g}_0 \mathbf{w} & \bar{P}_2 & \mathbf{w}^T \\ \bar{P}_2 & -I & \mathbf{0} \\ \mathbf{w} & \mathbf{0} & -I \end{bmatrix} < 0 \; . \\[2mm] -\bar{P}_2 < 0 \end{cases} \qquad (3.14)$$

The above LMIs can be solved numerically in the following manner. We increase the value of μ from zero in a fixed step, and check whether there is a feasible solution of LMI (4.27). We repeat the task until (4.27) has no solution. The final feasible solution is the optimal feedback gains $\mathbf{k}$.

Solving the above LMIs, we can obtain the optimal feedback gain matrix $\mathbf{k}$ and the positive matrix P_2 concurrently. The matrix P_2 will be used in the following stability analysis. We will find that the matrix P_2 obtained in this way can help us to find a more accurate stability region compared with a P_2 obtained through solving a Lyapunov equation as $A_0{}^T P_2 + P_2 A_0 = -Q$ with an arbitrarily selected positive matrix Q.

Define a domain B_R by $B_R = \{\mathbf{e} \in \mathbb{R}^{2(m+n)} \mid \|\mathbf{e}\|_2 < \alpha\}$ and $\dot{V}(\mathbf{e}) < 0$ in $B_R - \{\mathbf{0}\}$. If the LMI (3.13) stands for $\mathbf{e} \in \mathbb{R}^{2(m+n)}$, the closed loop system is globally asymptotically stable.

Remark 3.1 *If $B_R \neq \mathbb{R}^{2(m+n)}$, the system is locally attractive. In (3.13), μ_1, μ_2 and μ_3 are related with $\mathbf{e}$. With the maximum μ we obtained when solving (4.27), we can explore the region of $\mathbf{e}$ to*

satisfy (3.13), which makes $\dot{V} < 0$. However, it is too conservative. Therefore, we propose the

following numerical method to explore a less conservative B_R. We go back to (3.11), and B_R can

be expanded step by step from $\mathbf{e} = \mathbf{0}$ by checking the eigenvalues of the close-loop system matrix

$(A - \mathbf{gk})^T P_2 + P_2(A - \mathbf{gk}) + P_2{}^2 + \mu_3 I$, *until an eigenvalue becomes non-negative. A trade-off*

between the programming time and accurate of the stability range should be made when we

choose the length of each step.

Remark 3.2 *For different size of ϕ, B_R is different. As ϕ increases, μ_3 increases, hence the*

region B_R becomes smaller.

Remark 3.3 *The region of attraction (ROA) exists and can be estimated [35]. A simple estima-*

tion is provided by the set

$$\Omega_w = \{\mathbf{e} \in \mathbb{R}^{2(m+n)} \mid V(\mathbf{e}) \leq w\} \tag{3.15}$$

when Ω_w is bounded and contained in B_R. The largest set Ω_w that we can determine is by

choosing

$$w < \min_{\|\mathbf{e}\|=\alpha} V(\mathbf{e}) = \lambda_{min}(P_2)\alpha^2$$

The relationship between B_R and ROA is shown in Fig. 3.1 (a).
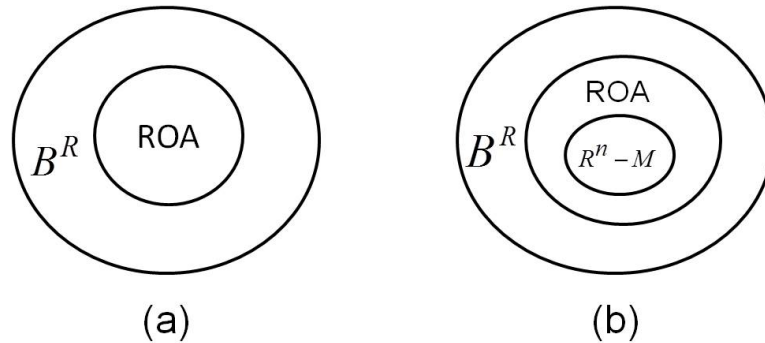
Figure 3.1: Stability Region.

<u>Scenario 2.</u> Assume that $\|\phi\|$ is of lower order in the state such that $\|\phi\|/\|\mathbf{e}\| \to 0$, $\forall t \in \mathbb{R}^+$ as

$\|\mathbf{e}\| \to \infty$ and $\|\phi\|_2$ is uniformly bounded by ϕ_b.

$$\dot{V} = \mathbf{e}^T \{(A_0 + \delta A - \mathbf{g}_0 \mathbf{w} P_2 - \delta \mathbf{g} \mathbf{w} P_2)^T P_2 + P_2 (A_0 + \delta A - \mathbf{g}_0 \mathbf{w} P_2 - \delta \mathbf{g} \mathbf{w} P_2)\} \mathbf{e} + \phi^T P_2 \mathbf{e} + \mathbf{e}^T P_2 \phi.$$

Choose a positive definite matrix $Z = \beta I$ and solve the following LMI

$$(A_0 + \delta A - \mathbf{g}_0 \mathbf{w} P_2 - \delta \mathbf{g} \mathbf{w} P_2)^T P_2 + P_2 (A_0 + \delta A - \mathbf{g}_0 \mathbf{w} P_2 - \delta \mathbf{g} \mathbf{w} P_2) < -Z, \qquad (3.16)$$

we have

$$\dot{V} \leq -\beta \|\mathbf{e}\|_2^2 + 2\lambda_{max}(P_2) \|\mathbf{e}\|_2 \cdot \phi_b. \qquad (3.17)$$

Apply Young's inequality, the LMI problem (3.16) changes into

$$\bar{P}_2 A_0{}^T + A_0 \bar{P}_2 - \mathbf{w}^T \mathbf{g}_0{}^T - \mathbf{g}_0 \mathbf{w} + \bar{P}_2{}^2 + (\mu_1 + \mu_2 + \beta) I + \mathbf{w}^T \mathbf{w} < 0$$

Further, check the conservative Lyapunov stable region B_R using the similar method as we discussed for scenario 1. B_R can be expanded step by step from states $\mathbf{e} = \mathbf{0}$ by checking the eigenvalues of the close-loop system matrix $(A - \mathbf{g}\mathbf{k})^T P_2 + P_2(A - \mathbf{g}\mathbf{k}) + Z$, until an eigenvalue becomes non-negative. The region of attraction Ω_w can also be estimated as (3.15). Denoting

$$M = \left\{ \mathbf{e} \in \mathbb{R}^{2(m+n)} \ \middle| \ \|\mathbf{e}\|_2 > \frac{\beta}{2\lambda_{max}(P_2)\phi_b} \right\},$$

We have that $\dot{V} < 0$ at the region $\{M \cap B_R\}$.

In this scenario, the closed-loop system may not be asymptotically stable or attractive at the origin because $\dot{V} > 0$ may happen in a neighborhood around the origin. Nevertheless, if B_R is $\mathbb{R}^{2(m+n)}$, the closed-loop system is globally uniformly ultimately bounded in the region $\{\mathbb{R}^{2(m+n)} - M\}$. If B_R is a bounded region, and $\{\mathbb{R}^{2(m+n)} - M\}$ is a subset of Ω_w, any state originating in Ω_w will be bounded. B_R, ROA and $\{\mathbb{R}^{2(m+n)} - M\}$ are described in Fig. 3.1 (b).

Scenario 3. In general, $\|\phi\|$ may not belong to any of the above cases but be their combinations. For instance, $\|\phi\| \leq c_1 + c_2 \|\mathbf{e}\| + c_3 \|\mathbf{e}\|^2$. In such circumstances, we can express the equal and

higher order part as $D\mathbf{e}$. The robust stability can be established through the method introduced in the scenario 2, while the LMI (3.16) should take D into consideration as is done in (3.11).

3.4   Numerical Validations

Simulations were conducted to verify the effectiveness of the proposed control scheme. For simulation, f_r is modeled as a combination of viscous friction and Coulomb friction, that is, $f_r = f_v \dot{x} + f_c sgn(\dot{x})$. Similarly, τ_f is modeled as $\tau_f = \tau_v \dot{\theta} + \tau_c sgn(\dot{\theta})$. Both frictions are vanishing terms and assumed to be unknown. Setpoint control of the wheel position is considered, and the pre-planned trajectory is as (2.14).

3.4.1   Linear Controller for System Without Uncertainties

First, the 2WMR system is considered in absence of uncertainties, i.e., $f_r = 0$, $\tau_f = 0$ and all the system parameters are known.

Case 1. In this case, we consider that the 2WMR travels on a flat surface, i.e., $\varphi = 0$. Initial states for the 2WMR system are $\mathbf{x} = [0,\ 0,\ 0.1,\ 0]^T$. LQR method is used to design the feedback gains. Choose $\{q_1,\ q_2,\ q_3,\ q_4\} = \{50,\ 0.1,\ 500,\ 1\}$, $R = 0.8$. We obtain the feedback gains as $\mathbf{k} = [-7.9057,\ -10.7948,\ -29.9739,\ -3.1183]$. The simulation results are shown in Fig. 3.2. The wheel reaches the desired setpoint smoothly with a small overshoot, the pendulum angular stays around zero.

Case 2. In this case, the 2WMR traveling on an inclined surface is considered. The slope angle is known as $\varphi = \pi/15$ rad. Initial states for the 2WMR system are $\mathbf{x} = [0,\ 0,\ 0.1,\ 0]^T$. Refer to (2.15), the reference position for the pendulum is $\theta_r = 0.2547$ rad. Feedback gains for the linear controller, $\mathbf{k} = [-7.9057,\ -10.9223,\ -29.9289,\ -3.1491]$, are obtained based on LQR method, where Q and R are chosen the same as in Case 1. The simulation results are shown in Fig. 3.3. The wheel reaches the desired setpoint smoothly with a small overshoot, while the
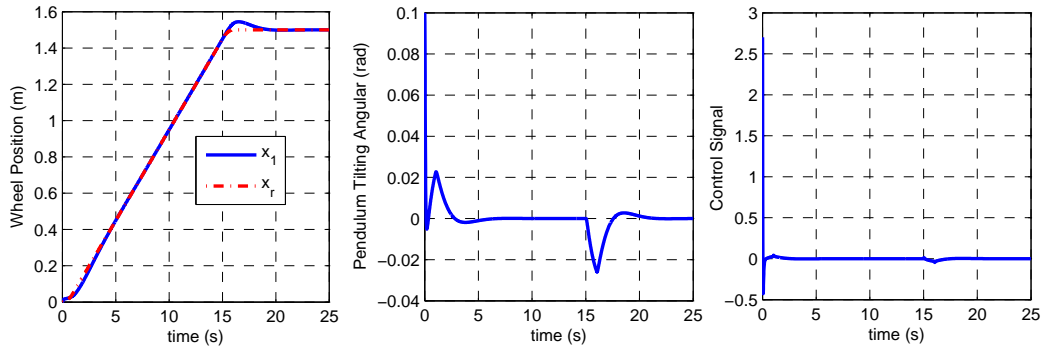
Figure 3.2: Case 1: time responses of x, θ and u under LQR based linear control. The 2WMR travels on a flat surface and the system is in absence of any uncertainties.

pendulum is balanced at the new equilibrium point $\theta_e = \theta_r = 0.2547$ rad. It is also observed that the control input is a positive constant when the 2WMR finally balances at the desired position. The simulation results are consistent with the theoretical analysis in Subsection 2.4.
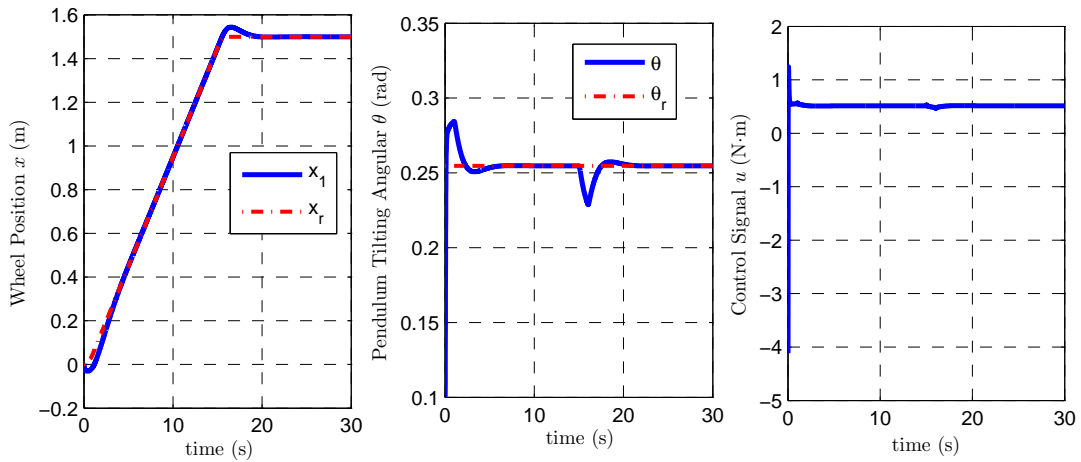
Figure 3.3: Case 2: time responses of x, θ and u under LQR based linear control. The 2WMR travels on an inclined surface with known slope angle $\varphi = \pi/15$ and the system is in absence of any uncertainties.

Case 3. In this case, we consider that the 2WMR travels on a flat surface, i.e., $\varphi = 0$. The LMI method is used to obtain the feedback gains for the linear controller. Numerical method is applied to solve the LMIs (4.27). μ is increased from 0 with step equals 0.005 until no feasible solution for (4.27). The maximum μ is 0.42 and the corresponding feedback gains are
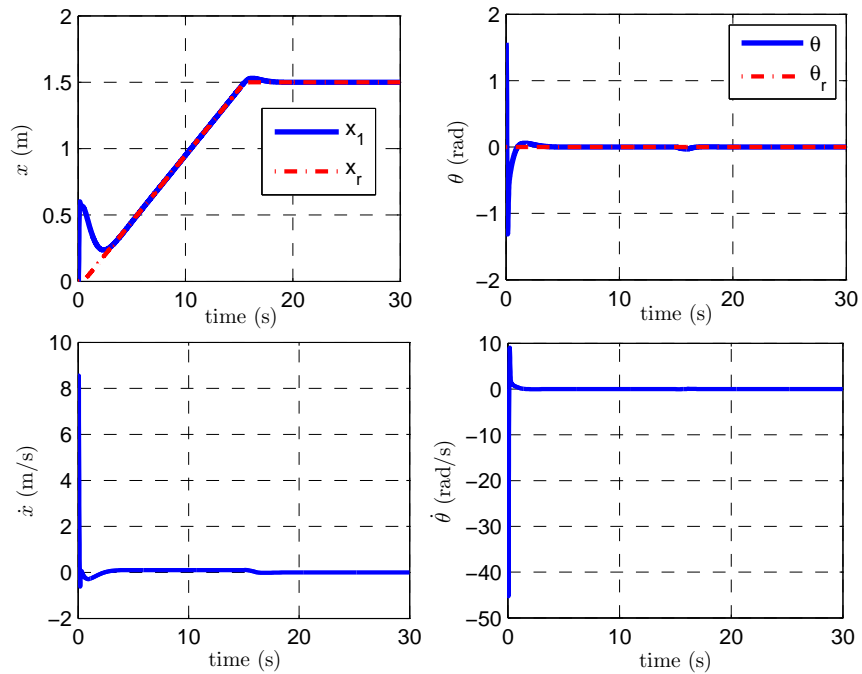
Figure 3.4: Case 3: time responses of x, $\dot{x}$, θ and $\dot{\theta}$ under LMI based linear control. The 2WMR travels on a flat surface and the system is in absence of any uncertainties.
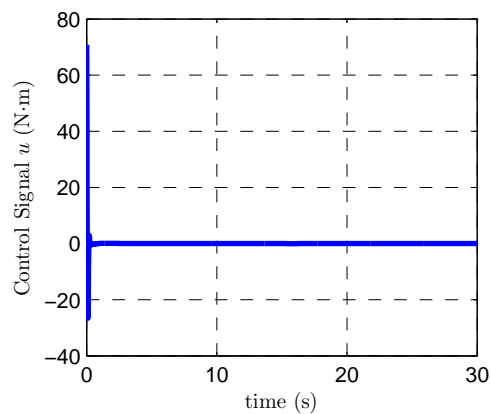
Figure 3.5: Case 3: time responses of u under LMI based linear control. The 2WMR travels on a flat surface and the system is in absence of any uncertainties.

$\mathbf{k} = 10^3 \times [-0.9416, \ -1.0350, \ -1.6971, \ -0.1804]$, which are quite large. Instead we choose

a more suitable solution as $\mathbf{k} = [-22.1976, \ -25.4919, \ -45.0711, \ -5.4233]$, at $\mu = 0.37$, and

the corresponding solution for P_2 is as

$$P_2 = \begin{bmatrix} 21.7333 & 23.0408 & 37.0954 & 4.1368 \\ 23.0408 & 26.1911 & 42.4524 & 4.7148 \\ 37.0954 & 42.4524 & 72.2187 & 7.7847 \\ 4.1368 & 4.7148 & 7.7847 & 0.8886 \end{bmatrix}.$$

By applying the obtained P_2 and $\mathbf{k}$ and using the proposed method introduced in Remark 3.1,

a conservative region of B_R is obtained as $B_R = \{|e_3| < 1.48\}$. By simulations, we find that the

actual working range is even larger. Fig. 3.4 shows the responses of the 2WMR and Fig. 3.5

shows the control profile. The initial states of the 2WMR are $\mathbf{x} = [0, \ 0, \ \pi/2, \ 0]^T$. The pendulum

is stabilized at the upright position within 5 seconds and the 2WMR finally reaches the desired

setpoint. During the time interval $t = 0 \sim 3$ s, the control priority is given to achieve the swing

up of the pendulum. It is noted that a large initial control signal is generated and the speed of

the wheels goes up to 8.5582 m/s. However, these responses are unlikely to appear in practice

because the capacity of the actuator is physically limited.

3.4.2 Linear Controller for System With Uncertainties

Case 4. In this case, we consider the 2WMR system in presence of the joint friction τ_f. The

LMI based linear controller is applied to control the 2WMR and the feedback gains are chosen

the same as in Case 3. As we have stated in Remark 3.2, the system stability region is related

with the size of ϕ. As the frictions increase, the system response could become unsatisfactory.

Fig. 3.6 shows the responses of the 2WMR when the joint friction is $\tau_f = 0.04\dot{\theta} + 0.06sgn(\dot{\theta})$.

For a clear observation, the tracking error of the wheel position e_1 instead of x_1 is plotted in the

first graph of Fig. 3.6. We can see that the pendulum can still be stabilized at the upright position

and the tracking error of the wheel position converges to zero finally.

Next, a larger joint friction, $\tau_f = 0.2\dot{\theta} + 0.3sgn(\dot{\theta})$, is considered existing in the system, and the simulation results are shown in Fig. 3.7. It is found that the pendulum and the wheel keep vibrating around the desired positions, which are not satisfactory responses and indicates the limited robustness of the linear controller.
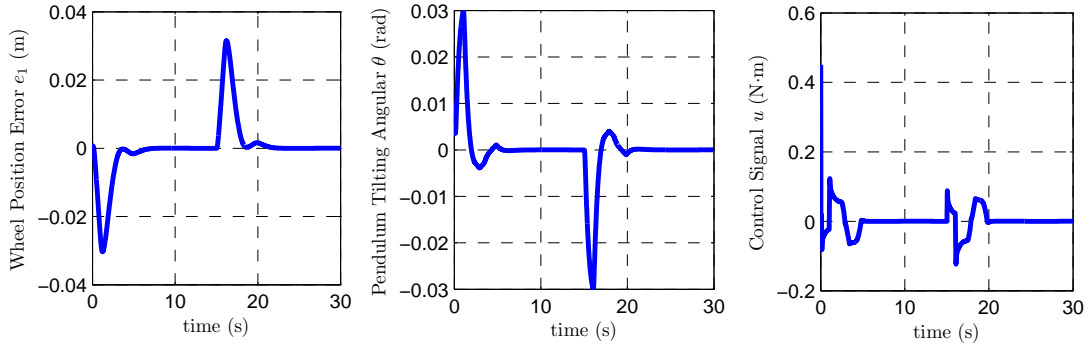
Figure 3.6: Case 4: time responses of e_1, θ and u under LMI based linear control. In simulations, system is considered in presence of the joint friction $\tau_f = 0.04\dot{\theta} + 0.06sgn(\dot{\theta})$.
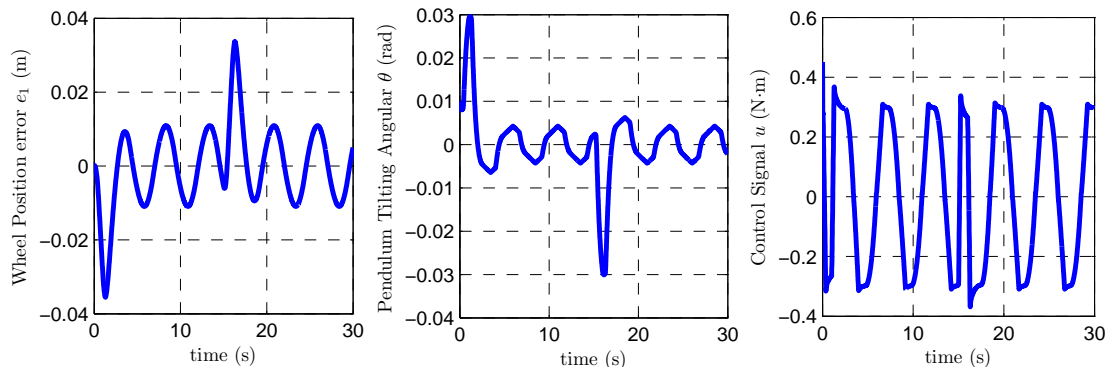
Figure 3.7: Case 4: time responses of e_1, θ and u under LMI based linear control. In simulations, system is considered in presence of the joint friction $\tau_f = 0.2\dot{\theta} + 0.3sgn(\dot{\theta})$.

Case 5. In this case, we consider the 2WMR system in presence of the ground friction f_r. The feedback gains for the linear controller are the same as in Case 4. Simulation results are shown in Fig. 3.8 and Fig. 3.9. The tracking error of the wheel position converges to zero at $t = 20$ s and the pendulum is balanced at the upright position. At the time interval $5 \sim 15$ s , the 2WMR reaches a steady state that the 2WMR travels with the constant speed 0.1 m/s, the

pendulum is balanced at $\theta = 0.0125$ rad and the tracking error of the wheel position exists. In Case 1, the system is in absence of frictions. When the 2WMR travels with a constant speed, the equilibrium position of the pendulum is $\theta = 0$ and the tracking error of the wheel position is zero.

The results obtained in Case 5 are consistent with the analysis in Section 2.3.2. When $f_r \neq 0$, the equilibrium of the pendulum is not the upright position, but related with the size of the ground friction. $\tau_s = r f_r$ is provided to overcome the effect of the ground friction. Since the ground friction is unknown to the designer, $\theta_r = 0$ is used in the controller design, which yields $e_3 = \theta - \theta_r \neq 0$ and $e_1 = (\tau_s - k_3 e_3)/k_1 \neq 0$. Although the ground friction brings a tracking error of the wheel position during the traveling, the system performance is still satisfactory. When the 2WMR stops at the desired setpoint at $t = 20$ s, the ground friction disappears, so does the tracking error of the wheel position.
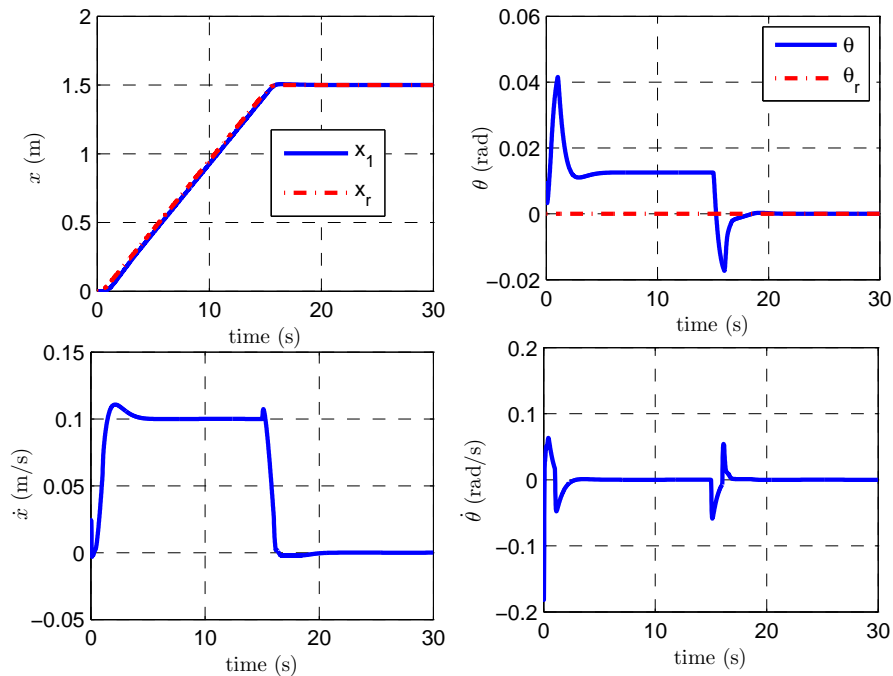
Figure 3.8: Case 5: time responses of x, $\dot{x}$, θ and $\dot{\theta}$ under LMI based linear control. In simulations, system is considered in presence of the ground friction $f_r = 0.2\dot{x} + 0.3 sgn(\dot{x})$.
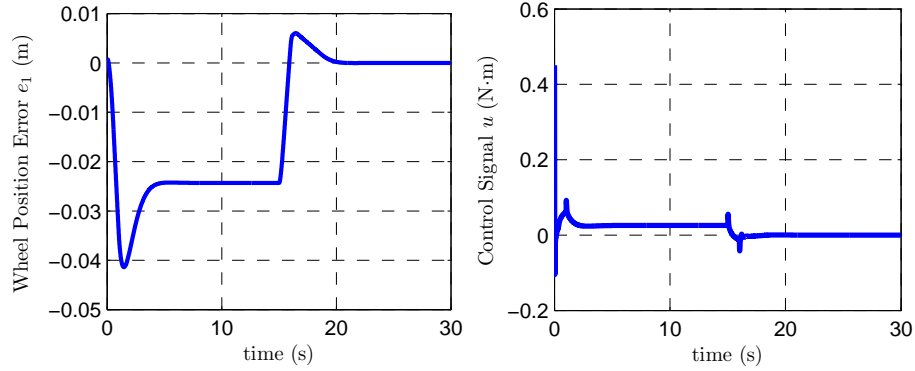
Figure 3.9: Case 5: time responses e_1 and u under LMI based linear control. In simulations, system is considered in presence of the ground friction $f_r = 0.2\dot{x} + 0.3sgn(\dot{x})$.

3.5   Implementation and Experiment Results

In simulations, an ideal model of the 2WMR is used and the control input is assumed to be unlimited. To stabilize the 2WMR system, the feedback gains can be chosen in a wide range as long as $A_0 - \mathbf{g}_0\mathbf{k}$ is Hurwitz, and the linear controller with higher gains provides better robustness. However, considering the existence of mismatch between the real-time system model and the mathematical model (2.1)(2.2), the feedback gains obtained from simulations may not function well on the real-time platform, thus need to be adjusted through experimental testings on the 2WMR prototype. For implementation, we consider a simple regulation task that is to balance the robot at the original position on a flat surface, i.e., $x_r = 0$, $v_r = 0$, and $\varphi = 0$.

By applying the linear controller with the feedback gains obtained from simulations, strong vibrations are observed, which can be explained as the following. For systems having backlash in the driving mechanism, large feedback gains could easily incur vibrations [68]. In our 2WMR system, the backlash is produced by the gearbox. To reduce or avoid vibrations, feedback gains for the velocity terms, k_2 and k_4, should be minimized [68]. From experimental testing, we observe that the system vibration reduces significantly as k_2 and k_4 decrease. It is also found that large feedback gains are necessarily needed for the position terms, including the tracking

error of the wheel position and the pendulum angle. If k_3 is too small, the pendulum could easily

fall down because the torque generated by the motor is not enough to overcome the effect of the

gravity. If k_1 is too small, the position control of the wheels fails that a steady state error exists

in the wheel position response.
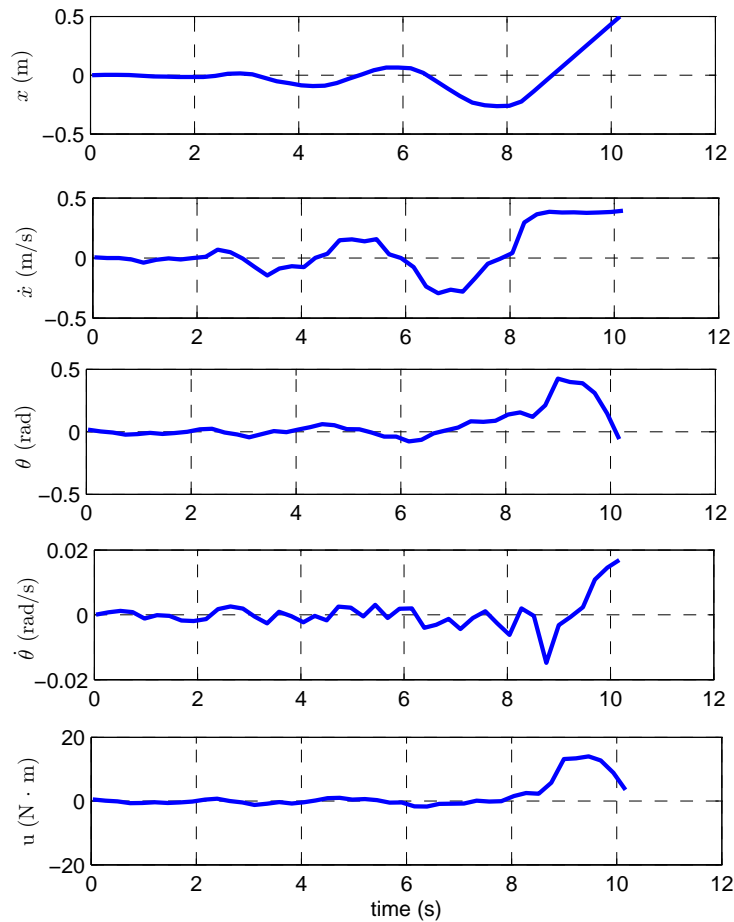
Figure 3.10: Experimental testing results for regulation task: time responses of x, $\dot{x}$, θ, $\dot{\theta}$ and u under the linear controller with feedback gains as $\mathbf{k} = [-10, \ -0.5, \ -35, \ -1.5]$. The 2WMR is placed on a flat surface.

Fig. 3.10 shows the experimental results for 2WMR system under the linear controller with

feedback gain as $\mathbf{k} = [-10, \ -0.5, \ -35, \ -1.5]$, it can be seen that the 2WMR is stabilized at

the first few seconds, however, becomes unstable in 10 seconds. From the response of the wheel

velocity $\dot{x}$, it is observed that the maximum speed that the wheels can achieve is around 0.4 m/s.
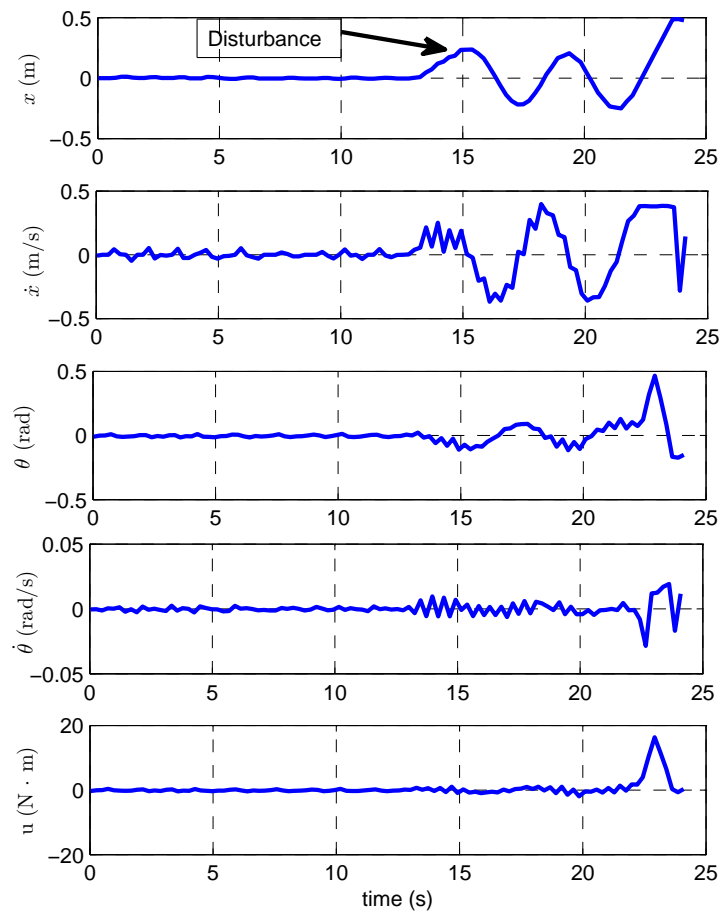
Figure 3.11: Experimental testing results for regulation task: time responses of x, $\dot{x}$, θ, $\dot{\theta}$ and u under the linear controller with feedback gains as $\mathbf{k} = [-20, \ -1.0, \ -70, \ -3]$. The 2WMR is placed on a flat surface.

To achieve a better performance, larger feedback gains $\mathbf{k} = [-20, \; -1, \; -70, \; -3]$ are used. Each feedback gain is twice as that used in the preceding testing. The experiment results are shown in Fig. 3.11. Compared with the results in the preceding testing, the responses of the 2WMR are improved. In the time interval $0 \sim 15$ s, the 2WMR can be consistently stabilized around the initial position. At $t = 15$ s, we push the 2WMR to the right about 0.22 m away from the origin, which can be considered as a disturbance to the system. After that, the system becomes unstable. It can be seen that the linear controller provides limited robustness to the exceptional disturbance, even when high gains are applied.

Next, balancing of the 2WMR on an inclined surface is considered. First, the control law in (3.2) is applied with $\theta_r = 0$ and $\tau_s = 0$. The experiment results are shown in Fig. 3.12 and Fig. 3.13. At the beginning, due to the effect of gravity, the 2WMR moves down along the slope. In about 25 seconds, the 2WMR is stabilized at $x = 0.4$ m. The pendulum balance position is $\theta_e = 0.135$ rad. From Fig. 3.13, it can be seen that after the 2WMR reaches a steady state, the average value of the control signal is positive.

To eliminate the steady state errors, $\theta_r = \theta_e = 0.135$ rad and $\tau_s = m_p l g \sin \theta_e = 0.2746$ N·m is applied. The results are shown in Fig. 3.14 and Fig. 3.15. The pendulum is initially placed around the equilibrium position. The 2WMR slightly moves down along the slope and finally is stabilized around the original position. The pendulum balances around $\theta_e = 0.135$ rad.

Images of the stabilized 2WMR are shown in Fig. 3.16, we can see that the pendulum balances at the upright position when it is placed on the flat surface but tilts rightward a bit when it is balanced on the inclined surface. The experiment results are consistent with the theoretical analysis in section 2.3.2.
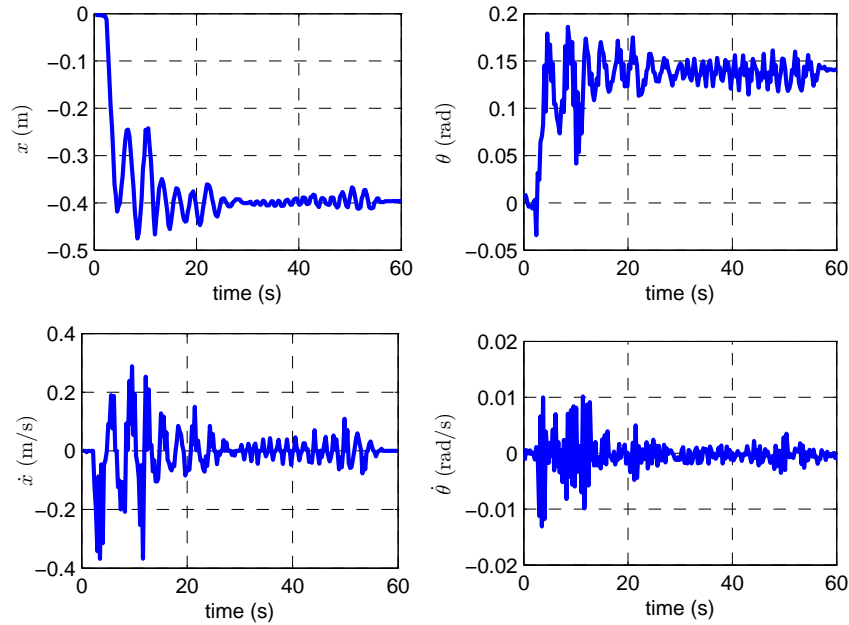
Figure 3.12: Experimental testing results for regulation task: time responses of x, $\dot{x}$, θ and $\dot{\theta}$ under the linear controller (3.2) with $\tau_s = 0$, $\theta_r = 0$ and the feedback gains as $\mathbf{k} = [-20, \; -1.0, \; -70, \; -3]^T$. The 2WMR is placed on an inclined surface.
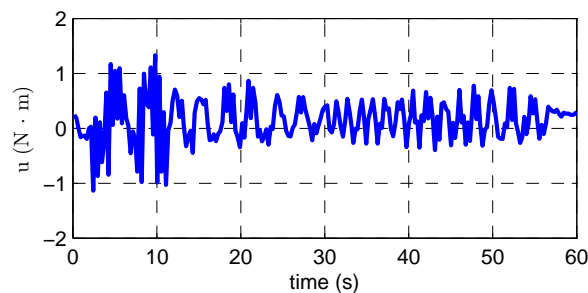
Figure 3.13: Experimental testing results for regulation task: time responses of u under the linear controller (3.2) with $\tau_s = 0$, $\theta_r = 0$ and the feedback gains as $\mathbf{k} = [-20, \; -1.0, \; -70, \; -3]$. The 2WMR is placed on an inclined surface.
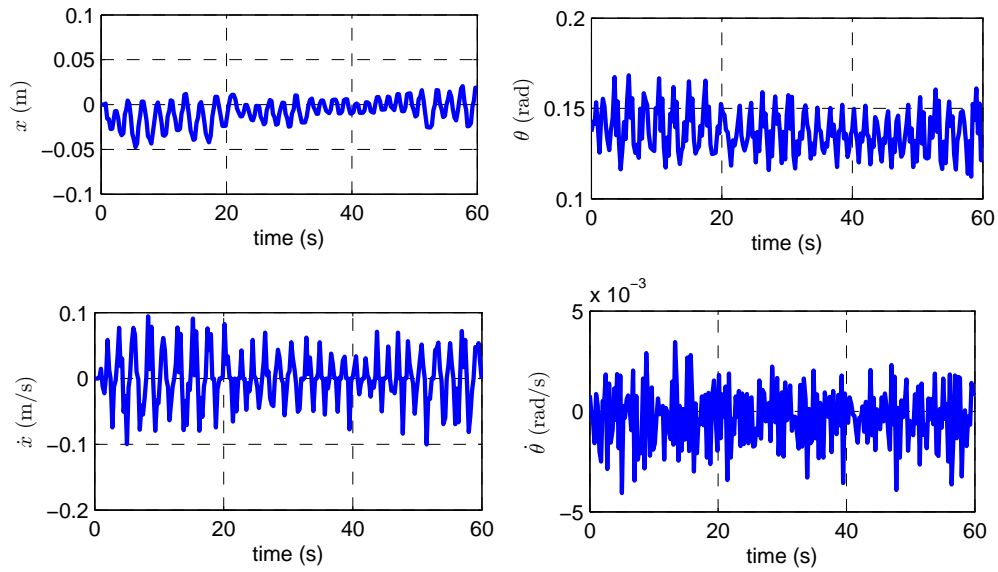
Figure 3.14: Experimental testing results for regulation task: time responses of x, $\dot{x}$, θ and $\dot{\theta}$ under the linear controller (3.2) with $\tau_s = 0.135$, $\theta_r = 0.2746$ and feedback gains as $\mathbf{k} = [-20, \ -1.0, \ -70, \ -3]$. The 2WMR is placed on an inclined surface.
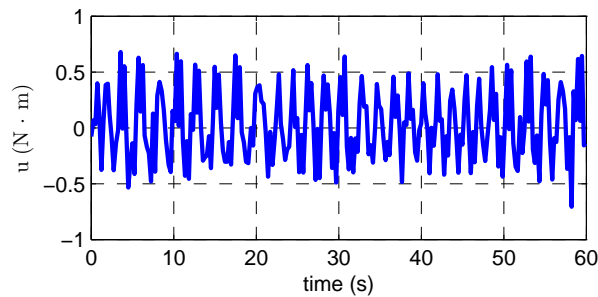
Figure 3.15: Experimental testing results for regulation task: time responses of u under the linear controller with (3.2) with $\tau_s = 0.135$, $\theta_r = 0.2746$ and feedback gains as $\mathbf{k} = [-20, \ -1.0, \ -70, \ -3]$. The 2WMR is placed on an inclined surface.
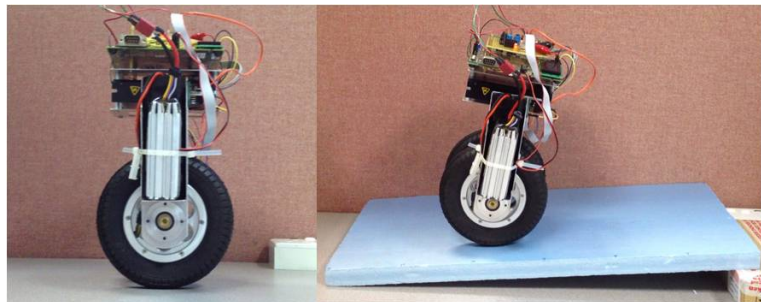
Figure 3.16: Images for regulation tasks. The 2WMR balanced on the flat and the inclined surface.

3.6   Conclusion and Discussion

The linear controller shows effectiveness in stabilizing the 2WMR. However, the robustness is limited. Differences between the simulation based validation and experiment based validation are observed. These discrepancies between the simulated and actual performance can be high-lighted by following main factors which have not been considered in the simulations: (i) effects of discretization; (ii) dynamic model of the actuator system; (iii) presence of noises in the sensor signals; (iii) existence of the gear backlash.

Chapter 4

A Sliding Mode Controller with Linear Sliding Surface

4.1 Introduction

SMC is a well known robust control approach for system in presence of model uncertainties and has been studied for control of wheeled inverted pendulum and similar underactuated mechanical systems [3, 29, 36, 48, 49, 57, 61, 81]. SMC utilizes a discontinuous control law to drive system state trajectory into a designer specified sliding surface and to maintain the system state trajectory on this surface for all the subsequent time. In standard SMC design for full actuated system, it is straightforward to conclude the convergence of the system states when system is in the sliding mode. However, for underactuated system, the standard SMC design and stability analysis are not applicable because the system has fewer inputs than the independent variables to be controlled. As a result, a nonlinear sliding manifold or in general an internal dynamic must be stabilized by proper selection of the sliding surface coefficients.

In this chapter, an SMC along with a linear sliding surface is proposed for control of the 2WMR system. The linear sliding surface is constructed by combining the two states of the wheel and two states of the pendulum in a linear form [3, 29, 48, 49], which brings four coeffi-

cients associated with the four states. The SMC law is derived by using Lyapunov theory, which guarantees the finite reaching time of the sliding surface and leads to a sliding manifold with all the matched uncertainties rejected. In the sliding mode, the sliding motion is determined by the four coefficients, however, in a complex and highly nonlinear form. Therefore, it is difficult to directly choose or tune the coefficients to achieve the desired sliding motion. To simplify the sliding surface design, the sliding manifold is linearized around the desired equilibrium point of the pendulum. Through a mathematical transformation, it is shown that the linearized sliding manifold is equivalent to a normal linear system that is under a full state linear feedback control with the freedom in choosing feedback gains. Now the sliding surface design becomes a nominal linear controller design, which is simple, systematic, and furthermore provides one extra degree of freedom in control. In this work, this degree of freedom is utilized to implement optimal or robust linear control techniques. Two alternative methods are adopted for the nominal linear controller design. One is based on LQR method, which leads to a stable sliding manifold that also exhibits optimality in terms of fast tracking convergence and low control cost. The other is based on LMI method and the resulting sliding manifold exhibits robustness with respecting to various unmatched uncertainties.

The main contributions of this chapter are summarized as follows.

(i) An SMC is proposed to control an underactuated 2WMR system in the presence of both matched and unmatched uncertainties. The proposed control methods and the obtained results can be extended to general underactuated systems with or without input coupling;

(ii) To avoid the difficulty in directly choosing the sliding surface coefficients, a new sliding surface design method is proposed. The sliding surface design is transformed into a nominal linear control design, which is simple, systematic and furthermore provides one extra degree of freedom in control. By utilizing the extra degree of freedom, various linear control techniques

can be incorporated in the SMC design. The resulting sliding manifold exhibits desirable prop-

erties besides stability, such as optimality and robustness. The existing works on SMC design

for underactuated systems only focused on the stabilization of the sliding manifold.

The remainder of this chapter is organized as follows. In Section 4.2, the design of an SMC

with a linear sliding surface is detailed. In Section 4.3, the sliding surface design is discussed. In

Section 4.4, simulation based case studies are presented. Section 4.5 presents the implementation

of the proposed SMC on the 2WMR platform. Conclusions are drawn in Section 4.6.

4.2 Sliding Mode Controller Design

4.2.1 SMC Design for System with Unmodeled Frictions

Recall the error dynamic model of the 2WMR in (2.12),

$$\dot{\mathbf{e}} = \eta(\mathbf{e}) + \mathbf{g}(\mathbf{e})[u + d_m(\mathbf{e},t)] + \mathbf{d}_u(\mathbf{e},t), \tag{4.1}$$

where η is the system nonlinear term, d_m is the lumped matched uncertainties, $\mathbf{d}_u$ is the lumped

unmatched uncertainties.

The following linear sliding surface is proposed

$$\sigma = \mathbf{c}\mathbf{e} = 0 \tag{4.2}$$

where $\mathbf{c}$ is a constant row vector, and $\mathbf{c}\mathbf{g}$ is uniformly invertible.

The SMC law is

$$u = -\frac{\mathbf{c}\eta + \rho\, sgn(\sigma)}{\mathbf{c}\mathbf{g}} \tag{4.3}$$

where $sgn(\cdot)$ is a signum function and

$$\rho = \rho_m + \rho_u + \rho_0, \tag{4.4}$$

with $\rho_m \geq |\mathbf{c}\mathbf{g}d_m|$, $\rho_u \geq |\mathbf{c}\mathbf{d}_u|$, and ρ_0 is a positive constant.

Theorem 4.1 *Under the SMC law (4.3), the 2WMR system can reach the defined sliding surface (4.2) in a finite time and maintain on it afterwards. In the sliding mode, the matched uncertainties will be completely nullified. Furthermore, we have the freedom to choose the vector **c** to stabilize the sliding manifold and meanwhile achieve other desirable properties.*

Proof : The derivative of σ is as

$$\dot{\sigma} = \mathbf{c}\dot{\mathbf{e}} = \mathbf{c}\eta + \mathbf{c}\mathbf{g}(u + d_m) + \mathbf{c}\mathbf{d}_u. \tag{4.5}$$

A quadratic Lyapunov function candidate is chosen as

$$V_1 = \frac{1}{2}\sigma^2. \tag{4.6}$$

Differentiating V_1 with respect to time t yields

$$\begin{aligned} \dot{V}_1 &= \sigma\dot{\sigma} \\ &= \sigma\left[\mathbf{c}\eta + \mathbf{c}\mathbf{g}(u + d_m) + \mathbf{c}\mathbf{d}_u\right]. \end{aligned} \tag{4.7}$$

Substituting the control law (4.3) into (4.7), we have

$$\begin{aligned} \dot{V}_1 &= \sigma\left[-\rho\, sgn(\sigma) - \mathbf{c}\mathbf{g}d_m - \mathbf{c}\mathbf{d}_u\right] \\ &\leq -\rho_0|\sigma| < 0, \end{aligned}$$

which implies a finite reaching time to the sliding surface, $\sigma = 0$, and the reaching time can be calculated as $t_{reach} \leq |\sigma(0)|/\rho_0$.

We can see that, under the same ρ_0, the reaching time t_{reach} reduces as $|\sigma(0)|$ decreases. As we stated in Section 2, the absolute values of the initial e_1 and e_2 are zero by applying the planned trajectory (2.13)(2.14), which yields a small $|\sigma(0)|$. Therefore, the sliding surface can be reached in a fairly short time.

After reaching the sliding surface, the system is in sliding mode and $\sigma = 0$, $\dot{\sigma} = 0$. Accordingly the equivalent control is derived from $\dot{\sigma} = 0$, as

$$u_{eq}(t) = -\frac{\mathbf{c}\eta}{\mathbf{cg}} - d_m - \frac{\mathbf{cd}_u}{\mathbf{cg}}$$

Define $\mathbf{e}_d = [e_{1,d},\ e_{2,d},\ e_{3,d},\ e_{4,d}]^T$ as the state vector in the sliding mode, and substitute the above $\mathbf{u}_{eq}(t)$ into (4.1), one obtains the sliding manifold as

$$\dot{\mathbf{e}}_d = \eta(\mathbf{e}_d) + \mathbf{g}(\mathbf{e}_d)(-\frac{\mathbf{c}\eta}{\mathbf{cg}}) + \mathbf{d}_{eq} \tag{4.8}$$

where

$$\mathbf{d}_{eq} = \left(I - \frac{\mathbf{gc}}{\mathbf{cg}}\right)\mathbf{d}_u. \tag{4.9}$$

In the sliding manifold, the matched uncertainty d_m is completely nullified. Furthermore, we have the freedom to choose the vector $\mathbf{c}$ to stabilize the sliding manifold and meanwhile achieve other desirable properties, such as robustness, optimality, etc.   Q.E.D.

4.2.2   SMC Design for System with Parameter Variations

From the practical point of view, the load of the pendulum m_p and slope angle of the traveling surface φ are most likely to vary. The system dynamic model with parameter uncertainties is expressed as:

$$\dot{\mathbf{e}} = \eta(\mathbf{e}) + \Delta\eta(\mathbf{e},\mathbf{p}) + [\mathbf{g}(\mathbf{e}) + \Delta\mathbf{g}(\mathbf{e},\mathbf{p})](d_m + u) + \mathbf{d}_u(\mathbf{e},t), \tag{4.10}$$

where η and $\mathbf{g}$ are known nominal parts, $\mathbf{p}$ represents the uncertain parameters, $\Delta\eta$ and $\Delta\mathbf{g}$ are uncertain parts. Define constants $m_{p,0}$, φ_0 the estimation values of m_p and φ, respectively. The known parts are $\eta = \eta(\mathbf{e},m_{p,0},\varphi_0)$ and $\mathbf{g} = \mathbf{g}(\mathbf{e},m_{p,0},\varphi_0)$, respectively. The unknown parts are $\Delta\eta = \eta(\mathbf{e},m_p,\varphi) - \eta(\mathbf{e},m_{p,0},\varphi_0)$ and $\Delta\mathbf{g} = \mathbf{g}(\mathbf{e},m_p,\varphi) - \mathbf{g}(\mathbf{e},m_{p,0},\varphi_0)$, respectively.

The SMC in (4.3) is applied with the following switching gain

$$\rho = \frac{1}{\varepsilon_b}(\rho_m + \rho_u + \rho_0), \tag{4.11}$$

where

$$\rho_m \geq |\mathbf{c}(\mathbf{g}+\Delta\mathbf{g})d_m|, \quad \rho_u \geq |\mathbf{c}\mathbf{d}_u| + |\mathbf{c}\Delta\eta| + \left|\frac{\mathbf{c}\Delta\mathbf{g}\mathbf{c}\eta}{\mathbf{c}\mathbf{g}}\right|, \quad \text{and} \quad \rho_0 > 0.$$

Theorem 4.2 *For system with parameter uncertainties, under the SMC law (4.3) with the switching gain (4.11), the 2WMR system can reach the sliding surface (4.2) in a finite time and maintain on it afterwards, under the condition $|\mathbf{c}\Delta\mathbf{g}(\mathbf{c}\mathbf{g})^{-1}| < 1 - \varepsilon_b$ ($\varepsilon_b > 0$). In the sliding mode, the desirable properties stated in* **Theorem 4.1** *also hold.*

Proof : Differentiating the sliding surface (4.2) with respect to time using (4.10) one obtains

$$\dot{\sigma}(t) = \mathbf{c}\dot{\mathbf{e}} = \mathbf{c}(\eta + \Delta\eta) + \mathbf{c}(\mathbf{g}+\Delta\mathbf{g})(u+d_m) + \mathbf{c}\mathbf{d}_u. \tag{4.12}$$

Substituting the SMC law (4.3) into the above we have

$$\begin{aligned}
\dot{\sigma}(t) &= \mathbf{c}(\eta+\Delta\eta) + \mathbf{c}(\mathbf{g}+\Delta\mathbf{g})\left[-\frac{\mathbf{c}\eta+\rho sgn(\sigma)}{\mathbf{c}\mathbf{g}}+d_m\right]+\mathbf{c}\mathbf{d}_u \\
&= -\rho sgn(\sigma) - \frac{\mathbf{c}\Delta\mathbf{g}}{\mathbf{c}\mathbf{g}}\rho sgn(\sigma) + \mathbf{c}(\mathbf{g}+\Delta\mathbf{g})d_m + \mathbf{c}(\mathbf{d}_u+\Delta\eta) - \frac{\mathbf{c}\Delta\mathbf{g}}{\mathbf{c}\mathbf{g}}\mathbf{c}\eta.
\end{aligned}$$

Differentiating the non-negative quadratic function in (4.6) with respect to time t yields

$$\begin{aligned}
\dot{V}_1 &= \sigma\dot{\sigma} \\
&= \sigma\left[-\rho sgn(\sigma) - \frac{\mathbf{c}\Delta\mathbf{g}}{\mathbf{c}\mathbf{g}}\rho sgn(\sigma) + \mathbf{c}(\mathbf{g}+\Delta\mathbf{g})d_m + \mathbf{c}(\mathbf{d}_u+\Delta\eta) - \frac{\mathbf{c}\Delta\mathbf{g}}{\mathbf{c}\mathbf{g}}\mathbf{c}\eta\right] \\
&\leq -\rho|\sigma| + \rho|\sigma|\cdot\left|\frac{\mathbf{c}\Delta\mathbf{g}}{\mathbf{c}\mathbf{g}}\right| + |\sigma\mathbf{c}(\mathbf{g}+\Delta\mathbf{g})d_m| + |\sigma\mathbf{c}\mathbf{d}_u| + |\sigma\mathbf{c}\Delta\eta| + \left|\frac{\mathbf{c}\Delta\mathbf{g}}{\mathbf{c}\mathbf{g}}\mathbf{c}\eta\sigma\right| \\
&= -|\sigma|\left(\rho - \left|\frac{\mathbf{c}\Delta\mathbf{g}}{\mathbf{c}\mathbf{g}}\right|\rho - |\mathbf{c}(\mathbf{g}+\Delta\mathbf{g})d_m| - |\mathbf{c}\mathbf{d}_u| - |\mathbf{c}\Delta\eta| - \left|\frac{\mathbf{c}\Delta\mathbf{g}}{\mathbf{c}\mathbf{g}}\mathbf{c}\eta\right|\right) \\
&\leq -|\sigma|\left(\varepsilon_b\rho - |\mathbf{c}(\mathbf{g}+\Delta\mathbf{g})d_m| - |\mathbf{c}\mathbf{d}_u| - |\mathbf{c}\Delta\eta| - \left|\frac{\mathbf{c}\Delta\mathbf{g}}{\mathbf{c}\mathbf{g}}\mathbf{c}\eta\right|\right).
\end{aligned}$$

Substituting the switching gain in (4.11) to the above inequality, we have

$$\dot{V}_1 \leq -\rho_0|\sigma| < 0.$$

Similarly, we conclude that the sliding surface can be reached in a finite time as $t_{reach} \leq |\sigma(0)|/\rho_0$.

In the sliding mode, the equivalent control is derived from $\dot{\sigma} = 0$, which is

$$u_{eq}(t) = -\frac{\mathbf{c}(\eta + \Delta\eta)}{\mathbf{c}(\mathbf{g} + \Delta\mathbf{g})} - d_m - \frac{\mathbf{c}d_u}{\mathbf{c}(\mathbf{g} + \Delta\mathbf{g})}.$$

Substituting the above $u_{eq}(t)$ into (4.10), one obtains the sliding manifold as (4.8) with

$$\mathbf{d}_{eq} = \left[I - \frac{(\mathbf{g} + \Delta\mathbf{g})\mathbf{c}}{\mathbf{c}(\mathbf{g} + \Delta\mathbf{g})} \right] \left(\mathbf{d}_u + \Delta\eta_u + \mathbf{g}\frac{\mathbf{c}\eta}{\mathbf{c}\mathbf{g}} \right). \tag{4.13}$$

In the sliding manifold, the matched uncertainty d_m is completely nullified. Sliding motion is

determined by the vector $\mathbf{c}$.   Q.E.D.

4.3   Sliding Surface Design

Under the proposed SMC in (4.3), the 2WMR system can reach the switching surface in a

finite time. When the system is in sliding mode, from (4.8), we can see that the sliding motion

is directly determined by the vector $\mathbf{c}$. In [29, 48, 49], the stabilization of the sliding manifold

is achieved by choosing the switching surface coefficients according to several established con-

straints. However, since the vector $\mathbf{c}$ affects the system performance in a complicated manner, it

is hard to predict the system responses from the information of $\mathbf{c}$, which is the main drawback of

the existing sliding surface designs. Another major drawback or difficulty in the sliding surface

design is the non-affine structure of the sliding manifold in the coefficients $\mathbf{c}$, as shown in (4.8).

To avoid the drawbacks, in this work, the sliding surface coefficients are determined indirectly,

by transforming the coefficients determination problem into a nominal linear controller design.

Hence the sliding surface design becomes simple, systematic, and furthermore provides one ex-

tra degree of freedom in control. Feedback gains for the nominal controller can be determined

through various systematic linear control design methods, which makes the system responses

predictable. In the transformation, relations are established between the sliding surface coeffi-

cients and the feedback gains. With the obtained feedback gains, the sliding surface coefficients

can be determined.

4.3.1 Problem Transformation

We linearize the sliding manifold (4.8) around the desired equilibrium point by assuming

$e_{3,d} \approx 0$, $\sin e_{3,d} \approx e_{3,d}$ and $e_{4,d}^2 \approx 0$. The obtained linearized sliding manifold is

$$\dot{\mathbf{e}}_d = \underbrace{\begin{bmatrix} 0 & 1 & 0 & 0 \\ 0 & 0 & a_{23} & 0 \\ 0 & 0 & 0 & 1 \\ 0 & 0 & a_{43} & 0 \end{bmatrix}}_{A} \mathbf{e}_d + \underbrace{\begin{bmatrix} 0 \\ g_{1,0} \\ 0 \\ g_{2,0} \end{bmatrix}}_{\mathbf{g}_0} u_0 + \underbrace{\left(I - \frac{\mathbf{g}_0 \mathbf{c}}{\mathbf{c}\mathbf{g}_0} \right) \mathbf{d}_u}_{\mathbf{d}_{eq,0}}, \tag{4.14}$$

with

$$a_{23} = -\frac{b_0 m_p l g \cos \theta_r}{ac - b_0^2},$$

$$a_{43} = \frac{a m_p l g \cos \theta_r}{ac - b_0^2},$$

$$g_{1,0} = \frac{c}{r(ac - b_0^2)} + \frac{b_0}{ac - b_0^2},$$

$$g_{2,0} = \frac{-b_0}{r(ac - b_0^2)} - \frac{a}{ac - b_0^2},$$

$$b_0 = m_p l \cos(\varphi + \theta_r),$$

and the system control input is as

$$u_0 = -\frac{c_1}{c_2 g_{1,0} + c_4 g_{2,0}} e_{2,d} - \frac{c_2 a_{23} + c_4 a_{43}}{c_2 g_{1,0} + c_4 g_{2,0}} e_{3,d} - \frac{c_3}{c_2 g_{1,0} + c_4 g_{2,0}} e_{4,d}. \tag{4.15}$$

When the 2WMR system is in the sliding mode, we have $\sigma = c_1 e_{1,d} + c_2 e_{2,d} + c_3 e_{3,d} + c_4 e_{4,d} = 0$,

thus,

$$e_{1,d} = -\frac{c_2}{c_1} e_{2,d} - \frac{c_3}{c_1} e_{3,d} - \frac{c_4}{c_1} e_{4,d}. \tag{4.16}$$

Let

$$\frac{c_1}{c_2 g_{1,0} + c_4 g_{2,0}} = k_2 - \frac{k_1}{c_1} c_2, \qquad (4.17)$$

$$\frac{c_2 a_{23} + c_4 a_{43}}{c_2 g_{1,0} + c_4 g_{2,0}} = k_3 - \frac{k_1}{c_1} c_3, \qquad (4.18)$$

$$\frac{c_3}{c_2 g_{1,0} + c_4 g_{2,0}} = k_4 - \frac{k_1}{c_1} c_4, \qquad (4.19)$$

the system control input (4.15) can be rewritten as

$$
\begin{aligned}
u_0 &= -(k_2 - \frac{k_1}{c_1} c_2) e_{2,d} - (k_3 - \frac{k_1}{c_1} c_3) e_{3,d} - (k_4 - \frac{k_1}{c_1} c_4) e_{4,d} \\
&= k_1 (\frac{c_2}{c_1} e_{2,d} + \frac{c_3}{c_1} e_{3,d} + \frac{c_4}{c_1} e_{4,d}) - k_2 e_{2,d} - k_3 e_{3,d} - k_4 e_{4,d} \\
&= -k_1 e_{1,d} - k_2 e_{2,d} - k_3 e_{3,d} - k_4 e_{4,d}. \qquad (4.20)
\end{aligned}
$$

To stabilize the nominal linear system, i.e., the linearized sliding manifold (4.14), various linear controller design methods could be applied to obtain the feedback gains $\mathbf{k} = [k_1, \ k_2, \ k_3, \ k_4]$, and $c_1 \sim c_4$ can be solved from relations (4.17)$\sim$(4.19).

Remark 4.1 *The four coefficients $c_1 \sim c_4$ are constrained by three equations (4.17)$\sim$(4.19), therefore there are innumerable solutions of $\mathbf{c}$ for a given $\mathbf{k}$. However, from (4.17)$\sim$(4.19), it can be concluded that the ratios between $c_1 \sim c_4$ are fixed. In this work, we choose c_1 be the free parameter, then $c_2 \sim c_4$ can be decided from (4.17)$\sim$(4.19) once c_1 is set.*

4.3.2   Nominal Linear Controller Design

Two alternative linear control design methods are introduced in this work.

When the 2WMR travels in a safe environment, a LQR based optimal linear controller is adopted to achieve an stable and optimal sliding manifold. The optimal control gain is as

$$\mathbf{k} = R^{-1} \mathbf{g}_0^T P_1,$$

where P_1 is the solution of the following Riccati equation

$$P_1 A + A^T P_1 - P_1 \mathbf{g}_0 R^{-1} \mathbf{g}_0^T P_1 + Q = 0.$$

where Q is the weight matrix for the error states $\mathbf{e}$ and R is the weighting factor for the control input. The details of the LQR based optimal design has been discussed in Section 3.3, thus is omitted here.

When the 2WMR travels in a severe environment with various uncertainties, robustness of the system is the main concern, thus a LMI based robust design is employed to address unmatched uncertainties.

Let $\mathbf{k} = \mathbf{w}P$, we have $u_0 = -\mathbf{w}P\mathbf{e}$. The nominal linear system (4.14) becomes

$$\dot{\mathbf{e}}_d = A\mathbf{e}_d - \mathbf{g}_0\mathbf{w}P\mathbf{e}_d + \mathbf{d}_{eq,0}. \tag{4.21}$$

Define a Lyapunov function $V_2 = \mathbf{e}_d^T P \mathbf{e}_d$, differentiating V_2 with respect to t yields

$$\begin{aligned} \dot{V}_2 &= \dot{\mathbf{e}}_d^T P \mathbf{e}_d + \mathbf{e}_d^T P \dot{\mathbf{e}}_d \\ &= (A\mathbf{e}_d - \mathbf{g}_0\mathbf{w}P\mathbf{e}_d + \mathbf{d}_{eq,0})^T P \mathbf{e}_d + \mathbf{e}_d^T P \{A\mathbf{e}_d - \mathbf{g}_0\mathbf{w}P\mathbf{e}_d + \mathbf{d}_{eq,0}\} \qquad (4.22) \\ &= \mathbf{e}_d^T [(A - \mathbf{g}_0\mathbf{w}P)^T P + P(A - \mathbf{g}_0\mathbf{w}P)]\mathbf{e}_d + \mathbf{d}_{eq,0}^T P \mathbf{e}_d + \mathbf{e}_d^T P \mathbf{d}_{eq,0}. \qquad (4.23) \end{aligned}$$

For $\mathbf{d}_{eq,0} = 0$, to make $\dot{V}_2 < 0$, we have the following sufficient condition

$$(A - \mathbf{g}_0\mathbf{w}P)^T P + P(A - \mathbf{g}_0\mathbf{w}P) + \mu I < 0, \tag{4.24}$$

with $\mu \geq 0$.

Assume the unmatched uncertainties $\mathbf{d}_{eq,0}$ is bounded by $\beta_1\|e_d\| + \beta_2$ with $(\beta_1, \beta_2 > 0)$, we have

$$\mathbf{d}_{eq,0}^T P \mathbf{e}_d + \mathbf{e}_d^T P \mathbf{d}_{eq,0} \leq 2\lambda_{max}(P)(\beta_1\|\mathbf{e}_d\|_2^2 + \beta_2\|\mathbf{e}_d\|_2), \tag{4.25}$$

thus

$$\dot{V}_2 < -\mu\|\mathbf{e}_d\|_2^2 + 2\lambda_{max}(P)(\beta_1\|\mathbf{e}_d\|_2^2 + \beta_2\|\mathbf{e}_d\|_2).$$

For system with only vanishing unmatched uncertainties, i.e., $\beta_1 \neq 0$ and $\beta_2 = 0$, we have $\dot{V} < 0$ if $\beta_1 < \mu/2\lambda_{max}(P)$. It can be concluded that the desired equilibrium $\mathbf{e}_d = \mathbf{0}$ is locally asymptotically stable. For system with both vanishing and non-vanishing unmatched uncertainties, i.e.,

$\beta_1 \neq 0$ and $\beta_2 \neq 0$, we have $\dot{V}_2$ is negative outside the set $\left\{ \|\mathbf{e}_d\| \leq 2\beta_2\lambda_{max}(P) / [\mu - 2\beta_1\lambda_{max}(P)] \right\}$,

under the condition that $\beta_1 < \mu / 2\lambda_{max}(P)$. We can conclude that $\|\mathbf{e}_d\|$ is ultimately bounded by

$$\|\mathbf{e}_d\| \leq \frac{2\beta_2\lambda_{max}(P)}{\mu - 2\beta_1\lambda_{max}(P)} = \frac{\beta_2}{\dfrac{\mu}{2\lambda_{max}(P)} - \beta_1}.$$

Based on the above analysis, we seek for solutions of $\mathbf{w}$ and P which can maximize $\mu / 2\lambda_{max}(P)$

such that the system could be robust against unmatched uncertainties, meanwhile the ultimate

bound of $\|\mathbf{e}_d\|$ can be minimized.

Pre and post multiplying (4.24) by P^{-1}, and letting $\bar{P} = P^{-1}$, we have

$$\bar{P}A^T + A\bar{P} - \mathbf{w}^T\mathbf{g}_0{}^T - \mathbf{g}_0\mathbf{w} + \mu\bar{P}^2 < 0, \tag{4.26}$$

which can be casted in the LMI form as

$$\begin{cases} \max \dfrac{\mu}{2\lambda_{max}(P)} \\[2em] \begin{bmatrix} \bar{P}A^T + A\bar{P} - \mathbf{w}^T\mathbf{g}_0{}^T - \mathbf{g}_0\mathbf{w} & \sqrt{\mu}\bar{P} \\ \sqrt{\mu}\bar{P} & -I \end{bmatrix} < 0 \\[2em] -\bar{P} < 0 \end{cases} \tag{4.27}$$

The above LMIs can be solved numerically.

4.4   Numerical Validations and Discussions

For simulation, f_r is modeled as $f_r = f_v\dot{x} + f_c sgn(\dot{x})$, where $f_v = 0.2$ and $f_c = 0.3$. τ_f is

modeled as $\tau_f = \tau_v\dot{\theta} + \tau_c sgn(\dot{\theta})$, where $\tau_v = 0.2$ and $\tau_c = 0.3$. Both frictions are vanishing

terms and assumed to be unknown. From the dynamic equation (2.12), it is evident that τ_f is the

matched uncertainty to the control input while f_r is the unmatched uncertainty. Initial states for

the 2WMR system are $\mathbf{x} = [0, 0, 0.1, 0]^T$.

Case 1. In this case, a linear controller based on LQR method, is applied to the 2WMR

system with and without the joint friction τ_f. The 2WMR travels on a flat surface. Choose
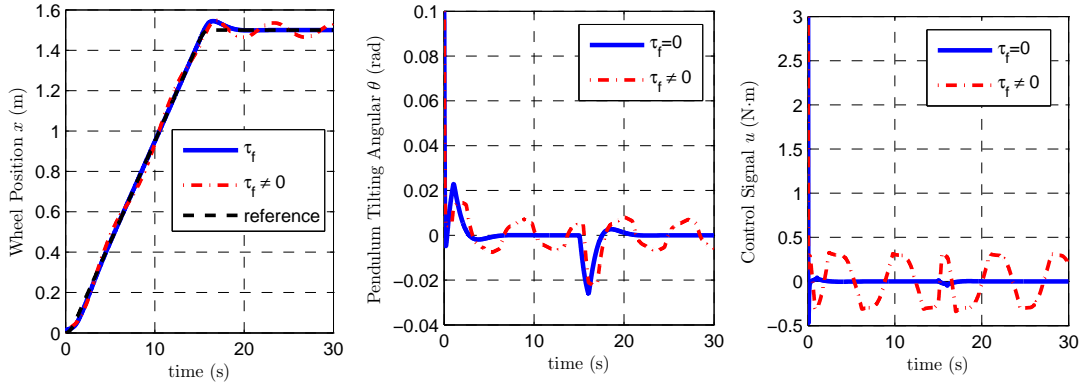
Figure 4.1: Case 1: time responses of x, θ and u under linear controller based on LQR. The 2WMR travels on a flat surface. System with and without the joint friction τ_f are considered.

$\{q_1, q_2, q_3, q_4\} = \{50, 0.1, 500, 1\}$, $R = 0.8$. We obtain the feedback gains as $\mathbf{k} = [-7.9057, -10.7948, -29.9739, -3.1183]$. The results are shown in Fig. 4.1. For the 2WMR system without the joint friction, the LQR based linear controller shows effectiveness that the wheel reaches the desired setpoint smoothly with a small overshoot, and the pendulum angle stays around zero. However, the LQR based linear controller can not function well when the joint friction exists in the 2WMR system. The pendulum and the wheel keep vibrating around the desired positions, which are not satisfactory responses.

Case 2. In this case, we consider only the joint friction τ_f exists in the 2WMR system, which is a matched uncertainty. The 2WMR travels on a flat surface. SMC is applied with parameters designed as the following. Refer to (2.15), the reference position for the pendulum is $\theta_r = 0$ since $\varphi = 0$, the switching gain is $\rho = 0.1 + |\mathbf{cg}|(0.3 + 0.2|x_4|)$. Feedback gains for the nominal controller u_0 are obtained based on LQR method.

(a). To compare the 2WMR responses under the SMC and the LQR based linear controller, the weighting matrices Q and R are chosen the same as in Case 1. The feedback gains are obtained as $\mathbf{k} = [-7.9057, -10.7948, -29.9739, -3.1183]$. Set $c_1 = 1$, solving (4.17)$\sim$(4.19) yields $[c_2, c_3, c_4] = [1.330530, 3.454665, 0.2738175]$. The results are shown in Fig. 4.2. The

2WMR reaches the desired setpoint smoothly and stays still afterwards, the pendulum is balanced at $\theta_e = 0$ and the control signal shows switching behavior. The sliding surface is reached at $t = 0.87\,s$, which is a fairly short time.

Comparing the results in Case 2 (a) with the results in Case 1 when $\tau_f = 0$, the performances are almost the same in terms of tracking error profiles and control profiles. However, in Case 1 the control system is directly designed by LQR, whereas in Case 2 (a), the control system is first designed by SMC in order to eliminate the effect caused by the matched uncertainty, and then the sliding surface is designed by LQR for the sliding manifold. Thus our new SMC approach achieves both robust and optimal properties.
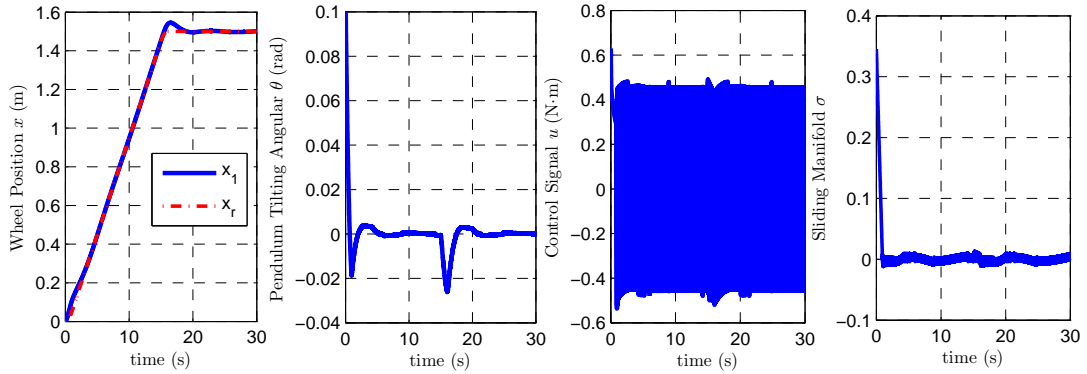
Figure 4.2: Case 2 (a): time responses of x, θ, u and σ under SMC. The 2WMR travels on a flat surface. Only matched uncertainty, the joint friction $\tau_f = 0.2\dot{\theta} + 0.3sgn(\dot{\theta})$, exists in the system. $R = 0.8$ is used in SMC design.

(b). To illustrate our discussion in *Section* 4 that the selection of the weighting matrices directly affects the system performance, we select the weighting matrix Q to be the same as in *Case* 2 (*a*), while the weighting factor for the control input to be $R = 0.08$, which is smaller than the one used in Case 2 (a). The obtained feedback gains are $\mathbf{k} = [-25.0000,\ -33.7972,\ -90.3320,\ -8.6977]$, which are larger than in Case 2 (a). Let $c_1 = 1$, solving (4.17)~(4.19) yields $[c_2,\ c_3,\ c_4] = [1.307674,\ 3.338392,\ 0.200306]$. The results are shown in Fig. 4.3. The 2WMR is stabilized and reached the desired setpoint. We can see the switching amplitude of the control
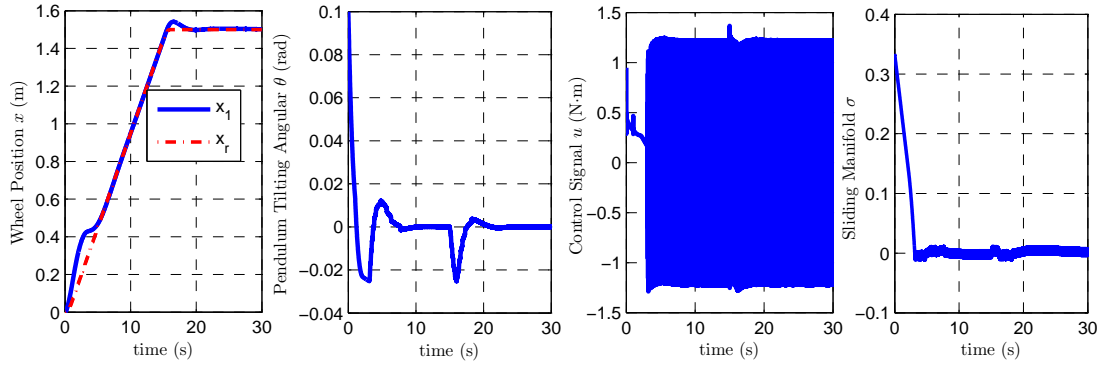
Figure 4.3: Case 2 (b): time responses of x, θ, u and σ under SMC. The 2WMR travels on a flat surface. Only matched uncertainty, the joint friction $\tau_f = 0.2\dot{\theta} + 0.3sgn(\dot{\theta})$, exists in the system. $R = 0.08$ is used in SMC design.

signal in Case 2 (b) is much larger than the one in Case 2 (a), which is due to the higher feedback gains used for the nominal linear controller in Case 2 (b). The results are consistent with the discussions in *Section* 4.

It is noticeable that the vector **c** used in Case 2 (b) is quite close to the one in Case 2 (a). In other words, a minor change of the vector **c** might lead to large changes in the system responses and the changes are unpredictable, which indicates the difficulty in tuning the vector **c** directly to achieve desired responses and shows the drawback of the the existing sliding surface designs. With our proposed design method, the sliding surface coefficients are determined indirectly. The sliding manifold is determined by the feedback gains of the nominal linear controller, which can be tuned in a systematic way. For instance, in the LQR design, we can choose more of control penalty in the weighting factor for the control input, so as to prevent overlarge control signals. The advantage of our proposed method is immediately obvious.

<u>Case 3.</u> In this case, we consider both frictions, τ_f and f_r, exist in the 2WMR system, i.e., the system is in the presence of both matched and unmatched uncertainties. The 2WMR travels on a flat surface. SMC is applied with $\rho = 0.1 + |\mathbf{cg}|(0.3 + 0.2|x_4|) + |(-cc_2 + bc_4)/(ac - b^2)| \cdot (0.3 + 0.2|x_2|)$, and all other parameters the same as in Case 2. The results are shown in Fig. 4.4. The

2WMR reaches the desired setpoint and the pendulum is finally balanced at the upright position, i.e., $\theta_e = 0$, which indicates that the proposed SMC is also robust to unmatched uncertainties.
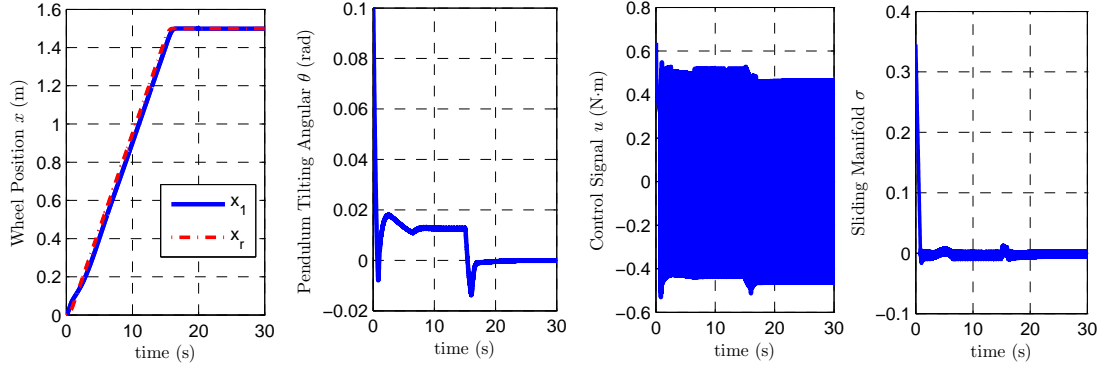
Figure 4.4: Case 3: time responses of x, θ, u and σ under SMC. The 2WMR travels on a flat surface. Both matched uncertainty, the joint friction $\tau_f = 0.2\dot{\theta} + 0.3sgn(\dot{\theta})$, and unmatched uncertainty, the ground friction $f_r = 0.2\dot{x} + 0.3sgn(\dot{x})$, exist in the system.
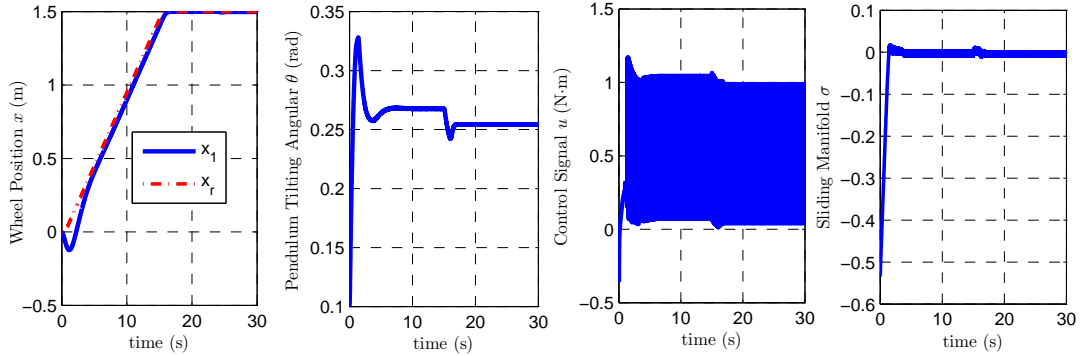
Figure 4.5: Case 4: time responses of x, θ, u and σ under SMC. The 2WMR travels on an inclined surface with known slope angle $\varphi = \pi/15$. Both matched uncertainty, the joint friction $\tau_f = 0.2\dot{\theta} + 0.3sgn(\dot{\theta})$, and unmatched uncertainty, the ground friction $f_r = 0.2\dot{x} + 0.3sgn(\dot{x})$, exist in the system.

Case 4. In this case, the 2WMR traveling on an inclined surface is considered. The slope angle is known as $\varphi = \pi/15$ rad. Both frictions τ_f and f_r exist in the system. SMC is applied with parameters designed as the following. Refer to (2.15), the reference position for the pendulum is $\theta_r = 0.2547$ rad. Feedback gains $\mathbf{k} = [-7.9057, \ -10.7535, \ -30.0154, \ -3.1275]$ for the nominal controller u_0 are obtained based on LQR method, where

Q and R are chosen the same as in Case 1. Next, let $c_1 = 1$, solving (4.17)$\sim$(4.19) yields

$[c_2, c_3, c_4] = [1.327784, 3.470293, 0.283022]$. The switching gain is the same as in Case 3.

The results are shown in Fig. 4.5, the unicycle reaches the desired setpoint, while the pendu-

lum is balanced at the new equilibrium point $\theta_e = \theta_r = 0.2547$ rad. The simulation results are

consistent with the theoretical analysis in Subsection 2.4.
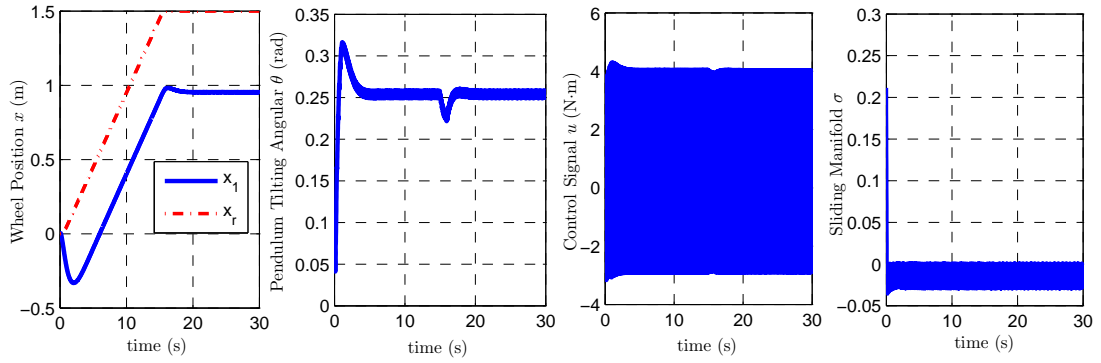
Figure 4.6: Case 5: time responses of x, θ, u and σ under SMC. The 2WMR travels on an inclined surface with unknown slope angle. Both matched uncertainty, the joint friction $\tau_f = 0.2\dot{\theta} + 0.3sgn(\dot{\theta})$, and unmatched uncertainty, the ground friction $f_r = 0.2\dot{x} + 0.3sgn(\dot{x})$ exist in the system.

Case 5. In this case, the 2WMR travels on the same surface as in Case 4. However, the s-

lope angle is assumed to be unknown to the designer, thus $\varphi_0 = 0$ and $\theta_r = 0$ are used in the

controller design. Both frictions τ_f and f_r exist in the system. SMC is applied. Feedback

gains $\mathbf{k} = [-7.4802, -11.2445, -26.9865, -5.5473]$ for the nominal controller u_0 are ob-

tained based on LMI method. Next, let $c_1 = 1$, solving (4.17)$\sim$(4.19) yields $[c_2, c_3, c_4] =$

$[1.241766, 2.113164, 0.1890710]$. The results are shown in Fig. 4.6. The pendulum is bal-

anced at the new balanced position θ_e, which is around $\theta = 0.2547$ rad, thus steady state error

for e_3 exist as $e_{3,s} = \theta_e - \theta_r \neq 0$. From $\sigma = \mathbf{c}e = 0$, steady-state error for e_1 also exist as

$e_{1,s} = -c_3 e_{3,s}/c_1 = -0.5382$ m, which meets the simulation results. Comparing the results in

Case 4 and Case 5, we can see the necessity of adjusting the reference position of pendulum

when the 2WMR travels on an inclined surface. θ_r cannot be computed according to (2.15) if system parameters involved are unknown. When task repeats, we obtain $\theta_r = \theta_e$, which can be incorporated in the controller design to eliminate steady-state errors.

4.5 Implementation and Experiment Results

4.5.1 Regulation Task

For implementation, we start with the regulation control of the 2WMR. The robot is placed on a flat surface. SMC is applied. The sliding surface coefficients are chosen according to the results obtained in simulations, as $\mathbf{c} = 0.25 \times [1, \ 1.33, \ 3.45, \ 0.27]$. However, strong vibrations are observed in the system responses. As we explained in the previous chapter, the vibration is mainly due to the existence of backlash. To reduce the vibration, the feedback gains for the velocity terms should be reduced. After adjustment, satisfactory results are obtained and the experiment results are shown in Fig. 4.7 and Fig. 4.8. By applying the SMC, the 2WMR stays around the original place and the pendulum is balanced around $\theta = 0$. The value of the defined sliding surface σ keeps around zero.
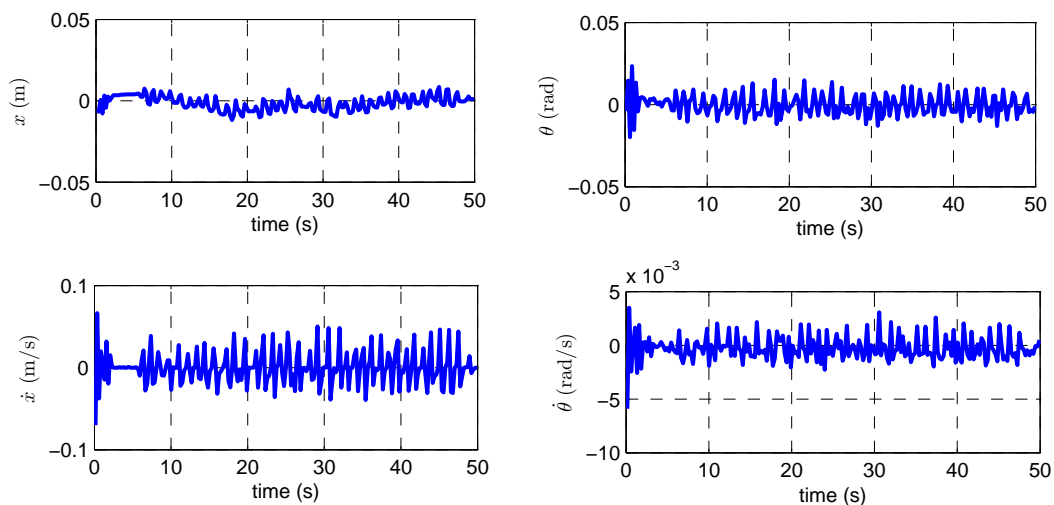
Figure 4.7: Experimental testing results for regulation task: time responses of x, θ, $\dot{x}$ and $\dot{\theta}$ under SMC. The 2WMR is placed on flat surface.
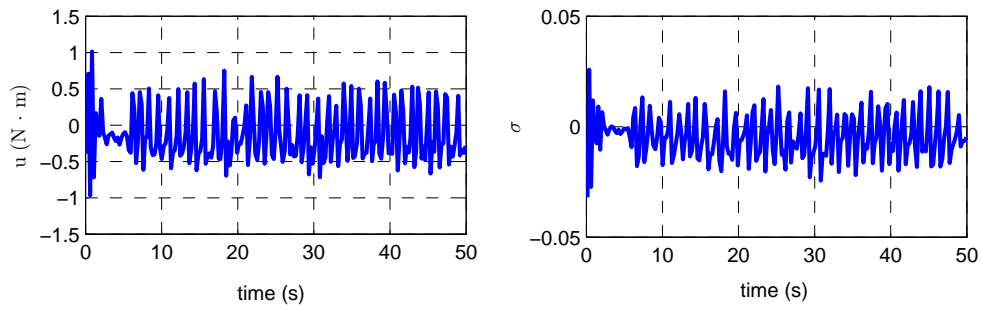
Figure 4.8: Experimental testing results for regulation task: time responses of u and σ under SMC. The 2WMR is placed on flat surface.
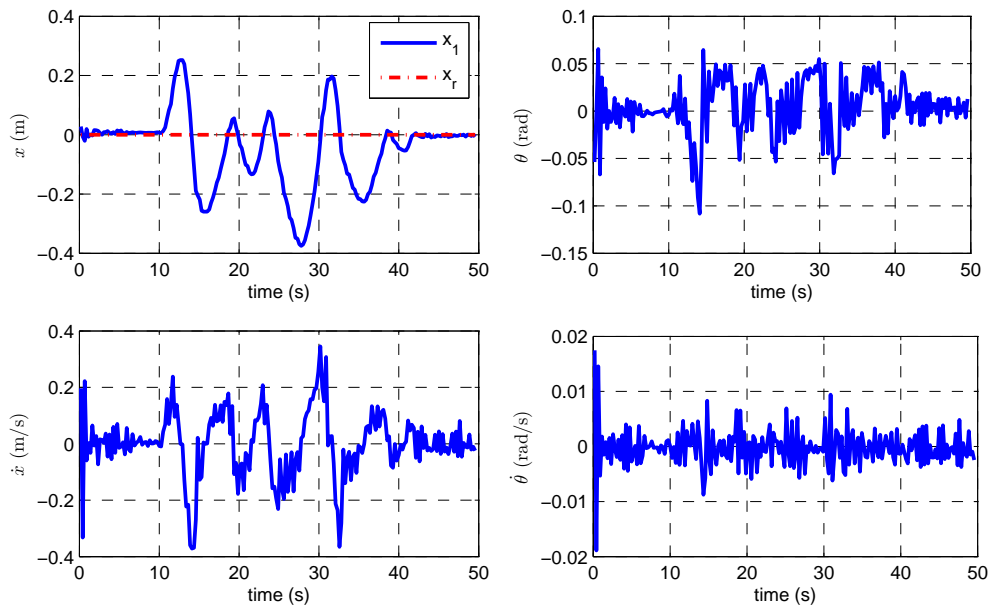
Figure 4.9: Experimental testing results for regulation task: time responses of x, θ, $\dot{x}$ and $\dot{\theta}$ under SMC. The 2WMR is placed on flat surface. A disturbance is added to the system at $t = 10$ s.

Similarly as we did in the previous chapter, a testing is conducted to check the robustness of the SMC. As shown in Fig. 4.9, we push the 2WMR to the right about 0.22 m at $t = 10$ s, which can be considered as an exceptional disturbance to the system. We can see that the 2WMR is finally stabilized at the initial position even a disturbance is added to the system, which indicates that SMC provides a better robustness than the linear controller. However, the transient response is still not satisfactory that the response of the wheel position shows oscillation and the settling

time is around 30 seconds. The reason is that when the exceptional disturbance is added to the

system, the system no long stays on the sliding surface. In such a situation, the system responses

are hardly predictable or even may become unstable.

4.5.2   Reaching a Setpoint

We consider the mobile robot travels on a flat surface, i.e., $\varphi = 0$. The reference trajectory

for the 2WMR is the same as in simulations. SMC is applied and the sliding surface coefficients

are chosen the same as for the regulation task. Experiment results are shown in Fig. 4.10 and

Fig. 4.11. The 2WMR reached the desired setpoint $x = 1.5$ m and stays there afterwards. The

pendulum is stabilized around the upright position. SMC shows effectiveness for setpoint control

of the 2WMR system.
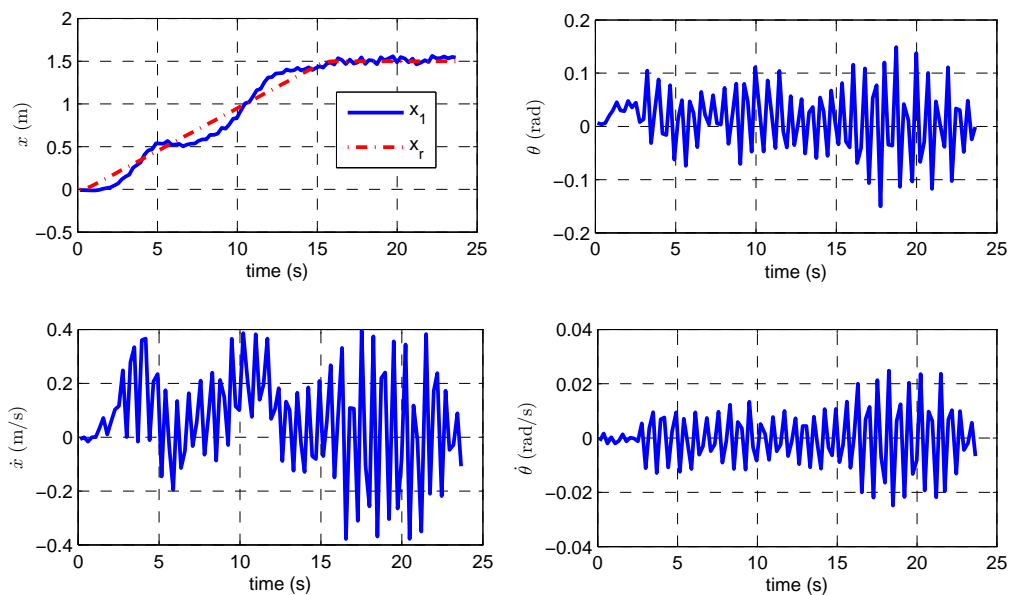
Figure 4.10: Experimental testing results for setpoint task: time responses of x, θ, $\dot{x}$ and $\dot{\theta}$ under
SMC. The 2WMR is placed on a flat surface. The reference trajectory (2.14) is applied.
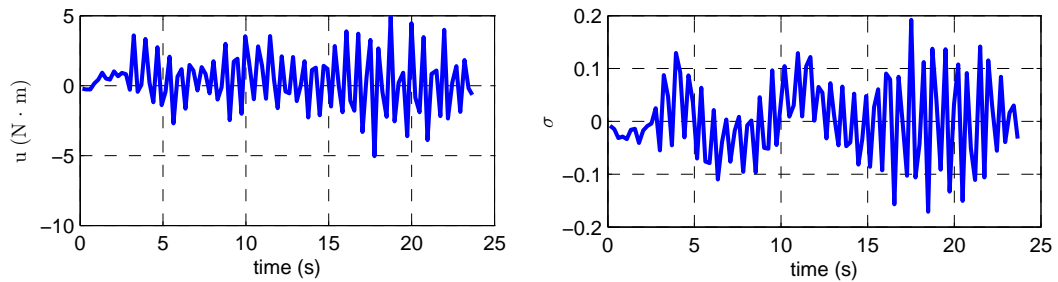
Figure 4.11: Experimental testing results for setpoint task: time responses of u and σ under SMC. The 2WMR is placed on a flat surface. The reference trajectory (2.14) is applied.

4.6 Conclusion

In this chapter, a novel design of SMC is presented. First, a linear sliding surface and the SMC are introduced. The system reaches the sliding surface in a finite time under the proposed SMC. Next, after the system reaches the sliding surface, the sliding surface design is discussed, which mainly focuses on choosing the sliding surface coefficients to stabilize the sliding manifold. To avoid the complexity on tuning the coefficients directly, we transform the problem into a simple nominal linear controller design problem, which not only simplifies the tuning process, but also provides one extra degree of freedom in control. By utilizing the extra degree of freedom, optimal and robust linear control techniques are incorporated in the SMC design. Intensive simulations and experiment testings are conducted to verify the effectiveness of the proposed SMC and satisfactory results are achieved.

Chapter 5

A Sliding Mode Controller With Integral Sliding Surface

5.1 Introduction

Design of SMC with linear sliding surface was discussed in the previous chapter. In this chapter, we propose an ISMC for the 2WMR. Integral-type sliding mode designs are proposed for controlling systems with both matched and unmatched uncertainties [10, 11, 76]. The sliding mode exists from the very beginning, therefore the system is more robust against perturbations than the other SMC systems with reaching phase. The ISMC is constructed by a nominal control part and a switching term. With the switching term, the matched uncertainties can be perfectly rejected. With the freedom to design a nominal control for the sliding manifold, ISMC can be easily incorporated with other robust control methods, such as LMI, H_∞, LQR, etc., to deal with the unmatched uncertainties. Furthermore, ISMC provides one more degree of choosing an appropriate projection matrix to reduce the effect of the unmatched uncertainties. In [11], the selection of the projection matrix is discussed for systems with constant input matrix.

First, we define a integral-type sliding surface and derive the control law by using Lyapunov theory. The sliding mode exists from the beginning and will be maintained. The resulting slid-

ing manifold is still underactuated, the resulting sliding manifold includes unmatched nonlinear terms and uncertainties, as well as a nominal controller. Considering the feasibility and simpleness in real implementation, a linear controller is adopted as the nominal controller. It is found that the linear controller is adequate to stabilize the sliding manifold around the equilibrium.

For setpoint control, undesired motions are observed in the real implementation, such as traveling backward or stopping for a short time during the traveling. To improve the system performance and obtain a smoother response, an algorithm is proposed to modify the pre-planned reference trajectory (2.14). With applying the modified reference trajectory, the 2WMR not only travels more smoothly but also arrives the setpoint in a shorter time. Steady state of the system is analyzed and zero steady state error for the wheel position is achieved by adding a compensation term in the nominal controller design. The value of the compensation term is obtained through a data-based approach and avoids the need of precise model information, which is impossible to obtain in practical.

The remainder of this chapter is organized as follows. In Section 5.2, the ISMC design is detailed. In Section 5.3, intensive simulation investigations are conducted to verify the effectiveness of the proposed ISMC. In Section 5.4, the implementation of ISMC on the real platform is given. Conclusions are drawn in Section 5.5.

5.2   Integral Sliding Mode Control Design

The following nonlinear integral-type sliding surface is proposed in [10] to handle systems with matched and unmatched uncertainties,

$$\sigma(\mathbf{e},t) = \mathbf{s}\mathbf{e}(t) - \mathbf{s}\mathbf{e}(t_0) - \int_{t_0}^{t} [\mathbf{s}\eta(\mathbf{e}) + \mathbf{sg}(\mathbf{e})\kappa(\mathbf{x},t)]d\tau = 0 \tag{5.1}$$

where $\kappa(\mathbf{e},t)$ is a nominal control, $\mathbf{s}$ is a 4×1 projection vector with freedom to design, and $\mathbf{sg}(\mathbf{e}) \neq 0$. Here we define $\mathbf{s} = [s_1, \ s_2, \ s_3, \ s_4]$, to satisfy $\mathbf{sg}(\mathbf{e}) \neq 0$, we have $cs_2 - bs_4 \neq 0$.

5.2.1 ISMC for System with Unmodeled frictions

First, we investigate the effect of frictions to the 2WMR system. As we stated in Chapter 4, the joint friction τ_f is a matched uncertainty, while the ground friction f_r is an unmatched uncertainty. Recall the error dynamic model of the 2WMR in (2.12),

$$\dot{\mathbf{e}} = \eta(\mathbf{e}) + \mathbf{g}(\mathbf{e})[u + d_m(\mathbf{e},t)] + \mathbf{d}_u(\mathbf{e},t), \tag{5.2}$$

where η is the system nonlinear term, d_m is the lumped matched uncertainties, $\mathbf{d}_u$ is the lumped unmatched uncertainties.

The control law is designed as

$$u(t) = \kappa(\mathbf{e},t) - \rho(\mathbf{e},t)sgn(\mathbf{sg}\sigma) \tag{5.3}$$

where the switching gain function is

$$\rho = \rho_m + \rho_u + \rho_0, \tag{5.4}$$

ρ_m is the upper bound of the matched uncertainty d_m, ρ_u is the upper bound of $\{\mathbf{sg}\}^{-1}\mathbf{sd}_u$, ρ_0 is a positive constant.

Theorem 5.1 *With the nonlinear integral-type sliding surface (5.1) and the controller (5.3), the global attractiveness of the sliding manifold is achieved. In the sliding mode, the matched uncertainties will be completely nullified. Further, the influence of unmatched uncertainties can be reduced with an extra degree of freedom provided by the vector* **s***.*

Proof : Differentiating the sliding surface (5.1) with respect to time t using (5.2) one obtains

$$\dot{\sigma}(t) = \mathbf{s}\dot{\mathbf{e}}(t) - \mathbf{s}\eta(\mathbf{e}) - \mathbf{sg}(\mathbf{e})\kappa(\mathbf{e}) = \mathbf{sg}(d_m + \frac{\mathbf{sd}_u}{\mathbf{sg}} + u - \kappa). \tag{5.5}$$

We choose a non-negative quadratic function $V = \sigma^2/2$. Differentiating V with respect to time t yields

$$\dot{V} = \sigma\dot{\sigma}.$$

Substituting $\dot{\sigma}$ in equation (5.5) into the above we have

$$\dot{V} = \sigma\mathbf{sg}\left(d_m + \frac{\mathbf{sd}_u}{\mathbf{sg}} + u - \kappa\right). \tag{5.6}$$

Substituting the ISMC law (5.3) into the above we obtain

$$
\begin{aligned}
\dot{V} &= \sigma\mathbf{sg}\left[d_m + \frac{\mathbf{sd}_u}{\mathbf{sg}} - \rho\, sgn(\mathbf{sg}\sigma)\right] \\
&\leq |\sigma\mathbf{sg}|\left(|d_m| + \left|\frac{\mathbf{sd}_u}{\mathbf{sg}}\right| - \rho\right) \\
&\leq -\rho_0|\sigma\mathbf{sg}| < 0.
\end{aligned}
$$

Since $\sigma(\mathbf{e}(t_0), t_0) = 0$, we can conclude that the controller (5.3) using the gain function (5.4) guarantees that the sliding mode $\sigma = 0$ can be maintained $\forall t \in [t_0, \infty)$.

In the sliding mode, $\sigma(t) = 0$, $\dot{\sigma}(t) = 0$, and define $\mathbf{e}_d$ as the state vector in the sliding mode. The equivalent control is derived from $\dot{\sigma} = 0$, which is

$$u_{eq}(t) = \kappa - d_m - \frac{\mathbf{sd}_u}{\mathbf{sg}}.$$

Substituting the above $u_{eq}(t)$ into (5.2), one obtains the sliding manifold

$$\dot{\mathbf{e}}_d(t) = \eta(\mathbf{e}_d) + \mathbf{g}(\mathbf{e}_d)\kappa(\mathbf{e}_d) + \delta, \tag{5.7}$$

where the matched uncertainty d_m is completely nullified, and

$$\delta = \begin{bmatrix} 0 \\ \delta_1 \\ 0 \\ \delta_2 \end{bmatrix} = \left(I - \frac{\mathbf{gs}}{\mathbf{sg}}\right)\mathbf{d}_u = \frac{g_2 d_{u1} - g_1 d_{u2}}{s_2 g_1 + s_4 g_2}\begin{bmatrix} 0 \\ s_4 \\ 0 \\ -s_2 \end{bmatrix}. \tag{5.8}$$

We can choose s_2 and s_4 to minimize the effect of the unmatched uncertainties δ in the sliding manifold. Referring to (5.8), when $s_2 = 0$ and $s_4 \neq 0$, the unmatched uncertainties in the sliding manifold only exist in the wheel subsystem, when $s_4 = 0$ and $s_2 \neq 0$, the unmatched uncertainties only exist in the pendulum subsystem. Since the pendulum subsystem is much more sensitive to uncertainties than the wheel subsystem, it is preferred to choose $\mathbf{s} = [0, 0, 0, s_4]$ and $s_4 \neq 0$.

Q.E.D.

5.2.2   ISMC for System with Parameter Uncertainties

Similarly as in Chapter 4, we consider that the parameter uncertainties exist in the 2WMR system. Recall the system dynamic model with parameter uncertainties, as in Section 4.2.2,

$$\dot{\mathbf{e}} = \eta(\mathbf{e}) + [\mathbf{g}(\mathbf{e}) + \Delta\mathbf{g}(\mathbf{e}, \mathbf{p})](d_m + u) + \mathbf{d}_u + \Delta\eta(\mathbf{e}, \mathbf{p}), \tag{5.9}$$

where η and $\mathbf{g}$ are known nominal parts, $\mathbf{p}$ represents the uncertain parameters, $\Delta\eta$ and $\Delta\mathbf{g}$ are uncertain parts. Define constants $m_{p,0}$, φ_0 the estimation value of m_p and φ, the known parts are $\eta = \eta(\mathbf{e}, m_{p,0}, \varphi_0)$, $\mathbf{g} = \mathbf{g}(\mathbf{e}, m_{p,0}, \varphi_0)$. The unknown parts are $\Delta\eta = \eta(\mathbf{e}, m_p, \varphi) - \eta(\mathbf{e}, m_{p,0}, \varphi_0)$, and $\Delta\mathbf{g} = \mathbf{g}(\mathbf{e}, m_p, \varphi) - \mathbf{g}(\mathbf{e}, m_{p,0}, \varphi_0)$.

Remark 5.1 *The sliding surface (5.1) is applied. The projection vector* $\mathbf{s}$ *could be chosen to make the sign of* $\mathbf{s}(\mathbf{g} + \Delta\mathbf{g})$ *be available and fixed. For example, with choosing* $\mathbf{s} = [0, 0, 0, s_4]$, *we have* $sgn[\mathbf{s}(\mathbf{g} + \Delta\mathbf{g})] = sgn[s_4 \cdot g_2(\mathbf{e}, m_p, \varphi)] = -sgn(s_4)$ *since* $g_2(\mathbf{e}, m_p, \varphi) < 0$.

The ISMC in (5.3) is applied and the switching gain function is as (5.4) with

$$\rho_m \;\geq\; |d_m|, \tag{5.10}$$

$$\rho_u \;\geq\; \left|\frac{\mathbf{s}\mathbf{d}_u}{\mathbf{s}(\mathbf{g} + \Delta\mathbf{g})}\right| + \left|\frac{\mathbf{s}\Delta\eta}{\mathbf{s}(\mathbf{g} + \Delta\mathbf{g})}\right| + \left|\frac{\mathbf{s}\Delta\mathbf{g}\kappa}{\mathbf{s}(\mathbf{g} + \Delta\mathbf{g})}\right|. \tag{5.11}$$

Theorem 5.2 *For system with parameter uncertainties, the sliding surface (5.1) and the ISMC (5.3) with a modified switching gain guarantee the existence of the sliding mode. In the sliding mode, the desirable properties stated in* **Theorem 5**.1 *also hold.*

Proof : Differentiating the sliding surface (5.1) with respect to time using (5.9) one obtains

$$\begin{aligned}
\dot{\sigma}(t) \;&=\; \mathbf{s}\dot{\mathbf{e}}(t) - \mathbf{s}\eta(\mathbf{e}) - \mathbf{s}\mathbf{g}(\mathbf{e})\kappa(\mathbf{e}) \\
&=\; [\mathbf{s}(\mathbf{g} + \Delta\mathbf{g})]\left\{ \frac{\mathbf{s}(\mathbf{d}_u + \Delta\eta) - \mathbf{s}\mathbf{g}\kappa}{\mathbf{s}(\mathbf{g} + \Delta\mathbf{g})} + u + d_m \right\}.
\end{aligned} \tag{5.12}$$

We choose a non-negative quadratic function $V = \sigma^2/2$. Differentiating V with respect to time

t yields

$$
\begin{aligned}
\dot{V} &= \sigma\dot{\sigma} \\
&= \sigma[\mathbf{s}(\mathbf{g}+\Delta\mathbf{g})]\left\{\frac{\mathbf{s}(\mathbf{d}_u+\Delta\eta)-\mathbf{sg}\kappa}{\mathbf{s}(\mathbf{g}+\Delta\mathbf{g})}+u+d_m\right\}.
\end{aligned}
$$

Substituting the SMC law (5.3) with the modified gains (5.10)(5.11) into the above we obtains

$$
\begin{aligned}
\dot{V} &= \sigma[\mathbf{s}(\mathbf{g}+\Delta\mathbf{g})]\left\{d_m+\frac{\mathbf{s}\mathbf{d}_u+\mathbf{s}\Delta\eta}{\mathbf{s}(\mathbf{g}+\Delta\mathbf{g})}+\frac{\mathbf{s}\Delta\mathbf{g}\kappa}{\mathbf{s}(\mathbf{g}+\Delta\mathbf{g})}-\rho\,sgn(\mathbf{sg}\sigma)\right\} \\
&\leq |\sigma\mathbf{s}(\mathbf{g}+\Delta\mathbf{g})|\left\{|d_m|+\left|\frac{\mathbf{s}\mathbf{d}_u}{\mathbf{s}(\mathbf{g}+\Delta\mathbf{g})}\right|+\left|\frac{\mathbf{s}\Delta\eta}{\mathbf{s}(\mathbf{g}+\Delta\mathbf{g})}\right|+\left|\frac{\mathbf{s}\Delta\mathbf{g}\kappa}{\mathbf{s}(\mathbf{g}+\Delta\mathbf{g})}\right|-\rho\right\} \\
&\leq -\rho_0|\sigma\mathbf{s}(\mathbf{g}+\Delta\mathbf{g})|<0.
\end{aligned}
$$

Since $\sigma(\mathbf{x}(t_0),t_0)=0$, we can conclude that the sliding mode $\sigma = 0$ can be maintained $\forall t \in$

$[t_0,\infty)$.

In the sliding mode, the equivalent control is derived from $\dot{\sigma} = 0$, which is

$$
u_{eq}(t) = \frac{\mathbf{sg}}{\mathbf{s}(\mathbf{g}+\Delta\mathbf{g})}\kappa-d_m-\frac{\mathbf{s}(\mathbf{d}_u+\Delta\eta)}{\mathbf{s}(\mathbf{g}+\Delta\mathbf{g})}.
$$

Substituting the above $u_{eq}(t)$ into (5.9), one obtains the sliding manifold as (5.7) with

$$
\delta = \left[I-\frac{(\mathbf{g}+\Delta\mathbf{g})\mathbf{s}}{\mathbf{s}(\mathbf{g}+\Delta\mathbf{g})}\right][\Delta\eta+\mathbf{d}_u-\mathbf{g}\kappa]. \tag{5.13}
$$

Q.E.D.

5.2.3 Linear Controller Design for the Sliding Manifold

The obtained sliding manifold (5.7) is still nonlinear and underactuated with the nominal

controller κ to be further designed. Considering the feasibility and simpleness in real implemen-

tation, a linear controller is employed, as

$$
\kappa = -\mathbf{k}\mathbf{e}, \tag{5.14}
$$

where $\mathbf{k} = [k_1, \ k_2, \ k_3, \ k_4]$.

The methods introduced in Chapter 3 can be directly applied to obtain the feedback gains for the linear controller.

5.2.4 Steady State Analysis

We define the steady state error vector as $\mathbf{e}_s = [e_{1,s}, \ e_{2,s}, \ e_{3,s}, \ e_{4,s}]^T$. When the 2WMR system enters steady state, from (2.6), we have the equilibrium point of the pendulum as

$$\theta_e = \arcsin \frac{r \sin \varphi (m_p + m_w)g + f_r}{m_p l g}. \tag{5.15}$$

In steady state, $e_{2,s} = 0$, $e_{4,s} = 0$, the nominal controller (5.14) becomes

$$\kappa = -k_1 e_{1,s} - k_3 e_{3,s}. \tag{5.16}$$

Substituting the above equation to the sliding manifold (5.7), we have

$$\eta_1 + g_1(-k_1 e_{1,s} - k_3 e_{3,s}) + \delta_1 = 0, \tag{5.17}$$

$$\eta_2 + g_2(-k_1 e_{1,s} - k_3 e_{3,s}) + \delta_2 = 0. \tag{5.18}$$

Refer to (5.8), for $\mathbf{s} = [0, \ 0, \ 0, \ s_4]$, we have $\delta_2 = 0$ in (5.18), thus

$$e_{1,s} = \frac{\eta_2}{g_2 k_1} - \frac{k_3 e_{3,s}}{k_1}, \tag{5.19}$$

where

$$\eta_2 = \frac{a m_p l g \sin \theta_e}{ac - b^2} + \frac{b(m_p + m_w)g \sin \varphi}{ac - b^2}, \tag{5.20}$$

$$g_2 = \frac{1}{r} \frac{-b}{ac - b^2} + \frac{-a}{ac - b^2}, \tag{5.21}$$

with $b = m_p l \cos(\theta_e + \varphi)$.

It is reasonable to choose $\theta_r = \theta_e$ which makes $e_{3,s} = 0$. The steady state error for the wheel position (5.19) becomes as

$$e_{1,s} = \frac{\eta_2}{g_2 k_1}. \tag{5.22}$$

Refer to (5.20), when $\theta_e \neq 0$ or $\varphi \neq 0$, we have $\eta_2 \neq 0$, yields $e_{1,s} \neq 0$, which is undesirable. Generally integral control could be applied to deal with the steady state error. However, considering that various time-varying measurement noise or disturbances exist in the real testing environment, the integral control may not function well.

In this work, to achieve a satisfying response with zero steady state error for the wheel position, i.e., $e_{1,s} = 0$, we add a compensation term β_c to the nominal controller in (5.14), the new nominal controller is as

$$\kappa = -\mathbf{k}\mathbf{e} + \beta_c, \tag{5.23}$$

in steady state,

$$\kappa = -k_1 e_{1,s} - k_3 e_{3,s} + \beta_c. \tag{5.24}$$

Substituting the above equation to the sliding manifold (5.7) and applying $e_{3,s} = 0$, now we have

$$e_{1,s} = \frac{\eta_2 + g_2 \beta_c}{g_2 k_1}. \tag{5.25}$$

To make $e_{1,s} = 0$, we have

$$\beta_c = -\frac{\eta_2}{g_2}. \tag{5.26}$$

Refer to (5.15) and (5.26), it is noted that the accurate model information is required to obtain θ_r and β_c. However, in (5.15), the friction f_r and slope φ are not known precisely, thus the value of θ_e cannot be calculated directly and the value of η_2 / g_2 in (5.26) is also not available.

Instead, in this work, we seek a data-based approach to determine the suitable θ_r and β_c that make $e_{1,s} = 0$, $e_{3,s} = 0$. First, $\theta_r = 0$ and $\beta_c = 0$ are applied in the controller design. $e_{1,s}|_{(\theta_r=0,\beta_c=0)}$ and θ_e are obtained from simulation or experiment results. We have $e_{3,s}|_{(\theta_r=0,\beta_c=0)} = \theta_e - 0 = \theta_e$, (5.19) becomes

$$e_{1,s}|_{(\theta_r=0,\beta_c=0)} = \frac{\eta_2}{g_2 k_1} - \frac{k_3 \theta_e}{k_1},$$

yields

$$\frac{\eta_2}{g_2} = k_1 e_{1,s}|_{(\theta_r=0,\beta_c=0)} + k_3 \theta_e. \tag{5.27}$$

As we stated in *Remark* 2.1, θ_e is fixed and irrelevant to controller parameters or control tasks if the 2WMR travels under the same circumstance. Refer to (5.20)(5.21), we conclude the value of η_2/g_2 is also irrelevant from controller parameters or control tasks. Substituting (5.27) to (5.26), the compensation term becomes

$$\beta_c = -k_1 e_{1,s}|_{(\theta_r=0,\beta_c=0)} - k_3 \theta_e.$$

Submitting the above equation to (5.23), we have

$$\kappa = -k_1 e_1 - k_2 e_2 - k_3(x_3 - \theta_e) - k_4 e_4$$
$$-k_1 e_{1,s}|_{(\theta_r=0,\beta_c=0)} - k_3 \theta_e,$$

that is

$$\kappa = -k_1 e_1 - k_2 e_2 - k_3 x_3 - k_4 e_4 + \gamma_c, \tag{5.28}$$

where $\gamma_c = -k_1 e_{1,s}|_{(\theta_r=0,\beta_c=0)}$.

We can find that in the nominal controller design, the information of θ_e is no longer needed while the information of $e_{1,s}|_{(\theta_r=0,\beta_c=0)}$ is still needed. Note that expression of the nominal controller in (5.23) with $(\theta_r = 0, \beta_c = 0)$ is the same as the one in (5.28) with $\gamma_c = 0$, we have

$$\gamma_c = -k_1 e_{1,s}|_{\gamma_c=0}. \tag{5.29}$$

For the convenience of expression in the later work, γ_c is regarded as the final form of the compensation term.

5.3 Numerical Validations

Simulations were conducted to verify the effectiveness of the proposed control scheme, as well as obtain suitable controller parameters before proceeding with the experiments. For simu-

lation, frictions f_r and τ_f are modeled the same as in Section 4.4, i.e., $f_r = f_v \dot{x} + f_c sgn(\dot{x})$, where $f_v = 0.2$, $f_c = 0.3$, and $\tau_f = \tau_v \dot{\theta} + \tau_c sgn(\dot{\theta})$, where $\tau_v = 0.2$, $\tau_c = 0.3$.

5.3.1 ISMC for System With Matched Uncertainties

First, we consider only the joint friction exists in the system, which is a matched uncertainty. The 2WMR travels on a flat surface, i.e., $\varphi = 0$. The initial states of the mobile robot are as $\mathbf{x} = [0, \ 0, \ 0.1, \ 0]^T$. ISMC is applied with $\mathbf{s} = [0, \ 0, \ 0, \ 1]$, $\rho = 0.1 + 0.2|x_4| + 0.3$. The parameters for the nominal controller (5.28) are as $\theta_r = 0$, $\gamma_c = 0$ and $\mathbf{k} = [-7.0711, \ -9.6708, \ -27.0228, \ -2.8418]$, which is obtained through LQR method by choosing $Q = \{50, 0.1, 500, 1\}$ and $R = 1$.

The simulation results are shown in Fig. 5.1. The 2WMR reaches the desired setpoint smoothly and the pendulum is balanced at $\theta_e = 0$. The 2WMR responses are almost the same as in Fig. 3.2 despite the presence of the joint friction τ_f, which demonstrates the effectiveness of ISMC in rejecting matched uncertainties. It is noted that control signal shows switching behavior.
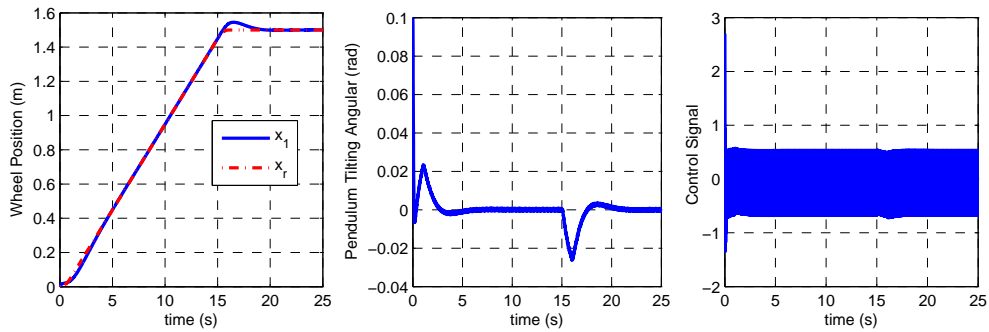
Figure 5.1: Time responses of x, θ and u under ISMC. In simulations, system is considered with the joint friction $\tau_f = 0.2\dot{\theta} + 0.3sgn(\dot{\theta})$, which is a matched uncertainty.

5.3.2 ISMC for System With both Matched Uncertainties and Unmatched Uncertainties

Two type of unmatched uncertainties exist in the system, one is due to the external disturbance and the other is due to the uncertain system parameters.

First, we consider the 2WMR system with the ground friction f_r and the joint friction τ_f. ISMC is applied with $\rho = 0.1 + 0.2|x_4| + 0.3 + br/(b+ar)(0.5|x_2|+1)$ and the nominal controller in (5.28). Other control parameters are chosen the same as in the preceding simulation. Applying $\gamma_c = 0$ in (5.28), from the simulation results, we found that the pendulum is balanced at the equilibrium point $\theta_e = 0.018\ rad$. The steady state error of the wheel position is $e_{1,s}|_{\gamma_c=0} = -0.0637\ m$. Next, $\gamma_c = -0.4504$ is computed according to (5.29) and applied in (5.28). The simulation results for the two cases, with and without the compensation term γ_c, are shown in Fig. 5.2. We can see that with the compensation, the 2WMR tracks the reference better and reaches the given setpoint $1.5\ m$ smoothly, which shows the effectiveness of the ISMC with the compensation term γ_c.
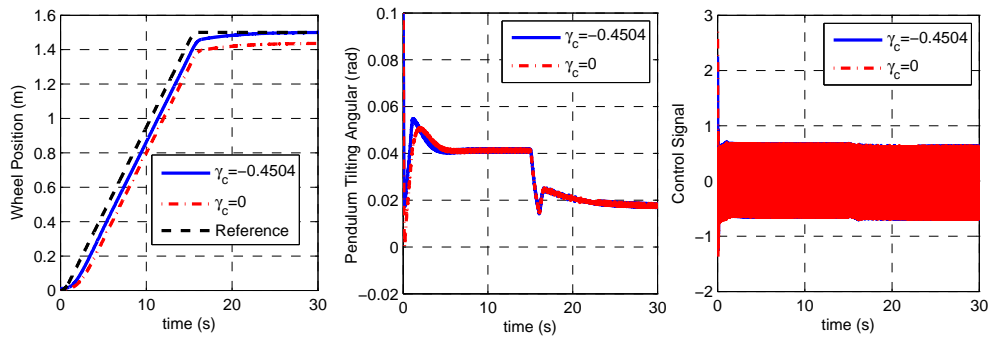
Figure 5.2: Time responses of x, θ and u under ISMC with and without the compensation term γ_c. In simulations, system is considered in presence of the joint friction $\tau_f = 0.2\dot{\theta} + 0.3sgn(\dot{\theta})$, and the ground friction $f_r = 0.5\dot{x} + sgn(\dot{x})$ which is a unmatched uncertainty.

Next, the system under parameter uncertainty is considered. We assume that the mobile robot travels on an inclined surface. $\varphi_0 = 0$ is used in sliding surface and controller design,

whereas the actual slope is $\varphi = \pi/15\ rad$. The frictions are also considered existing in the system. ISMC is applied with the nominal controller in (5.28). Similarly, first $\gamma_c = 0$ is used in (5.28). From the simulation results, we found that the pendulum is balanced at the equilibrium point $\theta_e = 0.275\ rad$. The steady state error of the wheel position is $e_{1,s}|_{\gamma_c=0} = -0.9991\ m$. Next $\gamma_c = -7.0647$ is computed according to (5.29) and used in (5.28). The simulation results for the two cases, with and without the compensation term γ_c, are shown in Fig. 5.3. ISMC shows the robustness to parameter uncertainties and a better response is achieved with adding the compensation term.
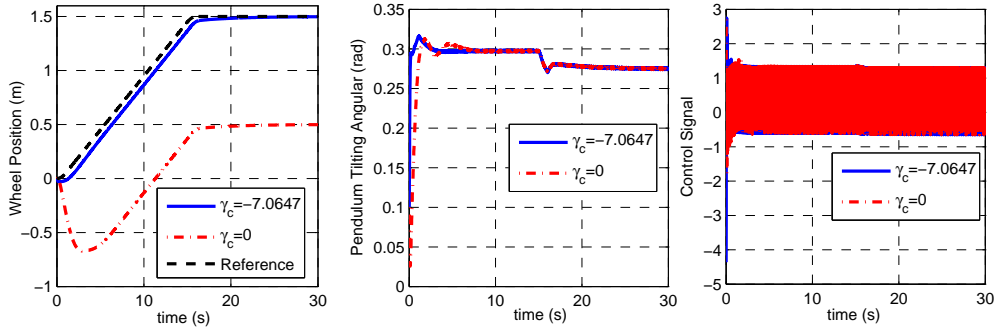
Figure 5.3: Time responses of x, θ and u under ISMC with and without the compensation term γ_c. In simulations, system is considered with the unmatched uncertainties caused by the uncertain of φ.

5.4   Implementation and Experiment Results

5.4.1   Regulation Task

For implementation, we start with a simple regulation control task that is to balance the robot at the original position. First, the robot is placed on a flat surface. ISMC is applied with $\rho = 0.2$. The projection vector is selected as $\mathbf{s} = [0, 0, 0, 0.05]$. The nominal linear controller $\kappa = -\mathbf{ke}$ is with $\mathbf{k} = [10, 0.5, 35, 3]$. The experiment results are shown in Fig. 5.4. We can see that the linear controller fails to stabilize the 2WMR system. By applying the ISMC, the 2WMR stays
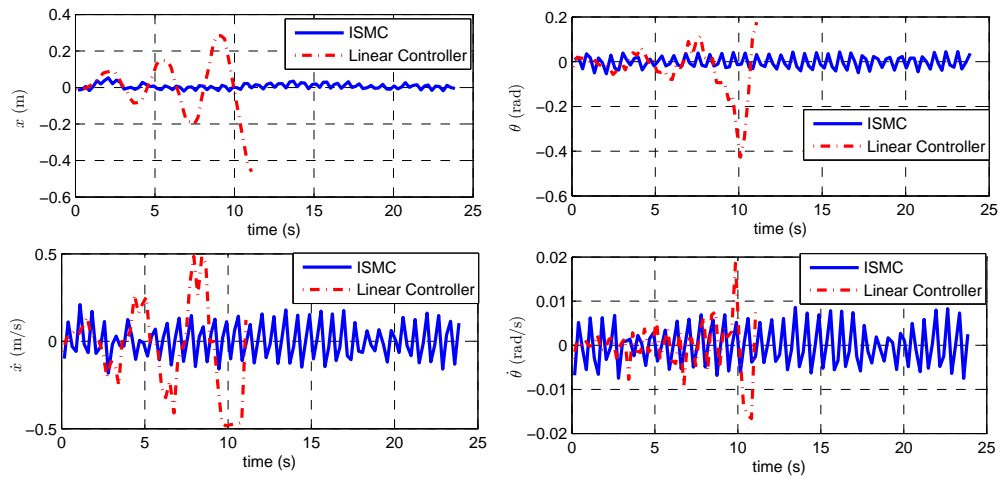
Figure 5.4: Experimental testing results for regulation task: time responses of x, θ, $\dot{x}$ and $\dot{\theta}$ under ISMC and linear controller. The 2WMR is placed on a flat surface.

around the original place and the pendulum is balanced around $\theta = 0$.

Similarly as we did in the previous chapters, a testing is conducted to check the robustness of the SMC with respecting to an exceptional disturbance. The experiment results are shown in Fig. 5.5. At $t = 18$ s, we push the 2WMR to the right about 0.15 m. The 2WMR is finally stabilized around the original position, however, the transit responses show oscillations.
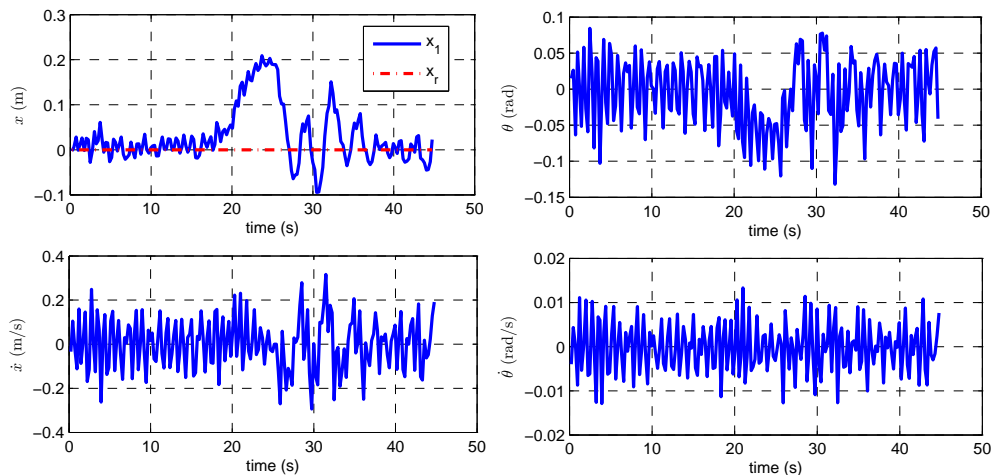
Figure 5.5: Experimental testing results for regulation task: time responses of x, θ, $\dot{x}$ and $\dot{\theta}$ under ISMC. The 2WMR is placed on a flat surface. A disturbance is added to the system at $t = 18$ s.

Next, the 2WMR is placed on an inclined surface and the slope angle φ is unknown. ISMC

is applied with the nominal linear controller controller in (5.28). For the first trial, we set $\gamma_c = 0$. The pendulum is balanced around $\theta_e = 0.1$ rad, however, steady state error of the wheel position exists, and $e_{1,s}|_{\gamma_c=0} = 0.35$ m. For the second trial, we use $\gamma_c = -3.5$, which is computed according to (5.29). Experiment results for the two cases, with and without the compensation term, are shown in Fig. 5.6. The steady state error for the wheel position is eliminated under ISMC with the compensation term, which is consistent with the theoretical analysis and simulation results.
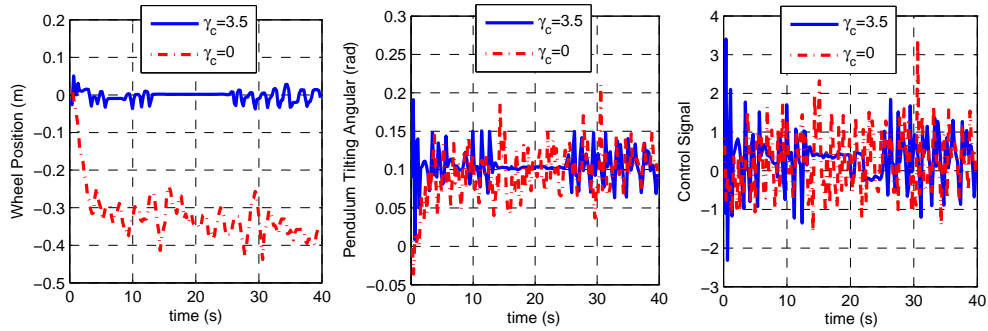
Figure 5.6: Experimental testing results for regulation task: time responses of x, θ and u under ISMC with and without the compensation term γ_c. The 2WMR is placed on an inclined surface.

5.4.2 Reaching a Setpoint

First, we consider the 2WMR travels on a flat surface, i.e., $\varphi = 0$. The references for the wheel position and velocity are the same as used in simulations. ISMC is applied with $\theta_r = 0$, $\gamma_c = 0$. All other controller parameters are chosen the same as for the regulation task. The experiment results are shown in Fig. 5.7. The 2WMR reaches the desired setpoint and stays there afterwards. ISMC shows the effectiveness for setpoint control of the 2WMR system.

However, the response of the wheel position is not satisfactory because the backward motion exists. When the real position of the 2WMR x_1 surpasses the given reference x_r, the 2WMR would stop for a while or travel backwards, to make $|x_1 - x_r|$, i.e., $|e_1|$ become smaller, which is natural in feedback control system. However, considering that our objective for the 2WMR is
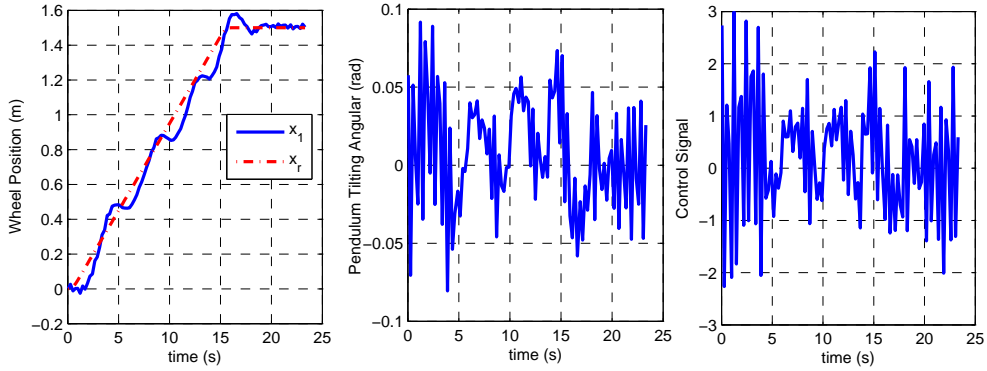
Figure 5.7: Experimental testing results for setpoint task: time responses of x, θ and u under ISMC. The 2WMR travels on a flat surface. The reference trajectory (2.14) is applied.

traveling forward to arrive the desired position, these motions are not desired.

To improve the 2WMR performance, especially the response of the wheel position, we propose a modified reference trajectory $x_{r,n}$ for the wheel position as the following.

$$
x_{r,n}(t+T_s) = \begin{cases} x_{r,n}(t)+v_rT_s & \text{if} \quad x_1(t) \leq x_{r,n}(t) < x_d \\ x_1(t)+v_rT_s & \text{if} \quad x_{r,n}(t) < x_1(t) < x_d \\ x_d & \text{if} \quad x_{r,n}(t) \geq x_d \text{ or } x_1(t) \geq x_d \end{cases} .
\tag{5.30}
$$

The idea is to avoid the undesired backward motion. The modified reference trajectory $x_{r,n}$ is adaptive in the sense that it is updated according to the current position of the 2WMR. When the wheel position x_1 surpasses the given reference $x_{r,n}$, we regard x_1 as the new starting point to generate the reference for the next sampling time, thus the error between the real position of the wheel and the reference, $e_1 = x_{r,n}(t+T_s) - x_1(t) = v_rT_s$, is guaranteed to be positive. As a result, the undesired backward motion is avoided and the 2WMR performance is improved.

Another test is conducted with applying the modified reference trajectory, and the design of ISMC is the same as in the preceding test. Experiment results are shown in Fig. 5.8. We can see that the response is much smoother and the 2WMR arrives the desired position in a shorter time.

Next, we consider the 2WMR travels on an inclined surface and the slope angle φ is unknown. ISMC is applied with the nominal linear controller controller in (5.28). For the first trial,
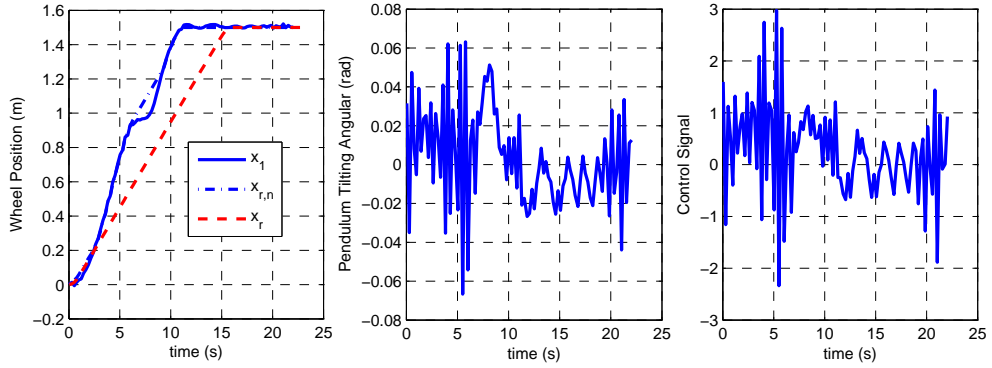
Figure 5.8: Experimental testing results for setpoint task: time responses of x, θ and u under ISMC. The mobile robot travels on a flat surface. Modified reference trajectory (5.30) is applied.

we set $\gamma_c = 0$, the experiment results are shown in Fig. 5.9. The pendulum is balanced around 0.05 rad. However, steady state error exists for the wheel position, and $e_{1,s}|_{(\theta_r=0,\gamma_c=0)} = 0.17\ m$.
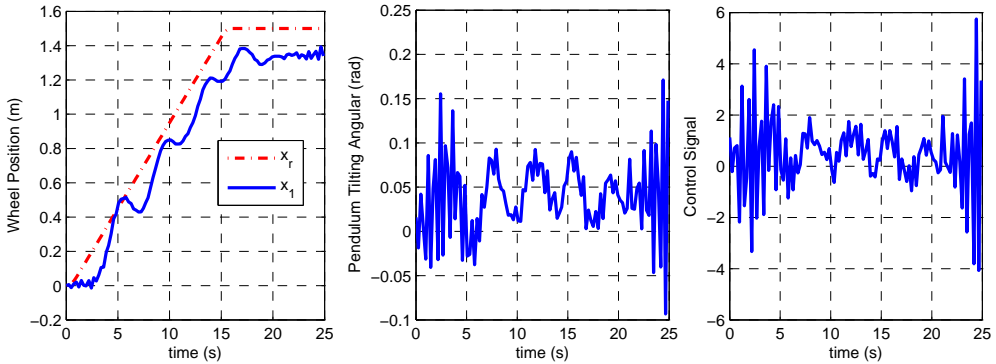
Figure 5.9: Experimental testing results for setpoint task: time responses of x, θ and u under ISMC with $\gamma_c = 0$. The 2WMR travels on an inclined surface with $\varphi = 2.5°$. The reference trajectory (2.14) is applied.

For the second trial, $\gamma_c = -1.7$ is computed according to (5.29) and applied in (5.28). The experiment results are shown in Fig. 5.10. Compared with the results in Fig. 5.9, we can see the robot tracks the given reference better and reaches the desired position without steady state error. However, the trajectory of the wheels x_1 is not smooth enough.

To obtain a smoother and faster response, similarly, the new reference (5.30) is used. ISMC applied is the same as in the preceding test. The experiment results are shown in Fig. 5.11. A
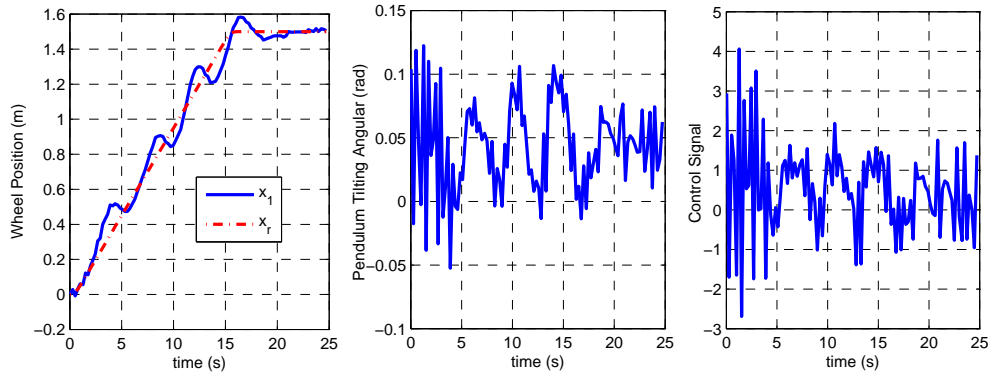
Figure 5.10: Experimental testing results for setpoint task: time responses of x, θ and u under ISMC with $\gamma_c = 0.17$. The 2WMR travels on an inclined surface with $\varphi = 2.5°$. The reference trajectory (2.14) is applied.

much smoother and faster response is observed.
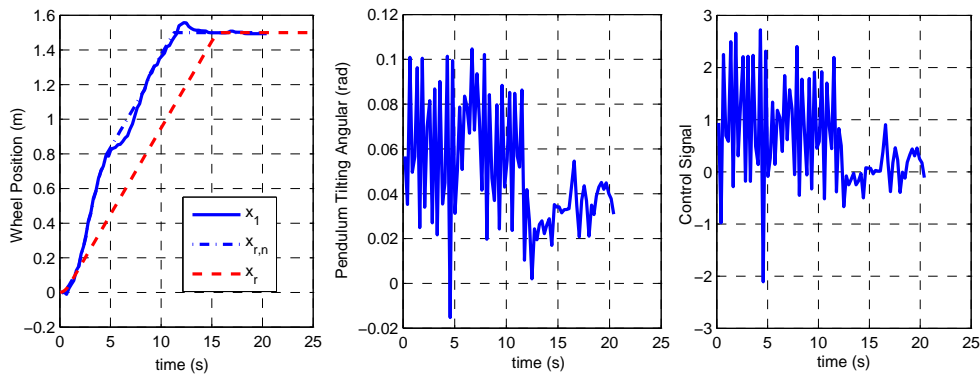
Figure 5.11: Experimental testing results for setpoint task: time responses of x, θ and u under ISMC with $\gamma_c = 0.17$. The 2WMR travels on an inclined surface with $\varphi = 2.5°$. Modified reference trajectory (5.30) is applied.

5.5 Conclusion

In this chapter, an ISMC is proposed. The sliding mode exists from the very beginning, therefore the system is more robust against uncertainties than the other SMC systems with reaching phase. The ISMC is constructed by a nominal control part and a switching term. With the switching term, the matched uncertainties are perfectly rejected. With the freedom to design a nominal

control for the sliding manifold, ISMC is incorporated with a linear controller. Strategies have been proposed to handle many practical problems regarding the implementation such as the reference trajectory design, eliminating the steady state error, rejecting the effect caused by the matched uncertainty and reducing the effects caused by the unmatched uncertainties. Simulation and experiment results are provided to validate the effectiveness and robustness of the ISMC.

Chapter 6

A Takagi-Sugeno Type Fuzzy Logic Controller

6.1 Introduction

Fuzzy logic control approach has been widely used in robotics control and applications as it provides user-friendly interface for controller design. In FLC design, the knowledge of the designers can be incorporated directly as a set of fuzzy rules. FLC design is in general model free, which is complementary to model-based control design. FLC offers a nonlinear controller with robustness for systems with parametric and functional uncertainties, as well as disturbances. The FLC design provides the flexibility in structure design and parameter selection, thus it can be easily incorporated with other control methods, such as LMI [28], sliding mode control [39], etc.

In [28], a fuzzy traveling and position control algorithm is proposed for a 2WMR without input coupling. The wheel position or position tracking error, is not used for computing the control input. The position control of the 2WMR is achieved through specifying a reference angle for the pendulum. The reference angle is the output of a fuzzy system, which has the inputs as the tracking error of the wheel position and the wheel velocity. Based on human experience,

forty-nine fuzzy rules are established to describe the relationship between the wheel states and the pendulum reference angle. For 2WMR without input coupling, the pendulum equilibrium position is always the upright position, while for 2WMR with input coupling, the equilibrium of the pendulum varies with respecting to the slope angle of the traveling surface and the ground friction. During the traveling, the ground friction is unknown to the designer, thus it is difficult to specify the value of the desired pendulum angle that could result in the desired motion of the wheels. As a result, the FLC proposed in [28] is limitedly applicable to the 2WMR without input coupling. In this work, to achieve the position control of the 2WMR, a Takagi-Sugeno (T-S) type FLC using full-state feedback is proposed. All the available states, including the wheel position, the wheel velocity, the pendulum tilting angle and the pendulum angle velocity, are used for feedback. The proposed FLC is applicable to 2WMR with or without input coupling. There are four inputs to the FLC and each of them is associated with two fuzzy labels, which yields in total 16 fuzzy rules in the FLC design.

A difficulty in FLC design is the lengthy tuning process for FLC parameters, which is usually trial and error in nature. There are two groups of controller parameters in the proposed FLC: the four range parameters for the fuzzy sets of four input variables, and eight output parameters for the output of the sixteen rules, considering the symmetry between the fuzzy rules. The range parameters are chosen using heuristic knowledge such as physical boundaries of input variables. The eight FLC output parameters cannot be easily decided through empirical investigation, because they jointly determine the control effectiveness and any change of a single parameter would affect the overall system response. It is difficult to make clear the relations among the eight parameters because the underacuated 2WRM system shows complex behaviors. The limitation of the heuristic knowledge motivates us to explore partially model-based design. Considering that the FLC is essentially a state feedback controller with varying feedback gains, we introduce a

simple method by aligning the FLC output with a linear feedback control output at eight particular operating points of the four dimensional state space, where each operating point represents a specific scenario with only one rule being activated while remaining fifteen rules are inhibited. As such, each time we can determine one FLC output parameter. The linear controller is designed based on a linearized model of the 2WMR and feedback gains are first obtained through LQR method by simulation and later manually tuned during the implementation, as in [68].

The main contributions of this chapter are summarized as follows.

(i) An FLC is proposed for real time control of the 2WMR. The designed FLC is also applicable to underactuated systems without input coupling, such as the 2WMR prototype built in [28]. Compared with FLC designed in [28], the proposed FLC has fewer fuzzy rules and parameters to be determined, which implies a simpler design.

(ii) The proposed FLC is a synthesized design which utilizes both the human knowledge and the model information. The FLC structure and membership function is determined using heuristic knowledge. The FLC output parameters are determined based on the output of a linear controller by specifying the 2WMR system states at sixteen particular operating points in the 4D state space, which avoids the difficulty in manual tuning. The new FLC outperforms a linear controller since it provides varying feedback gains that are desirable for real-time control of the 2WMR platform. Compared with the model-free designs in [12, 13, 71], the FLC is simpler in mathematics, furthermore, it provides a user-friendly design interface, thus is easy to understand.

The remainder of this chapter is organized as follows. In Section 6.2, the design procedure of the FLC is detailed. In Section 6.3, the implementation of FLC on the real platform is given. Conclusions are drawn in Section 6.4.

6.2   The FLC Design

We adopt T-S type FLC for the simplicity of controller structure and easiness in the FLC parameter tuning. With full-state feedback, we have four inputs to FLC. For each input we use two fuzzy labels, Positive (P) and Negative (N), for fuzzification. Therefore there are in total $2^4 = 16$ fuzzy rules.

6.2.1   The Structure of FLC

The four error states (e_1, e_2, e_3, e_4) are the inputs to the FLC. Each of the 4 input variables is associated with two fuzzy sets P and N, respectively, and the degree to which set they belong to is determined by membership function illustrated in Fig. 6.1.
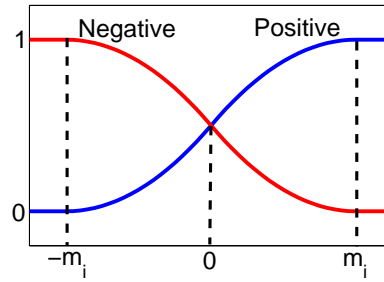
Figure 6.1: Membership function used for FLC. The range of inputs is specified by an interval $[-m_i, m_i]$, $i = 1, 2, 3, 4$. Two fuzzy sets, denoted by P and N, are described by their membership functions, respectively. The membership function of P is a smooth curve described by a function as (6.1). The membership function of N is the complementary to that of P.

A built-in membership function in the Matlab toolbox, named as S-shaped membership function, is used to represent fuzzy set P and given as below,

$$
\mu_P(e_i) = \begin{cases} 0 & (e_i < -m_i) \\ 2\left(\dfrac{e_i + m_i}{2m_i}\right)^2 & (-m_i \le e_i \le 0) \\ 1 - 2\left(\dfrac{m_i - e_i}{2m_i}\right)^2 & (0 \le e_i \le m_i) \\ 1 & (e_i > m_i) \end{cases}, \tag{6.1}
$$

where μ_P is the matching degree to fuzzy set P. The matching degree to fuzzy set N, denoted as

μ_N, is complementary to μ_P, i.e., $\mu_N = 1 - \mu_P$. The fuzzy set N is represented by another built-in

membership function in the matlab toolbox, named as Z-shaped membership function, which is

complementary to the S-shaped membership function.

There are three reasons to employ the Z-shaped and S-shaped membership functions. First,

the Z-shaped and S-shaped membership functions are appropriate to represent the concepts of

positive and negative. Second, the Z-shaped and S-shaped membership functions are second-

order polynomials, which are suitable for the implementation of the FLC because of their easi-

ness in computing. Third, the FLC using S-shape and Z-shaper membership functions provides

varying gains that are desirable for control of the 2WMR. The third point will be explained later.

Range parameters $[m_1, \ m_2, \ m_3, \ m_4]$ are determined by taking the physical constraints of

the 2WMR system into consideration. m_1 specifies the range of e_1, the tracking error of the

wheel position. Considering that the radius of the wheel is 0.08 m, we assume that the maximum

allowable tracking error of the wheel position is around the wheel circumference 0.5 m, thus m_1

is chosen to be 0.5 m. m_2 specifies the range of e_2, the tracking error of the wheel speed. Through

experimental investigation, we found that the maximum wheel speed is around 0.45 m/s under

the capacity of the DC-motor used. However, it is also noted that when the 2WMR travels at the

maximum speed, the system normally become unstable, hence m_2 is chosen to be 0.35 m/s. m_3

specifies the range of pendulum angular displacement. We consider the pendulum moves within

a safe range around the balanced position and choose $m_3 = \pi/6$ rad, that is 30°. m_4 specifies the

range of pendulum angular velocity and is chosen to be 0.2 rad/s, that is 11.5°/s.

The structure of FLC is T-S type, which consists of rules of the following form

R^i : If $(e_1$ is $A_1{}^i)$ AND $(e_2$ is $A_2{}^i)$ AND $(e_3$ is $A_3{}^i)$ AND $(e_4$ is $A_4{}^i)$, THEN $(u_i = \tau_i)$,

where $A_1{}^i, \ A_2{}^i, \ A_3{}^i, \ A_4{}^i \in \{P, N\}$ are fuzzy sets or fuzzy labels, u_i is the rule output, τ_i is a

constant representing the desired control torque. Each fuzzy rule describes a specific relationship between the fuzzy inputs and output.

Each rule contributes to the final FLC output according to matching for the IF part of the fuzzy rule. The TS-type fuzzy inference takes a weighted average of the individual outputs for each rule. The output τ_i $(i = 1 \sim 16)$ for each rule is weighted by the firing strength μ_{R^i}, which is calculated as shown in Fig. 6.2.
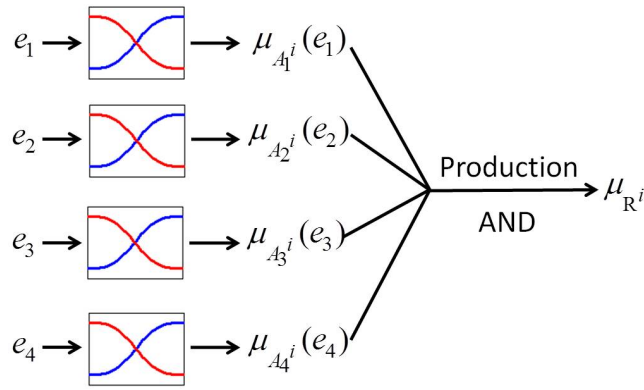
Figure 6.2: Sugeno-type fuzzy inference for the ith rule ($i = 1 \sim 16$). Each input, e_j ($j = 1 \sim 4$), yields two membership values $\mu_N(e_j)$ and $\mu_P(e_j)$. For individual fuzzy rules, $A_j{}^i$ is specified as either P or N, accordingly, the value of $\mu_{A_j{}^i}(e_j)$ used for calculation of μ_{R^i} is either $\mu_P(e_j)$ or $\mu_N(e_j)$. The AND logic operator in the antecedent part is chosen to be the production of four fuzzy membership values.

Table 6.1 shows the sixteen rules of the FLC for the 2WMR system. According to the table, the first IF-THEN rules can be expressed as

$$R^1 : \text{If } (e_1 \text{ is P}) \text{ AND } (e_2 \text{ is P}) \text{ AND } (e_3 \text{ is P}) \text{ AND } (e_4 \text{ is P}), \text{ THEN } (u_i = \tau_i),$$

and the firing strength for the first rule is

$$\mu_{R^1} = \mu_P(e_1)\mu_P(e_2)\mu_P(e_3)\mu_P(e_4).$$

The final output of the fuzzy controller is calculated by aggregating all sixteen rules in the

Table 6.1: Fuzzy Rules

Rule	$e_1(x - x_r)$	$e_2(\dot{x} - v_r)$	$e_3(\theta - \theta_r)$	$e_4(\dot{\theta})$	Torque
1	P	P	P	P	$\tau_1 = n_1$
2	P	N	P	P	$\tau_2 = n_2$
3	N	P	P	P	$\tau_3 = n_3$
4	N	N	P	P	$\tau_4 = n_4$
5	P	P	P	N	$\tau_5 = n_5$
6	P	N	P	N	$\tau_6 = n_6$
7	N	P	P	N	$\tau_7 = n_7$
8	N	N	P	N	$\tau_8 = n_8$
9	P	P	N	P	$\tau_9 = -n_8$
10	P	N	N	P	$\tau_{10} = -n_7$
11	N	P	N	P	$\tau_{11} = -n_6$
12	N	N	N	P	$\tau_{12} = -n_5$
13	P	P	N	N	$\tau_{13} = -n_4$
14	P	N	N	N	$\tau_{14} = -n_3$
15	N	P	N	N	$\tau_{15} = -n_2$
16	N	N	N	N	$\tau_{16} = -n_1$

weighted form

$$u_{flc} = \frac{\sum_{i=1}^{16} \mu_{\mathrm{R}^i} \tau_i}{\sum_{i=1}^{16} \mu_{\mathrm{R}^i}}.$$

Due to the symmetry in fuzzy rules design, we have $\sum_{i=1}^{16} \mu_{\mathrm{R}^i} = 1$, which yields

$$u_{flc} = \sum_{i=1}^{16} \mu_{\mathrm{R}^i} \tau_i. \tag{6.2}$$

6.2.2   FLC Output Parameter Tuning

The tuning of the FLC output value of each rule is a critical issue as it directly determines the control signal. First, note the skew symmetry between the ith rule and the $(17-i)$th rule ($i = 1 \sim 8$), that the input variables have opposite fuzzy labels P and N, we have the output skew symmetry that the two rules give the same control amplitude n_i but opposite directions. Therefore, there are eight output parameters in total to be determined.

Essentially, the FLC could be regarded as a feedback controller but with varying feedback gains,

$$u_{flc} = -\mathbf{k}(\mathbf{e})\mathbf{e}. \tag{6.3}$$

To stabilize the 2WMR system, feedback control should be taken appropriately for all states. A simple linear feedback controller can help to reveal how a feedback controller works, which inspires us to tune the eight output parameters $(n_1 \sim n_8)$ using the knowledge of a linear feedback controller.

The linear controller

$$\kappa = -\mathbf{k}\mathbf{e}, \tag{6.4}$$

where $\mathbf{k} = [k_1,\ k_2,\ k_3,\ k_4]$, is designed based on a linearized dynamic model at the desired equilibrium point and LQR method is applied to obtain the feedback gains. The detailed design of the LQR based linear controller is presented in Section 3.3, thus is omitted here.

The FLC output parameters are tuned in the following manner. At first, let one rule be fully activated and other 15 inhibited by setting the four input variables at the limits of their ranges ($\pm m_i$), respectively. For instance, for rule R_1 corresponding to $e_1 = $ P, $e_2 = $ P, $e_3 = $ P, $e_4 = $ P, we choose $e_i = m_i$, $i = 1, 2, 3, 4$. Then we can compare the output of the first fuzzy rule τ_1 with the output of the linear controller (6.4) with the same values of the four error quantities. In such circumstances, the value of linear controller output given by (6.4) is equal to the first FLC rule output, i.e., $\tau_1 = n_1 = -k_1 m_1 - k_2 m_2 - k_3 m_3 - k_4 m_4$. In this way we can determine all eight FLC output parameters τ_i, $i = 1, \cdots, 16$.

The advantages of using a linear controller to facilitate the FLC design are given as below. (1) There is lack of systematic parameter design for FLC in general. Trial and error design is time consuming due to the high dimension of parametric space, and often yields poor performance. It would be even more difficult to determine the FLC output parameters in this work because the 2WMR system is an underactuated and highly nonlinear system, which shows complex behaviors, especially the motions of the wheels. For instance, let the 2WMR be initially balanced at the origin, and a setpoint task with $x_d > 0$ is assigned, i.e., the robot is supposed to move forward. From human knowledge, a positive torque should be applied to drive the wheels move forward. However, through investigations, we found that to achieve a stable response, a negative torque should be applied at first, which makes the wheels move backward and the pendulum tilt rightward a bit. After that, the wheels start to move forward. In fact, this is the typical control behavior of non-minimum phase systems, and according to our theoretical analysis in Section 2.3.3, the underactuated 2WMR has an unstable internal dynamics. Considering the 2WMR complex behaviors, in this work, to determine the FLC output parameters, we utilize both the system model information and the knowledge of a linear feedback controller. The resulting FLC is able to produce a control signal profile that tallies with the desired one for non-minimum

phase systems.

(2) The linear control design based on LQR method offers a systematic design and can reveal how a feedback controller works. By aligning the FLC output with a linear controller output at sixteen particular operating points, at least it is guaranteed that the FLC uses the right feedback.

(3) For implementation, the parameter tuning is inevitable due to the difference between simulation and experiment. In this work, we do not need to tune the 16 FLC output parameters directly. Instead, we tune the four feedback gains for the linear controller, according to which, the FLC output parameters are computed. Thus, the tuning of the FLC output parameter in this work is much simpler than that in general FLC designs.

6.2.3   Steady State Analysis

As we discussed in Section 2.3.2, when system enters steady state, the pendulum equilibrium point is as

$$\theta_e = \arcsin \frac{r \sin \varphi (m_p + m_w)}{m_p l}. \tag{6.5}$$

Define the steady state error vector as $\mathbf{e}_s = [e_{1,s}, \, e_{2,s}, \, e_{3,s}, \, e_{4,s}]^T$, to make $e_{3,s} = 0$, it is reasonable to choose the reference for the pendulum angular as $\theta_r = \theta_e$. For the 2WMR with input coupling, when it is stabilized on a inclined surface ($\varphi \neq 0$), a torque, denoted as τ_s, should be provided to overcome the effect of gravity, and

$$\tau_s = r \sin \varphi (m_p + m_w) g. \tag{6.6}$$

At steady state, we have $(e_{2,s}, \, e_{3,s}, \, e_{4,s}) = (0, \, 0, \, 0)$, which yields $[\mu_P(e_{i,s}), \, \mu_N(e_{i,s})] = [0.5, \, 0.5]$, $i = 2, 3, 4$. It follows that

$$\mu_{R_i} = \begin{cases} \mu_P(e_1) \cdot 0.5^3 & \text{for } i = 1, \, 2, \, 5, \, 6, \, 9, \, 10, \, 13, \, 14 \\ \mu_N(e_1) \cdot 0.5^3 & \text{for } i = 3, \, 4, \, 7, \, 8, \, 11, \, 12, \, 15, \, 16 \end{cases}$$

The FLC in (6.2) becomes

$$u_{flc,s} = 0.125[\mu_{\text{P}}(e_{1,s}) - \mu_{\text{N}}(e_{1,s})] \sum_{i=1}^{8} n_i \tag{6.7}$$

When applying the FLC designed in (6.2) to the 2WMR which travels on an inclined surface, at steady state, we have $u_{flc,s} = \tau_s$. From the above equation, we have $\mu_{\text{P}}(e_{1,s}) - \mu_{\text{N}}(e_{1,s}) \neq 0$ since $\tau_s \neq 0$. From the membership function in (6.1), we can conclude that $e_{1,s} \neq 0$, i.e., there is a steady state error in the response of the wheel position.

In this work, to achieve a satisfactory response with zero steady-state error for the wheel position, i.e., $e_{1,s} = 0$, we introduce a compensation term β_c in the controller design, and $\beta_c = \tau_s$. The new control law is as

$$u = u_{flc} + \tau_s. \tag{6.8}$$

With the compensation term, now we have $u_{flc,s}$ in (6.7) equals zero, and $e_{1,s} = 0$.

6.3 Implementation and Experiment Results

6.3.1 Regulation Task

For implementation, we start with a simple control task that is to balance the 2WMR at the original position on a flat surface, i.e., $x_r = 0$, $v_r = 0$, and $\varphi = 0$.

Feedback gains for the linear controller (6.4) are obtained through LQR method and later manually tuned during the implementation, as presented in section 3.5. Based on the obtained feedback gains $\mathbf{k} = [-10, \ -0.5, \ -35, \ -1.5]$, the FLC output parameters are computed in the way introduced in section 6.2.2, and we have: $[n_1, \ n_2, \ n_3, \ n_4, \ n_5, \ n_6, \ n_7, \ n_8] = [23.79, 23.44, 13.79, 13.44, 23.19, 22.84, 13.19, 12.84]$. FLC in (6.8) is applied with $\tau_s = 0$ and $\theta_r = 0$. The experiment results are shown in Fig. 6.3. The FLC shows effectiveness that the 2WMR stays around the original position and the pendulum is balanced around $\theta = 0$. At
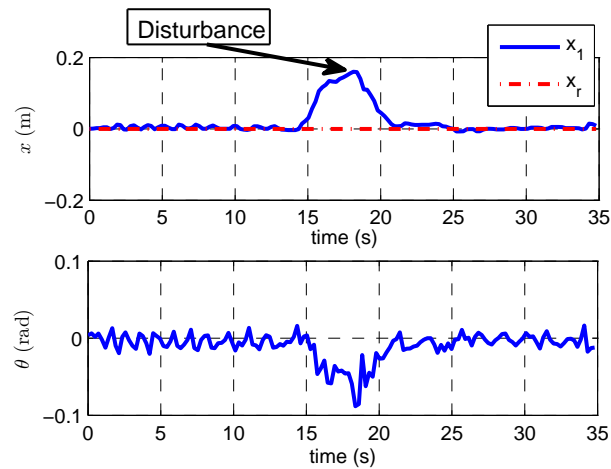
Figure 6.3: Experimental testing results for regulation task: time responses of x and θ under the FLC proposed in this work. The 2WMR is placed on a flat surface.

$t = 15$ s, we push the 2WMR to the right about 0.15 m, which can be considered as a disturbance to the system. The 2WMR moves backward and stops at the origin position within 3 seconds.
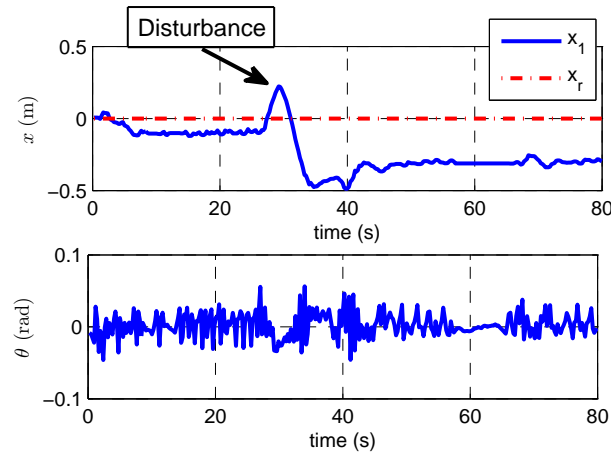
Figure 6.4: Experimental testing results for regulation task: time responses of x and θ under the FTPC [28]. The 2WMR is placed on a flat surface.

For comparison, the fuzzy traveling and position controller (FTPC) proposed in [28] is used to control the 2WMRs. Fig. 6.4 shows the experimental results for the 2WMR system under the FTPC [28]. The pendulum of the 2WMR can be stabilized, however, the wheel position control failed that steady state errors exist in the wheel position response, which shows the limitation

of the FTPC. From the experimental results shown in Fig. 6.3 and Fig. 6.4, it is evident that the

FLC proposed in this work provides a better performance than the FTPC proposed in [28] when

controlling the 2WMR.
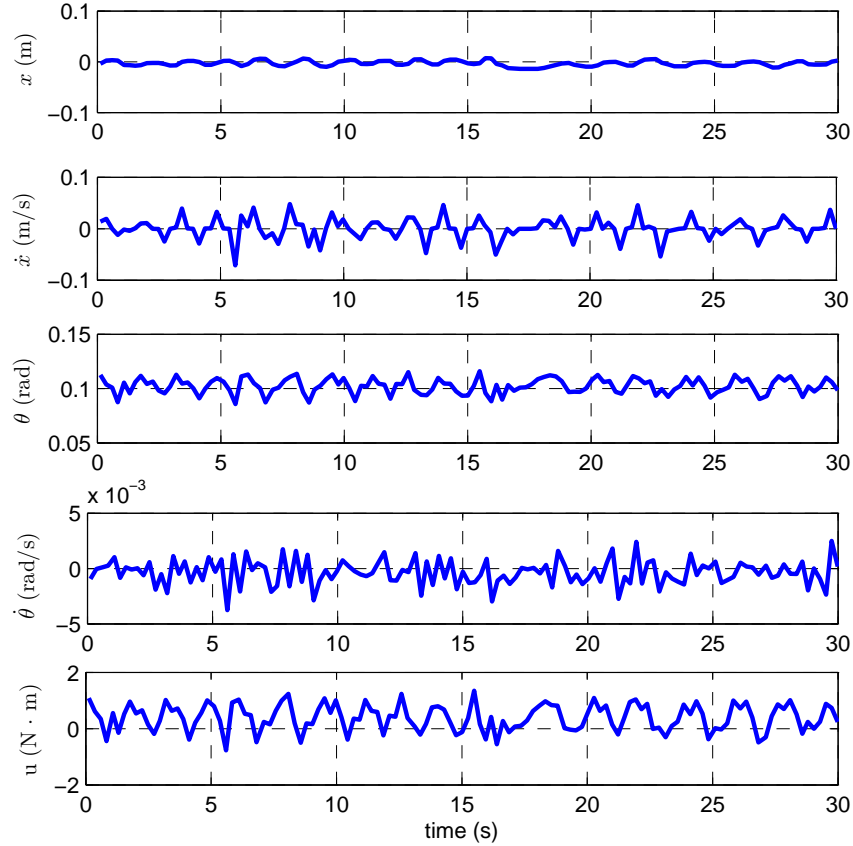
Figure 6.5: Experimental testing results for regulation task: time responses of x, $\dot{x}$, θ, $\dot{\theta}$ and u under FLC with $\theta_r = 0.09$ rad, $\tau_s = 0.1855$ N· m. The mobile robot is placed on inclined surface with $\varphi = 4.3°$.

Next, the robot is placed on an inclined surface with the slope angle $\varphi = 4.3°$. According

to (6.5) and (6.6), we have $\theta_r = 0.09$ rad and $\tau_s = 0.1855$ N·m. FLC in (6.8) is applied. Other

control parameters are chosen the same as in the preceding test. The experiment results are shown

in Fig. 6.5. The FLC shows effectiveness that the 2WMR stays around the original position and

the pendulum is balanced around $\theta = 0.1$ rad. It is also observed that the average value of the

control signal is positive.
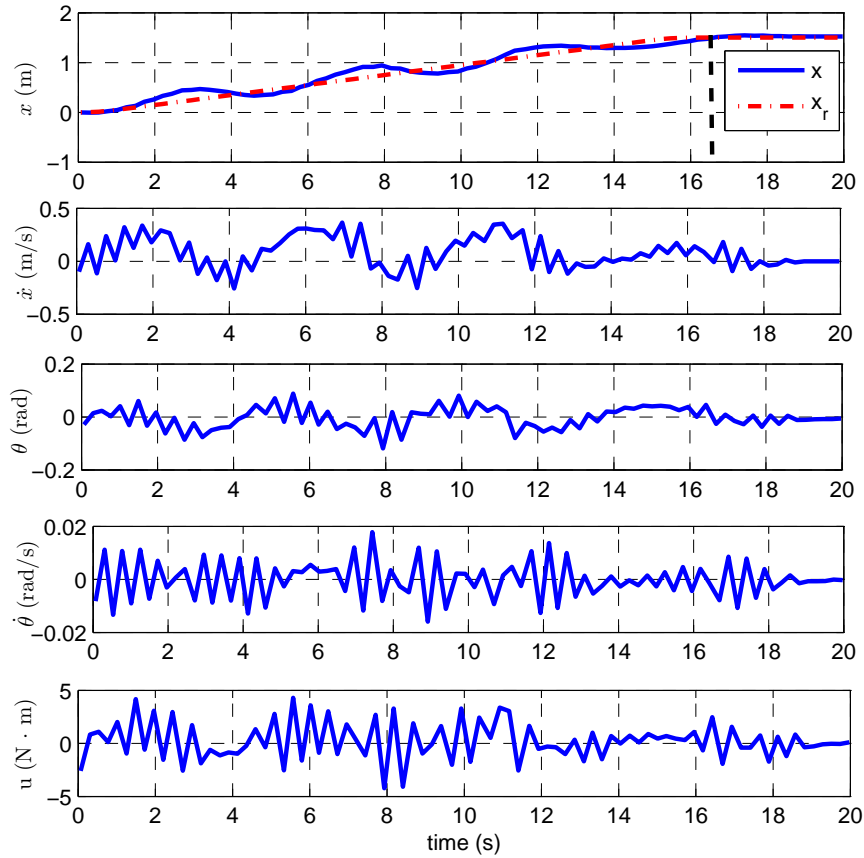
Figure 6.6: Experimental testing results for setpoint task: time responses of x, $\dot{x}$, θ, $\dot{\theta}$ and u under FLC with $\theta_r = 0$, $\tau_s = 0$. The mobile robot travels on flat surface. The reference trajectory (2.14) is applied.

6.3.2 Setpoint Task

First, we consider the 2WMR travels on a flat surface, i.e., $\varphi = 0$. The pre-planned references for the wheel position and velocity are applied, as shown in Fig. 2.4. The FLC parameters are chosen the same as for the regulation task. Experiment results are shown in Fig. 6.6. The 2WMR reaches the desired setpoint $x_d = 1.5$ m at $t = 16.5$ s and stays there afterwards. FLC shows the effectiveness for setpoint control of the 2WMR system. However, the response of the wheel position is not satisfactory because the backward motion exists.

To improve the 2WMR performance, especially the response of the wheel position, the modified reference trajectory $x_{r,n}$ in (5.30) is applied. The design of FLC is the same as in the

preceding test. Experiment results are shown in Fig. 6.7. We can see that the robot reaches the desired setpoint $x_d = 1.5$ m at $t = 13$ s and the pendulum is balanced around $\theta = 0$, i.e., the upright position. Compared with the results shown in Fig. 6.6, it is evident that the response of the wheel position in Fig. 6.6 is much smoother and the 2WMR arrives the desired position in a shorter time, which shows the effectiveness of the proposed modified reference trajectory $x_{r,n}$.
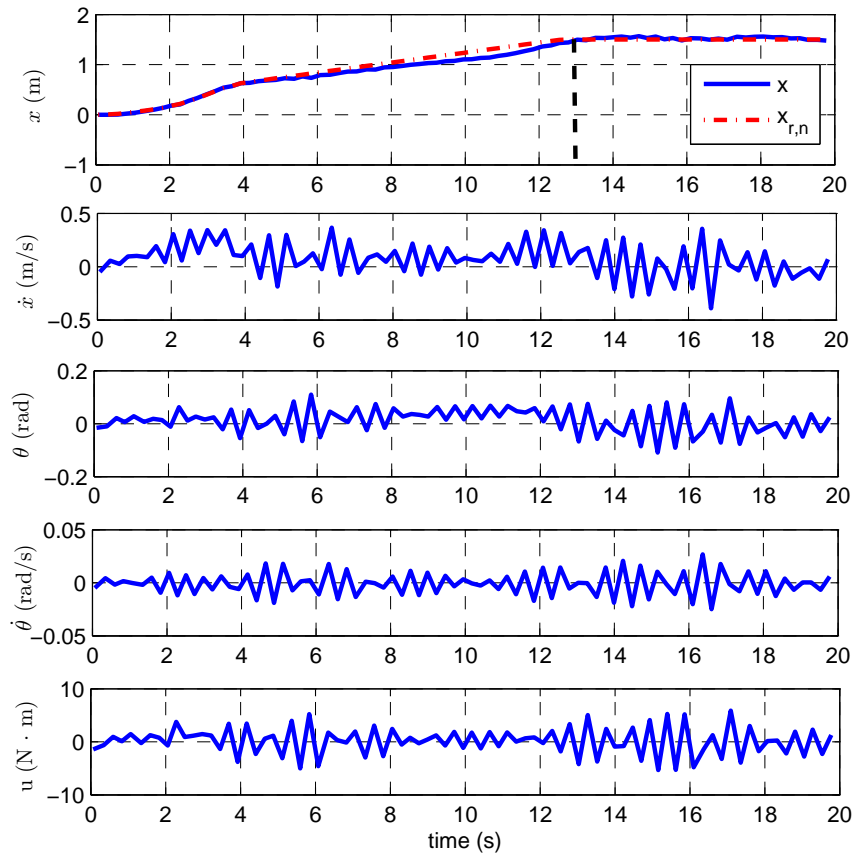
Figure 6.7: Experimental testing results for setpoint task: time responses of x, $\dot{x}$, θ, $\dot{\theta}$ and u under FLC with $\theta_r = 0$, $\tau_s = 0$. The mobile robot travels on flat surface. Modified reference trajectory (5.30) is applied.

Next, we consider the mobile robot travels on an inclined surface with the slope angle $\varphi = 2.45°$. According to (6.5) and (6.6), we have $\theta_r = 0.05$ rad and $\tau_s = 0.1$ N·m. To obtain a smooth and fast response, similarly, the reference trajectory in (5.30) is used. The experiment results are shown in Fig. 6.8. we can see that the robot travels smoothly and reaches the desired position

without steady state error. The pendulum is balanced around $\theta = 0.05$ rad.
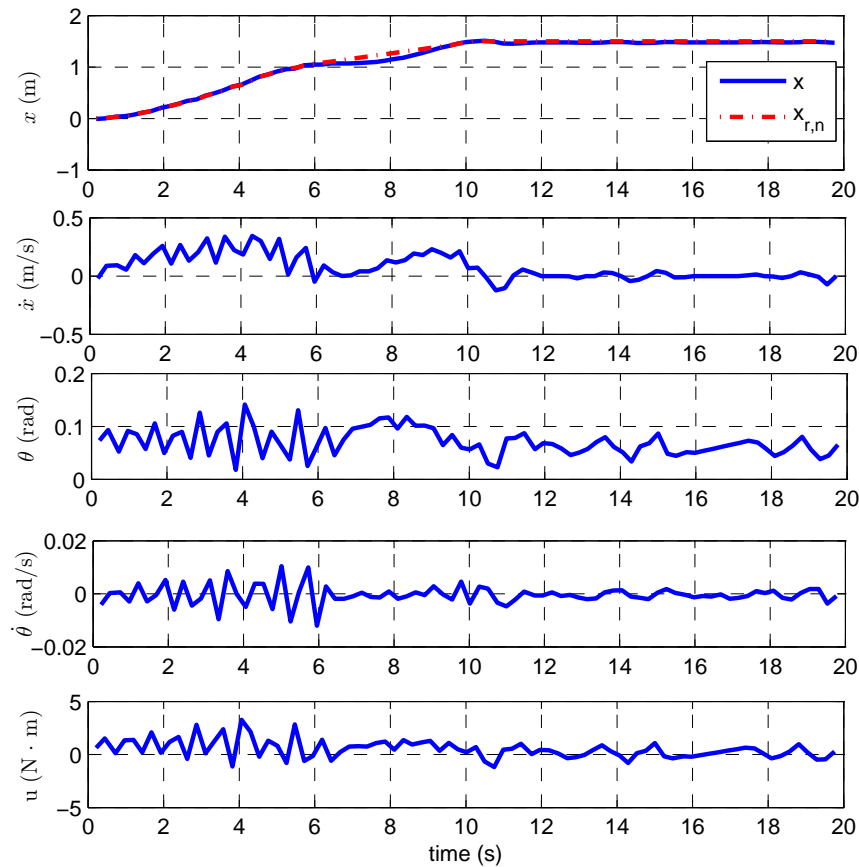
Figure 6.8: Experimental testing results for setpoint task: time responses of x, $\dot{x}$, θ, $\dot{\theta}$ and u under FLC with $\theta_r = 0.05$ rad, $\tau_s = 0.106$ N·m. The mobile robot travels on inclined surface with $\varphi = 2.5°$. Modified reference trajectory (5.30) is applied.

6.3.3 Discussions

From experimental testings, it is found that the designed FLC outperforms the linear controller. For linear controller with fixed feedback gains, when high gains are applied, the system does not perform well during the traveling and when low gains are applied, the system could easily become unstable for regulation task or after the setpoint is reached. The FLC shows effectiveness for various control tasks under a group of fixed controller parameters. The reason is that FLC functions as a feedback controller with varying gains, as we stated in Subsection III B. For

a clear explanation, we have conducted the following analysis. Fig. 6.9 shows the comparisons between the fixed feedback gains of a linear controller and the equivalent feedback gains of the FLC, which are computed in the following manner,

$$k_i = \frac{u_{flc}}{e_i} \ \text{ at } \ e_j = 0 \ \ (i, j = 1, 2, 3, 4 \text{ and } j \neq i).$$

For the calculation of k_1, let $(e_2, e_3, e_4) = (0, 0, 0)$, from Fig. 6.1, we have $[\mu_P(e_j), \mu_N(e_j)] = [0.5, 0.5]$, $j = 2, 3, 4$. It follows that

$$\mu_{R^i} = \begin{cases} \mu_P(e_1) \cdot 0.5^3 & \text{for } i = 1,\ 2,\ 5,\ 6,\ 9,\ 10,\ 13,\ 14 \\ \mu_N(e_1) \cdot 0.5^3 & \text{for } i = 3,\ 4,\ 7,\ 8,\ 11,\ 12,\ 15,\ 16 \end{cases}$$

We have

$$k_1(e_1) = \frac{u_{flc}}{e_1} = \frac{0.125[\mu_P(e_1) - \mu_N(e_1)]}{e_1} \sum_{i=1}^{8} n_i. \tag{6.9}$$

Similarly, we have

$$k_j(e_j) = \frac{u_{flc}}{e_j} = \frac{0.125[\mu_P(e_j) - \mu_N(e_j)]}{e_j} \sum_{i=1}^{8} n_i, \ \ j = 2, 3, 4. \tag{6.10}$$

Since $\sum_{i=1}^{8} n_i$ is a constant, it can be concluded that the equivalent feedback gains of the FLC are determined by the membership functions.

From Fig. 6.9, we can see that $|k_j|$ drops as e_j increase, which is desirable for the real implementation. When the states of the 2WMR are close to the desired values, i.e., the error states **e** are small, the control signal is small. High gains are needed to achieve robustness, considering the fact that the real-time platform is under various uncertainties, such as joint friction, ground friction, backslash, unmodeled motor dynamics, etc. When the states of the 2WMR are away from the desired values, i.e., the error states **e** are large, a group of relatively lower gains are preferred, considering that the motor capacity is limited and the control signal could be saturated if high gains are applied, which would devastate the effectiveness of the feedback controller. FLC with the selected membership function (6.1) provides such varying gains that are adapted to the
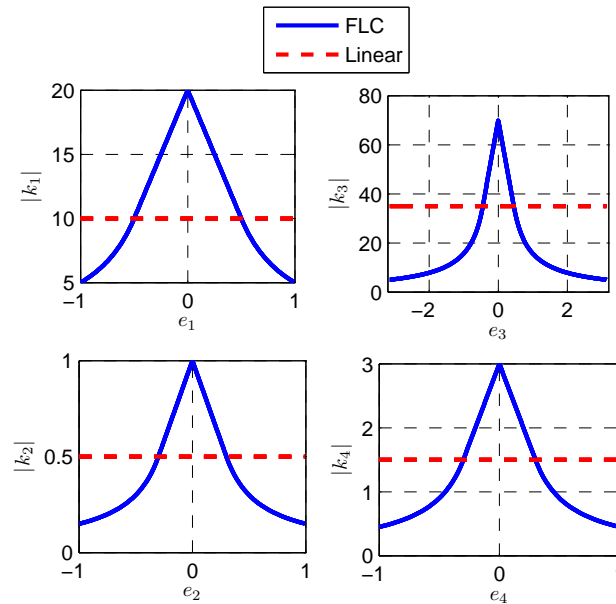
Figure 6.9: Comparisons between the fixed feedback gains of a linear controller and the equivalent feedback gains of the FLC.

current states of the 2WMR, which indicates the advantage of the selected membership functions and explains that the designed FLC outperforms the linear controller.

6.4 Conclusions

In this chapter, synthesized design of a T-S type fuzzy logic controller for an underactuated 2WMR is presented. The FLC design is based on both human experience and information of the system dynamic model. The proposed FLC is successfully implemented on the real-time platform and shows effectiveness. The new FLC outperforms a linear controller, even though the FLC output parameters are tuned according the output of the linear controller at certain operating points. The design procedure indicates that we can easily extend a linear controller to a nonlinear one like FLC to achieve better performance.

Chapter 7

Synthesized Design of a Fuzzy Logic Controller with Iterative Learning

7.1 Introduction

The controllers proposed in the previous three chapters are model based designs. Considering that system model is usually quite difficult to obtain in practice, model free or partially model free designs are preferred in real life applications. In this chapter, our aim is to develop a pure FLC without incorporating any model-based controller, and hence an accurate mathematic model is not required.

In [38], an adaptive FLC is proposed for a wheeled inverted pendulum with parametric and functional uncertainties, which is a model free design. The use of fuzzy approximations avoids the need to develop a highly accurate mathematic model. However, the fuzzy approximator uses 324 fuzzy rules and computation for the control signal could be time-consuming. In general, application of model-free FLC design for real life plants could be problematic considering the large number of fuzzy rules and controller parameters to be determined. Furthermore, the heuristic knowledge could be limited for control of system which has complex dynamic or behaves in a complicated manner, such as the underactuated 2WMR. A better alternative is to synergize a

model-free design with heuristic knowledge and a model-based design with an available plant model, so that all information relevant to the control system can be fully utilized in FLC design.

Similarly as in Chapter 6, for the simplicity in design, a T-S type FLC is adopted. On the basis of human experience, an FLC with three input variables and six fuzzy rules is first explored for regulation control. Six controller parameters need to be tuned. Three range parameters specify the universe of discourse of the input variables and were chosen using heuristic knowledge such as the physical boundaries for the input variables. The other three are output parameters that determine control output values for individual rules. In general, it is difficult to determine the output parameters based only on human intuition or heuristics.

The limitations of heuristic knowledge and model-free design motivate us to explore design based partially on a model. To capture the correct feedback control action for each state, a linear controller is designed based on a linearized model of the 2WMR. The linearization is performed around the desired balance position, when the inverted pendulum is upright. Necessary conditions for the feedback gains are established to ensure local stability around the desired equilibrium point. Next, conditions for selection of the FLC output parameters are identified, which makes parameter determination much easier. Considering the presence of uncertainties and disturbances in practice, an FLC with integral action is further proposed.

To improve FLC performance and avoid tedious manual tuning, a partially model-free iterative learning tuning (ILT) method is used to tune the FLC output parameters. The ILT process consists of three steps. First, a number of cost functions chosen to characterize 2WMR behavior are calculated according to 2WMR responses in the time domain. Next, an iterative learning algorithm is derived to minimize the cost functions and then used to update the FLC output parameters. After parametric updating, the same motion control task is executed again and the 2WMR responses are recorded for the next ILT run. The ILT only requires the process gradient infor-

mation in selecting the learning gain, and hence guarantees learning convergence. Furthermore, the gradient can be numerically approximated when gradient information is not available [80]. In this sense, the ILT is partially model-free.

The main contributions and originality of this chapter are summarized as follows.

(i) Synthesized FLC design is proposed for velocity control of the underactuated 2WMR system in the presence of disturbances and model uncertainties. The synthesized design consists of three phases: determination of the FLC structure through heuristic knowledge about the 2WMR; quantitative determination of the output parameters for stabilization of the 2WMR; and tuning of the FLC output parameters using ILT. The main idea behind the proposed methodology is to maximize utilization of all the information available, which is achieved by combining partially model-based and partially model-free designs, and hence improve the FLC performance.

(ii) Compared with model-based control design, the synthesized FLC design has the advantage that it does not require an accurate model of 2WMR system. The fuzzy rules, membership functions, direction of control action for the fuzzy output parameters, and cost function selection for the ILT are all determined by human experience. The relative amplitudes of the output parameters for different fuzzy rules are determined based on a linearized model. However, the values of the 2WMR parameters are not required to be known in the linearized model. Compared with conventional FLC and FLCs designed in [38] [70], the synthesized FLC developed in this work has fewer fuzzy rules and fewer parameters to be determined, which implies a simpler design.

(iii) The synthesized FLC is intelligent in the sense that learning is incorporated in FLC parameter tuning. Selection of the objective functions is based on human experience and the choice of different key features from the 2WMR responses is flexible for meeting different control requirements. The learning process is similar to human learning, which utilizes knowledge about not only successful but also unsuccessful trials.

The remainder of this chapter is organized as follows. In Section 7.2, FLC designs are elaborated, including the basic FLC structure, FLC speed control, and FLC speed control with integral action. The principle of ILT is presented in Section 7.3 and the FLC output parameters are updated using ILT. Conclusions are drawn in Section 7.4.

7.2   Synthesized Design of FLC

FLC with three input variables is first explored for the regulation task. We focus on determining the output parameter for each fuzzy rule, which is critical in T-S FLC design. First, to simplify the FLC design, a minimum number of fuzzy rules are used, which yields a minimum number of output parameters to be determined. Second, the direction of the control action (sign of the output parameters, positive or negative) is chosen by following the direction of the pendulum tilt angle. Next, the relative amplitudes of the output parameters for different rules are analyzed using the feedback knowledge of a linear controller, which is designed based on a linearized model of the 2WMR. Linearization is performed around the desired balance position, namely when the inverted pendulum is upright. Necessary conditions for the feedback gains are established to ensure local stability around the desired equilibrium point. Considering the presence of uncertainties and disturbances for a practical 2WMR, FLC with integral action is further proposed.

7.2.1   Fuzzy Logic Speed Controller

States $(x_2, x_3, x_4) = (\dot{x}, \theta, \dot{\theta})$ are the FLC input variables. Each of the input variables is associated with two fuzzy sets, positive (P) and negative (N). The membership functions adopted to represent the fuzzy sets P and N are the same as in Chapter 6, which are illustrated in Fig. 6.1. Let μ_P and μ_N denote the degree of matching to the fuzzy sets P and N, respectively. μ_P is given by (6.1) and $\mu_N = 1 - \mu_P$. The parameters $[m_1, m_2, m_3]$ in the membership function

Table 7.1: Fuzzy rules for the speed controller in the regulation task

Rule	$\dot{x}$	θ	$\dot{\theta}$	u
1	$\times$	P	P	$\tau_1 = +n_1$
2	P	P	N	$\tau_2 = +n_2$
3	N	P	N	$\tau_3 = +n_3$
4	P	N	P	$\tau_4 = -n_3$
5	N	N	P	$\tau_5 = -n_2$
6	$\times$	N	N	$\tau_6 = -n_1$

are determined under consideration of the physical constraints of the 2WMR system, as we have discussed in Chapter 6.

To derive fuzzy rules, we start with a regulation control task, namely, $v_r = 0$. Since there are three input variables and each variable is associated with two fuzzy sets P and N, we could have $2^3 = 8$ fuzzy rules in total. However, to simplify the FLC design, the number of fuzzy rules is minimized by combining several cases into one. Table 7.1 summarizes the six FLC rules, where $\times$ denotes either N or P. Fig. 7.1 shows a graphical representation of the six rules corresponding to six scenarios. Let $(\cdot, \cdot, \cdot)$ denote a fuzzy state with respect to three variables $(\dot{x}, \theta, \dot{\theta})$ and $\cdot$ is either P or N. R^1 is a combination of the two cases (P,P,P) and (N,P,P), and R^6 is a combination of the two cases (P,N,N) and (N,N,N).

FLC consists of rules in the following form:

$$\text{R}^i : \text{If } (\dot{x} \text{ is } A_i) \text{ AND } (\theta \text{ is } B_i) \text{ AND } (\dot{\theta} \text{ is } C_i), \text{ THEN } (u_i = \tau_i),$$

where $A_i, B_i, C_i \in \{\text{P,N}\}$ are fuzzy sets, u_i is the rule output and τ_i is a constant representing the inferred control torque. Each fuzzy rule describes a specific relationship between the FLC inputs and output.

Each rule contributes to the final FLC output according to matching for the IF part of the
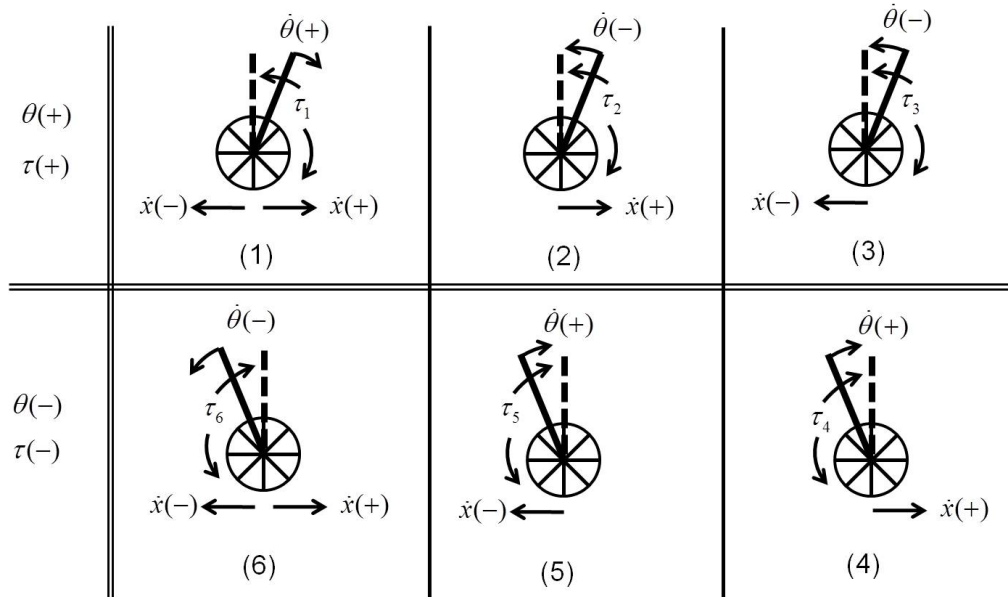
Figure 7.1: Graphical representation of the fuzzy rules corresponding to six scenarios. Each scenario is associated with a rule, namely, scenario (i) is associated with rule i for $i = i, \cdots, 6$. The control priority is to balance the pendulum. When θ is P, as shown in scenarios (1)–(3), a positive torque is provided so that the wheels move rightwards and the pendulum moves anticlockwise, regardless of the values of $\dot{x}$ and $\dot{\theta}$. Likewise, when θ is N, as shown in scenarios (4)–(6), a negative torque is provided so that the wheels move leftwards and the pendulum moves clockwise. In this way, rules 1–3 have positive outputs and rules 4–6 have negative outputs.
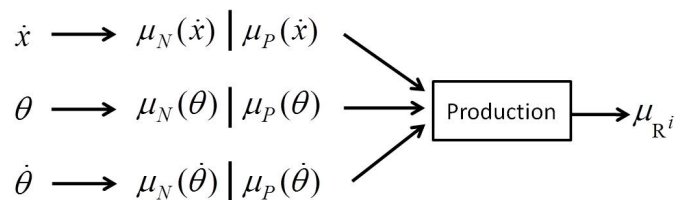
Figure 7.2: T-S type fuzzy inference for the ith rule of the FLC. Each input yields two membership values, μ_N and μ_P. The AND logic operator is chosen for production of the fuzzy membership values.

fuzzy rule. The output τ_i for each rule is weighted by the firing strength μ_{R^i} for that rule. The calculation for the firing strength for each rule is shown in Fig. 7.2. The TS-type fuzzy inference takes a weighted average of the individual outputs for each rule, and the final output of the fuzzy controller is computed as

$$u = \frac{\sum_{i=1}^{6} \mu_{R^i} \tau_i}{\sum_{i=1}^{6} \mu_{R^i}}, \tag{7.1}$$

Now we derive the amplitudes of the control outputs. Note the skew symmetry between scenarios (1) and (6), and hence rules 1 and 6, whereby the input variables have opposite fuzzy labels P and N. We have output skew symmetry whereby the two rules give the same control amplitude n_1 but in opposite directions. Similar skew symmetry can be observed between rules 2 and 5, and between rules 3 and 4. Thus, only three output parameters $n_i > 0$, $(i = 1, 2, 3)$ need to be determined. In scenario (1), the pendulum tilt angle and angular velocity are in the same direction $(\theta > 0, \dot{\theta} > 0)$, and thus the pendulum tends to fall down clockwise. In scenarios (2) and (3), the pendulum tilt angle and angular velocity are in opposite directions $(\theta > 0, \dot{\theta} < 0)$, and thus the pendulum returned to the balance position. Intuitively, a larger torque should be applied in scenario (1) to bring the pendulum back to the balance position, i.e., we should choose $n_1 > n_i$ $(i = 2, 3)$.

Next we need to decide the relative amplitudes of n_2 and n_3. The only difference between scenarios (2) and (3) is the direction of the wheel velocity, and thus deciding the relative amplitudes of n_2 and n_3 involves control of the wheels. However, the difference in velocity is not adequate for deciding the relative amplitudes of n_2 and n_3. From Newton's mechanical law, pendulum motion is related to wheel acceleration instead of velocity, as we can observe from the 2WMR dynamic equations (2.1) and (2.2). In many practical control tasks, acceleration is not available. For mechanical systems such as a 2WMR, the full state feedback uses only position

and velocity information.

Since n_2 and n_3 cannot be decided using intuitive derivation or heuristic knowledge, trial and error is an alternative. Through numerical tests, we find that $n_2 < n_3$ yields unstable responses, and $n_2 > n_3$ leads to stable behavior. Nevertheless, in this study we seek a systematic way to determine the FLC parameters, in particular the relative amplitudes of n_2 and n_3.

FLC can be regarded as a state feedback controller with varying feedback gains. In fact, from Fig. 7.2 and (7.1), the control output can be expressed as $u = -\mathbf{k}(\mathbf{x})\mathbf{x}$. To stabilize the 2WMR system, feedback control should be taken appropriately for all states. A linear controller helps to reveal how a feedback controller works. Based on the linearized model in (A.5), we design a linear controller as

$$u = -\mathbf{k}\mathbf{x} = -k_2 x_2 - k_3 x_3 - k_4 x_4, \tag{7.2}$$

where $\mathbf{k} = [k_2,\ k_3,\ k_4]$ is the feedback gain vector. To ensure local stability of the desired equilibrium point, all feedback gains need to be negative, i.e., $k_2 < 0$, $k_3 < 0$, $k_4 < 0$ (refer to Appendix A.3).

Remark 7.1 *Conditions $k_i < 0$, $(i = 2,3,4)$ are established without knowing the values of the 2WMR parameters.*

Note that the feedback term associated with x_2 is $-k_2 x_2$. In scenario (2), where x_2 is P, $-k_2 x_2 > 0$. On the contrary, in scenario (3), where x_2 is N, $-k_2 x_2 < 0$. Thus, when states (x_3, x_4) in scenario (2) are of the same value as in case (3), the control output in scenario (2) should be greater than that in case (3). Therefore, we have $n_2 > n_3$, which is consistent with the numerical tests.

The FLC with six rules is directly applicable to setpoint control by replacing x_2 with e_2 as the first input variable. To verify the effectiveness of the proposed FLC, choose $[n_1,\ n_2,\ n_3] =$

[5, 2, 1.5]. The desired velocity for the wheel is $v_r = 0.2$ m/s. The results are shown in Fig. 7.3.

Setpoint control of the wheel velocity is achieved while the pendulum is balanced.

Figure 7.3: Time responses of the wheel velocity, the pendulum tilt angle and the control signal profile under setpoint control with $v_r = 0.2$ m/s. The FLC consists of six rules.

In practice, disturbances and model uncertainties exist in the 2WMR system, such as friction f_r and slope φ. Assume that the 2WMR travels on a tilted surface with $\varphi = 2°$ and the friction is $f_r = 0.2\dot{x} + 0.1sgn(\dot{x})$. The results are shown in Fig. 7.4. The 2WMR fails to follow the desired velocity of 0.2 m/s; in other words, the FL speed controller is not robust for exogenous disturbances and model uncertainties.

Figure 7.4: Time responses of the wheel velocity, the pendulum tilt angle and the control signal profile under setpoint control $v_r = 0.2$ m/s in the presence of unknown friction and slope. The FLC consists of six rules.

7.2.2   Fuzzy Logic Speed Controller With Integral Action

To enhance the FLC robustness, we introduce another input, $E_I = \int_0^t (\dot{x} - v_r)d\tau$, which is the integration of the wheel velocity error. Input E_I is also associated with two fuzzy sets P and N, and the degree to which set the values belong to is determined by the membership functions illustrated in Fig. 6.1. We assume that the average value of the velocity tracking error e_2 for the whole test time, i.e., $1/t_s \cdot \int_0^{t_s} (\dot{x} - v_r)d\tau$, should be approximately 0.1 m/s. Thus, the range for E_I is chosen to be approximately $m_1 = 0.1t_s$ m. The ranges of other input variables $(e_2, \theta, \dot{\theta})$ are as $[m_2, m_3, m_4] = [0.5, \pi/3, 2]$.

For a conventional FLC design, we could have $2^4 = 16$ fuzzy rules. Similarly, the number of fuzzy rules is minimized to simplify the FLC design. Fuzzy rules are shown in Table 7.2. R^1 is a combination of four cases, (P,P,P,P), (P,N,P,P), (N,P,P,P) and (N,N,P,P), and R^{10} is a combination of four cases, (P,P,N,N), (P,N,N,N), (N,P,N,N) and (N,N,N,N). Here R^1 and R^{10} describe the same cases as R^1 and R^6 do in Table 7.1. R^2 and R^3 in Table 7.2 are obtained from R^2 in Table 7.1 with additional P and N for E_I. Similarly, we establish rules $R^4 \sim R^9$.

FLC consists of rules in the following form:

R^i : If $(E_I$ is $A_i)$ AND $(e_2$ is $B_i)$ AND $(e_3$ is $C_i)$ AND $(e_4$ is $D_i)$, THEN $(u_i = \tau_i)$,

where A_i, B_i, C_i, $D_i \in \{P,N\}$ are fuzzy sets, u_i is the rule output and τ_i is a constant representing the inferred control torque.

There are five output parameters, n_1–n_5, to be determined. First, considering that θ and $\dot{\theta}$ are in the same direction in R^1 and R^{10}, based on the analysis in Section 7.2.1, we have $n_1 > n_i > 0$ $(i = 2, 3, 4, 5)$. Next, we use feedback knowledge from a linear controller to determine the relative amplitude of n_2–n_5 because intuitive derivation is not straightforward.

With the additional state E_I, we have an augmented linearized state space model as given in (A.9). Now the linear feedback control law is $u = -\mathbf{ke}$ with $\mathbf{k} = [k_1, k_2, k_3, k_4]$. To ensure local

Table 7.2: Fuzzy rules for a speed controller with integral action for the setpoint task

Rule	E_I	$e_2(\dot{x}-\dot{x}_r)$	$e_3(\theta-0)$	$e_4(\dot{\theta}-0)$	u
1	$\times$	$\times$	P	P	$\tau_1 = +n_1$
2	P	P	P	N	$\tau_2 = +n_2$
3	N	P	P	N	$\tau_3 = +n_3$
4	P	N	P	N	$\tau_4 = +n_4$
5	N	N	P	N	$\tau_5 = +n_5$
6	P	P	N	P	$\tau_6 = -n_5$
7	N	P	N	P	$\tau_7 = -n_4$
8	P	N	N	P	$\tau_8 = -n_3$
9	N	N	N	P	$\tau_9 = -n_2$
10	$\times$	$\times$	N	N	$\tau_{10} = -n_1$

stability of the desired equilibrium point, all the feedback gains need to be negative (refer to Appendix A.4).

The relative amplitudes of the output parameters are determined by adopting the method used in Section 3.2. Between R^2 and R^3 or R^4 and R^5, the only difference in fuzzy inputs is P and N for E_I. Thus, the control output for rules with positive E_I should be greater than that for rules with negative E_I, that is, $n_2 > n_3$, $n_4 > n_5$. Between R^2 and R^4 or R^3 and R^5, the only difference in fuzzy inputs is P and N for e_1. Thus the control output for rules with positive e_2 should be greater than that for rules with negative e_2, that is, $n_2 > n_4$ and $n_3 > n_5$. To simplify the design, we could choose $n_3 = n_4$. To summarize, we have $n_2 > n_3 = n_4 > n_5$.

Calculation of the firing strength for each rule is shown in Fig. 7.5. The final output of the fuzzy controller is computed as

$$u = \frac{\sum_{i=1}^{10} \mu_{R_i} \tau_i}{\sum_{i=1}^{10} \mu_{R_i}}. \tag{7.3}$$

FLC with ten rules is applied with $[n_1, n_2, n_3, n_4, n_5] = [8, 4.5, 1.2, 1.2, 0.6]$, and param-

$$E_1 \longrightarrow \mu_N(E_1)\big|\mu_P(E_1)$$

$$e_2 \longrightarrow \mu_N(e_2)\big|\mu_P(e_2)$$

$$\theta \longrightarrow \mu_N(\theta)\big|\mu_P(\theta)$$

$$\dot{\theta} \longrightarrow \mu_N(\dot{\theta})\big|\mu_P(\dot{\theta})$$

Production $\longrightarrow \mu_{R^i}$
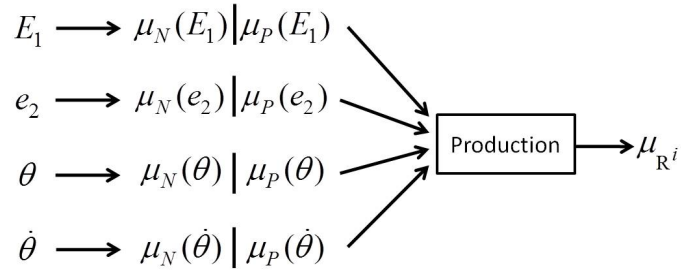
Figure 7.5: T-S type fuzzy inference for the ith rule of the FLC with integral action.

eter ranges $[m_1, m_2, m_3, m_4] = [5, 0.5, \pi/3, 2]$. The friction and slope are present as in the preceding example. The simulation results are shown in Fig. 7.6. The wheel velocity reaches the desired value of 0.2 m/s while the pendulum is balanced at a new equilibrium point, $\theta = 1.5011°$. The results can be explained as follows.

When system is in a steady state, we have $\ddot{x},\ \ddot{\theta},\ \dot{\theta} = 0$. From the 2WMR dynamic equation (2.1), $\tau = \sin\varphi(m_w + m_p)gr + rf_r$ is obtained. From (2.2), we obtain $\theta = \arcsin(\tau/m_plg)$. It is clear that to maintain a constant velocity, a constant torque is needed to overcome the effects of friction and slope, which thus results in a new balance position for the pendulum.
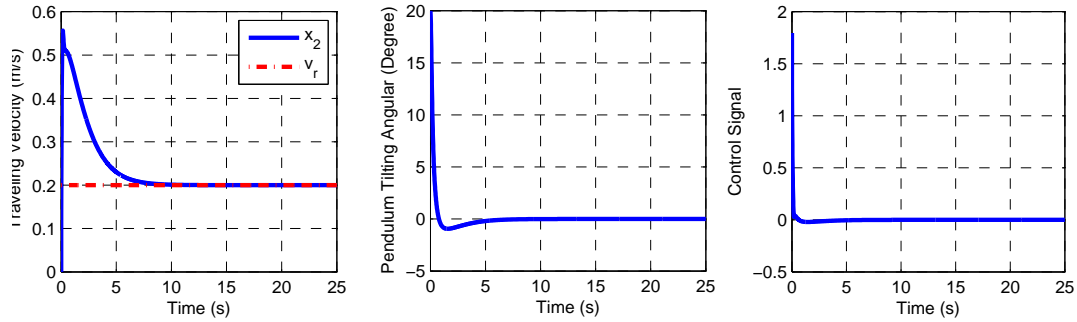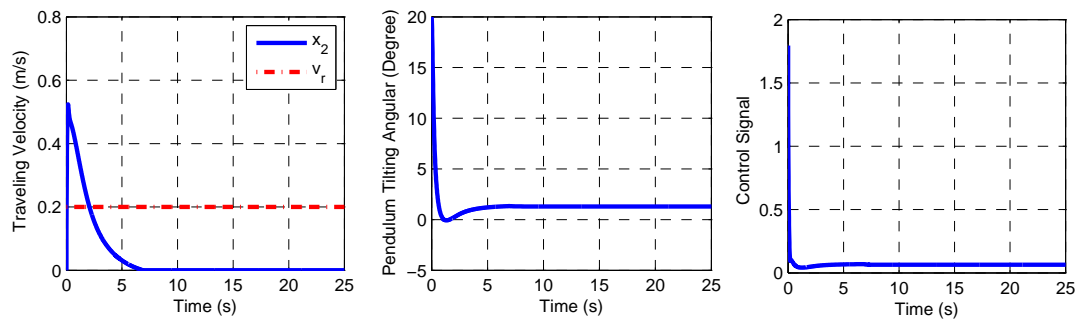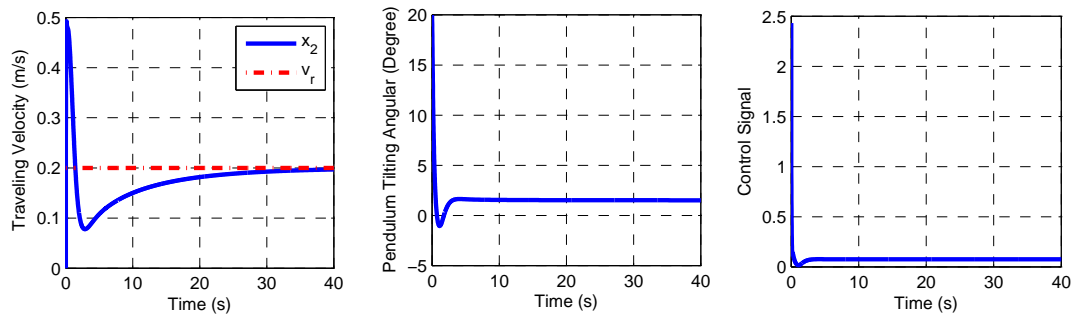

Figure 7.6: Time responses of the wheel velocity, the pendulum tilt angle and the control signal profile under setpoint control with $v_r = 0.2$ m/s in the presence of unknown friction and slope. The FLC consists of ten rules.

7.3 FLC With Iterative Tuning

The relative amplitudes of n_i are given in the previous section. Parameter tuning now needs to be addressed, but manual tuning is a tedious and time-consuming process. Tuning becomes even more challenging when model mismatch exists, for instance when the pendulum mass m_p and slope φ are unknown and if the actuator dynamics are not modeled. We use ILT to tune the output parameters. This problem is formulated as a minimization process with respect to a selected cost function. Parameter tuning is carried out via an updating law that is derived using gradient information to minimize the cost function iteratively. The result after tuning is an optimal solution with respect to the formulated cost function. With the ILT, the FLC design allows unstable system responses in the first few trials, so the initial values for the output parameters can be freely assigned. Given that the system response is unstable with the initial parameters, after the first IL tuning stage, a stable response can be reached. After further fine tuning, stable and fairly good performance can be achieved.

7.3.1 Selection of The Cost Function

Let t_s denote the time duration for an evaluation period. We consider the overall performance in the interval $[t_0, t_s]$. Different indices and features of 2WMR behavior can be used to evaluate the control performance, which can be either a stable or an unstable response. From a practical point of view, if $|\theta| > \pi/2$, we consider that the controller failed. We define t_w as the total time for which the pendulum stays above the horizontal plane, i.e., $|\theta| < \pi/2$ for $t \in [0, t_w]$.

For an unstable response $(t_w < t_s)$, the following index can be used to evaluate the performance:

$$G_1 = \frac{10}{t_w + 0.01}.$$

A smaller G_1 implies a larger t_w and hence a more stable response.

For a stable response $(t_w = t_s)$, the following indexes can be chosen to evaluate the 2WMR performance. To keep the pendulum around the balance position, we can use

$$\int_0^{t_s} |\theta|^q dt, \quad \text{or} \quad \max(|\theta|),$$

where q is a positive number. To avoid sharp changes in the pendulum angle and reduce pendulum oscillation, we can use

$$\int_0^{t_s} |\dot{\theta}|^q dt, \quad \text{or} \quad \max(|\dot{\theta}|).$$

To achieve a velocity tracking task, we may consider

$$\int_0^{t_s} |e_2|^q dt, \quad \text{or} \quad \max(|e_2|).$$

Since saturation problems commonly exist in real situations, to avoid a large control signal we can use

$$\int_0^{t_s} |u|^q dt, \quad \text{or} \quad \sum n_i \ (i = 1, \cdots, 5).$$

When multiple performance indexes are taken into consideration, controller design and tuning become a multi-objective optimization issue, which can be reduced to a scalar case using weighted sums. For instance, a cost function as the weighted sum of all the indices is

$$G_2 = \mathbf{w}^T \mathbf{f}, \tag{7.4}$$

where $\mathbf{w}$ is a vector of weighting coefficients and $\mathbf{f}$ is a vector of selected indices.

We can take various costs, not limited to those mentioned above, into consideration, such as the settling time, model nonlinearities and the linear approximation error. To meet different

control requirements, we need to choose different performance indices and different weighting values.

Remark 7.2 *The cost function is selected based on human experience, which captures the key features of the 2WMR response.*

For fuzzy logic speed controller with integral action, there are five output parameters, n_i ($i = 1, 2, 3, 4, 5$), to be determined. Note that $n_1 > n_2 > n_3 = n_4 > n_5$. We define $p_1 = n_1 - n_2$, $p_2 = n_2 - n_3$ and $p_3 = n_4 - n_5$, and denote $\mathbf{p} = [p_1, p_2, p_3]^T$, where p_1, p_2, $p_3 > 0$. n_5 is fixed at a given value, although it can also be learned. $\mathbf{p}$ is tuned to achieve satisfactory performance.

The tuning procedure for $\mathbf{p}$ can be divided into two parts. For a given initial value of $\mathbf{p}$, denoted as $\mathbf{p}_0$, if the first trial fails (i.e., unstable position), the cost function J is chosen to be G_1. The objective is to increase the time t_w for which a stable response lasts, and finally reach $J_{min} = 10/(t_s + 0.01)$, whereby the updated $\mathbf{p}$ makes the pendulum stay above the horizontal plane during the whole evaluation period. Then we switch to cost function $J = G_2$ for fine tuning. Note that now the optimal design is to minimize the cost function J by updating $\mathbf{p}$, which is in fact a search task:

$$\min_{\mathbf{p} \in \Omega_{\mathbf{p}}} J(\mathbf{e}, \mathbf{p}),$$

where $\Omega_{\mathbf{p}} = \{\mathbf{p} \in \mathbb{R}^3 | p_1 > 0, \ p_2 > 0, \ p_3 > 0\}$.

We propose the following typical first-order ILT law:

$$\mathbf{p}_{i+1} = \mathbf{p}_i - \gamma_i J_i,$$

where the subscript i denotes the ith updating, $\mathbf{p} = [p_{1,i}, \ p_{2,i}, \ p_{3,i}]^T$. $\gamma_i = [\gamma_{1,i}, \ \gamma_{2,i}, \ \gamma_{3,i}]^T$ is a learning gain vector that should be chosen to ensure the convergence of J_i. To speed up the learning process, the learning gain is chosen to be the inverse of the gradient $\partial J/\partial p$. When the

gradient is not available analytically, a numerically computed gradient can be used [80]. Note that

$$J(\mathbf{p}_{i+1}) = J(\mathbf{p}_i) + [J(\mathbf{p}_{i+1}) - J(\mathbf{p}_i)] = J(\mathbf{p}_i) + \frac{dJ(\mathbf{p}^*)}{d\mathbf{p}}(\mathbf{p}_{i+1} - \mathbf{p}_i),$$

where $\mathbf{p}^*$ is a value between $\mathbf{p}_i$ and $\mathbf{p}_{i+1}$.

Substituting the ILT law, we have

$$J(\mathbf{p}_{i+1}) = \left[1 - \frac{dJ(\mathbf{p}_i^*)}{d\mathbf{p}}\gamma_i\right]J(\mathbf{p}_i). \qquad (7.5)$$

To guarantee a contractive mapping in (7.5), the following condition should be satisfied:

$$\left|1 - \frac{dJ(\mathbf{p}_i^*)}{d\mathbf{p}}\gamma_i\right| < 1.$$

We define $D_{j,i} = \dfrac{dJ(\mathbf{p}_i^*)}{dp_{j,i}}$ $(j = 1,2,3)$, which is estimated numerically as

$$\hat{D}_{j,i} = \frac{J(\mathbf{p}_i) - J(\mathbf{p}_{i-1})}{p_{j,i} - p_{j,i-1}}. \qquad (7.6)$$

Then the learning gain is $\gamma_{j,i} = \lambda_j / \hat{D}_{j,i}$, where λ_j is a constant gain and $0 < \lambda_j \leq 1$.

For the first iteration, the gradient information is unavailable. We can choose a sufficiently small learning gain. An alternative is to update each element of $\mathbf{p}$ in opposite directions (increasing and decreasing directions), which yields eight ($2^3 = 8$) directions in 3D space, and select the best result for the next updating.

For the learning gain selection, theoretically, the objective function J converges faster as λ_i increases. However, in this study we use a numerical method to estimate the gradient information as in (7.6); the information might not be accurate if there is a large difference in response between consecutive iterations due to parameter updating. A small λ_i allows the parameters be updated slowly and provides a better learning result. Conversely, the number of learning iterations increases as λ_i decreases.

7.3.2   Learning Results

A setpoint control task is considered with $v_r = 0.2$ m/s. The initial states are $(\dot{x}, \theta, \dot{\theta}) = (0, 20°, 0)$. The pendulum load is $m_p = 8$ kg, the slope is $\varphi = 30°$ and friction is $f_r = 0.2\dot{x} + 0.1sgn(\dot{x})$. The total time for evaluation is 40 s.

FLC with integral action is applied with the same parameter ranges and output parameters as in the preceding example, which yields $\mathbf{p} = [3.5,\ 3.3,\ 0.6]^T$. However, the pendulum falls down at $t = 0.77$ s. We conclude that the FLC with parameters that stabilize the 2WMR system for $m_p = 1.45$ kg and $\varphi = 2°$ in the preceding example does not work when $m_p = 8$ kg and $\varphi = 30°$.

The ILT method is applied with the cost function $J = G_1$. The learning gains are $[\lambda_1, \lambda_2, \lambda_3] = [0.5, 0.3, 0.3]$. The learning process is iterated until $t_w = t_s$. $\mathbf{p} = [4.7379,\ 4.4608,\ 0.8111]^T$ is obtained after IL tuning. The results are shown in Figs. 7.7 and 7.8. The pendulum stays above the horizontal plane during the whole evaluation period. However, the overshoot of the wheel velocity is large and a steady-state error for the wheel velocity exists. The maximum pendulum angle is $27.1°$. Thus, the system performance is still poor and further fine tuning is required.
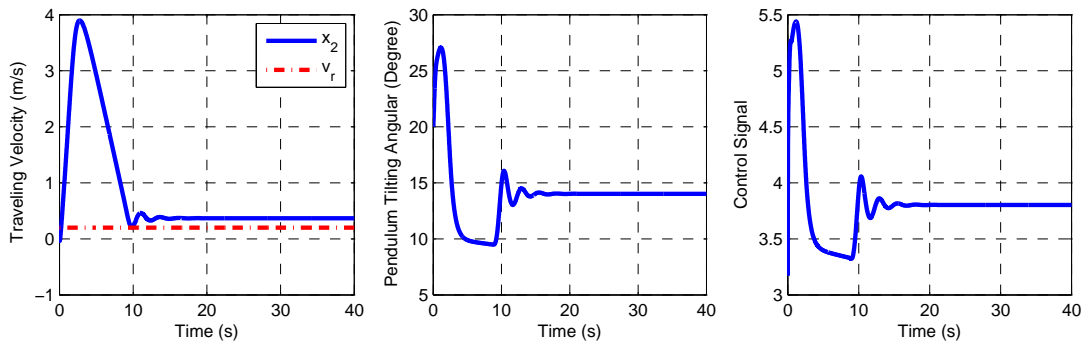
Figure 7.7: Time responses of the wheel velocity, the pendulum tilt angle and the control signal profile after four learning iterations with the cost function G_1. Before learning, $[n_1,\ n_2,\ n_3,\ n_4,\ n_5] = [8,\ 4.5,\ 1.2,\ 1.2,\ 0.6]$; after learning, $[n_1,\ n_2,\ n_3,\ n_4,\ n_5] = [10.6098, 5.8719, 1.4111, 1.4111, 0.6]$.

Next, ILT is applied with cost function $J = G_2$ and the following cost function is used
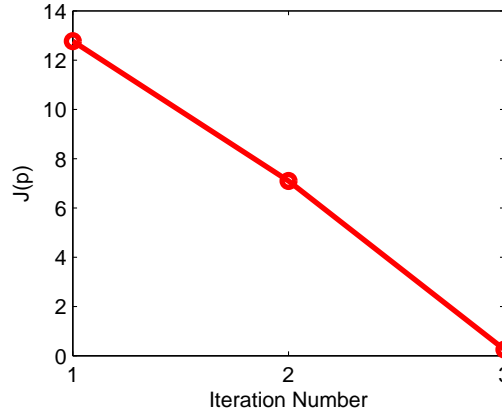
Figure 7.8: Evolution of the cost function G_1.

$$G_2 = \int_0^{t_s} [w_1|\theta(t)| + w_2|\dot{x}(t) - v_r(t)| + w_3|u(t)|]dt. \tag{7.7}$$

A smaller G_2 implies a smaller deviation from the equilibrium or setpoint. The weighting factors in the cost function chosen are $w_1 = 750$, $w_2 = 750$ and $w_3 = 600$. The initial value of $\mathbf{p}$ is $[4.7379, 4.4608, 0.8111]^T$, which is the result after four learning iterations with G_1. Learning gains are chosen as $[\lambda_1, \lambda_2, \lambda_3] = [0.3, 0.3, 0.3]$. The learning process is iterated until J no longer decreases. We obtain $\mathbf{p} = [7.6416, 7.1947, 1.3081]^T$ after ILT. The results are shown in Figs. 7.9 and 7.10. It is clear that the 2WMR responses improve after fine tuning. Compared with the results in Fig. 7.7, the wheels can perfectly track the desired velocity with no tracking error and the pendulum remains in a smaller range around the balance position.

For comparison, ILT is applied with an alternative cost function for fine tuning:

$$G_2 = w_1\max(|\theta|) + w_2\max(|e_1|) + w_3(p_1 + p_2 + p_3). \tag{7.8}$$

The weighting factors in the cost function were $w_1 = 100$, $w_2 = 800$ and $w_3 = 20$. The other parameters and initial conditions were the same as in the preceding example. The learning process was iterated until J no longer decreased. We obtained $\mathbf{p} = [6.9954, 6.5863, 1.1975]^T$ after learning tuning over iterations. The results are shown in Figs. 7.11 and 7.12. Compared with
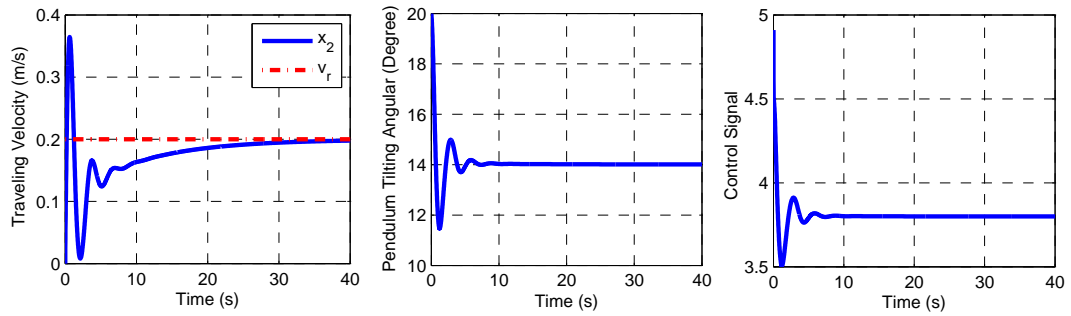
Figure 7.9: Time responses of the wheel velocity, the pendulum tilt angle and the control signal profile after fine-tuning of three iterations with the cost function (7.7). Before learning, $[n_1, \ n_2, \ n_3, \ n_4, \ n_5] = [10.6098, \ 5.8719, \ 1.4111, \ 1.4111, \ 0.6]$; after learning, $[n_1, \ n_2, \ n_3, \ n_4, \ n_5] = [16.7444, \ 9.1028, \ 1.9081, \ 1.9081, \ 0.6]$.
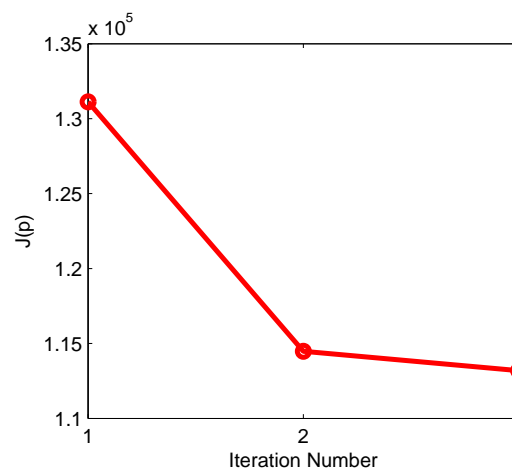
Figure 7.10: Evolution of the cost function G_2 given in (7.7).

the preceding simulation results, it is evident that ILT with different cost functions leads to quite similar results, which indicates the flexibility in choosing cost functions.
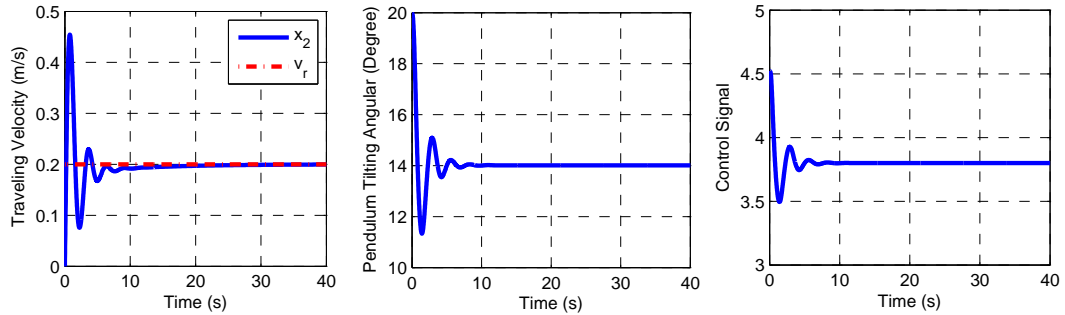
Figure 7.11: Time responses of the wheel velocity, the pendulum tilt angle and the control signal profile after fine-tuning of five iterations with the cost function (7.8). Before learning, $[n_1, n_2, n_3, n_4, n_5] = [10.6098, 5.8719, 1.4111, 1.4111, 0.6]$; after learning, $[n_1, n_2, n_3, n_4, n_5] = [15.3792, 8.3838, 1.7975, 1.7975, 0.6]$.
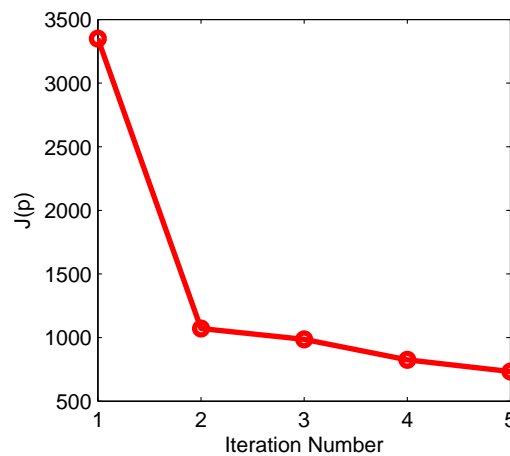
Figure 7.12: Evolution of the cost function G_2.

7.4   Conclusion

In this chapter, synthesis of a design for T-S FLC for an underactuated 2WMR was described. The FLC design is based on both human experience and information from the dynamic model of the system. The effectiveness of the FLC and ILT was verified using simulations. The proposed

FLC is simple and easy to apply. The ultimate objective of the design is to maximize the utilization of system information from either human experience or an analytical model. As a result, the design is easily understood and offers great flexibility. Our next aim is to address implementation on a real-time platform.

Chapter 8

Conclusions

This thesis presents the design of linear and nonlinear control algorithms for control of an underactuated 2WMR. A 2WMR prototype is developed and used to demonstrate and verify the effectiveness of the proposed control algorithms. Considering that various uncertainties exist in the real time 2WMR system, robustness is addressed in the control system design.

Linear controller is simple and easy to implement, however, provides limited robustness. Nonlinear controllers such as SMC or FLC are robust. However, a major difficulty in the design and implementation of the nonlinear controllers is the determination and tuning of the controller parameters. To avoid the difficulty in the nonlinear controller design, in this thesis, synthesized designs of linear and nonlinear control techniques are proposed. The nonlinear controller parameters are determined based on the knowledge of a linear controller, which makes the nonlinear control design become simple, systematic and easy to implement. Furthermore, the feedback gains for the linear controller are free to be chosen, thus an extra degree of freedom is obtained in control.

8.1 Summary

The summary of this thesis is as follows.

In Chapter 2, the design and modeling of the underactuated 2WMR are presented. By studying the zero dynamics of the 2WMR system, it is shown that the pendulum is inherently unstable at the desired equilibrium point. To stabilize the 2WMR, full-state feedback control is indispensable.

In Chapter 3, a full-state feedback linear controller is proposed. Two alternative methods are proposed to obtain the feedback gains for the linear controller. One is an optimal design based on LQR technique and the other is a robust design based on LMI technique. The stability analysis of the 2WMR nonlinear system with uncertainties is given when the system is under the LMI based linear control. Based on theoretical analysis, simulation and experiment results, it is concluded that the robustness of the linear controller is limited.

In Chapter 4 and Chapter 5, two types of SMC are proposed. The main advantages of the SMC are: (1) SMC is applicable to systems with various type of uncertainties, as long as the upper bounds of the uncertainties are known, in other words, the SMC design requires less information of the uncertainties in comparison with classical control techniques. (2) In the ideal sliding mode, all uncertainties which are in the control range space, namely, matched uncertainties are nullified. The SMC design consists of two phases: (1) sliding surface design that stabilizes the sliding manifold and satisfies some performance specifications; (2) switching control law design that guarantees the system to reach the sliding surface in a finite time and maintain on the surface afterwards. For the first phase of SMC design, linear and integral type sliding surfaces are proposed in Chapter 4 and Chapter 5, respectively. For the second phase of SMC design, Lyapunov's direct method is employed to derive the SMC laws.

In Chapter 4, the linear sliding surface is constructed by combining the two states of the wheel and two states of the pendulum in a linear form. For sliding surface design, the selection of the sliding surface coefficients is a sophisticated design issue because those coefficients are

non-affine in the sliding manifold. To avoid the difficulty in directly choosing the sliding surface coefficients, a new sliding surface design method is proposed. The sliding surface design is transformed into a nominal linear control design, which is simple, systematic and furthermore provides one extra degree of freedom in control. By utilizing the extra degree of freedom, various linear control techniques can be incorporated in the SMC design. The resulting sliding manifold exhibits desirable properties besides stability, such as optimality and robustness.

In Chapter 5, a nonlinear integral-type sliding surface is adopted in the SMC design, namely, an ISMC is proposed. The sliding mode exists from the very beginning, therefore the system is more robust against uncertainties than the other SMC systems with reaching phase. The ISMC is constructed by a nominal control part and a switching term. With the switching term, the matched uncertainties are perfectly rejected. With the freedom to design a nominal control for the sliding manifold, ISMC is incorporated with a linear controller.

Chapter 6 and Chapter 7 present synthesized design of T-S FLCs. The FLC design is based on both human experience and information of the system dynamic model. A difficulty in FLC design is the lengthy tuning process for FLC parameters, especially the output parameters. In Chapter 6, the FLC output parameters are tuned according the output of a linear controller at certain operating points. The linear control techniques introduced in Chapter 2 can be employed and incorporated in the FLC design. The new FLC outperforms a linear controller because it provides varying feedback gains, which are adapted to the current states of the 2WRM. In Chapter 7, a synthesized FLC is developed without incorporating any model-based controller, and hence an accurate mathematic model is not required. The synthesized design consists of three phases: determination of the FLC structure through heuristic knowledge about the 2WMR; quantitative determination of the output parameters for stabilization of the 2WMR; and tuning of the FLC output parameters using iterative learning tuning (ILT). The main idea behind the proposed

Table 8.1: Comparisons between the controllers proposed.

Control Method	Robustness			Optimality	Stability
	Unmodeled Frictions	Parameter Uncertainties	Exceptional Disturbance		Analysis
Linear Controller	Limited	Limited	Limited	Suboptimal	Provided
SMC	Good	Good	Limited	Suboptimal	Provided
ISMC	Good	Good	Fair	Suboptimal	Provided
FLC	Good	Fair	Good	Suboptimal	None
FLC with ILT	Good	Good	Good	Optimal	Provided
Complexity of algorithm: FLC > SMC, ISMC > Linear controller.					
User friendly: FLC > Linear controller > SMC, ISMC.					
Flexibility in design: FLC with ILT > FLC, and ISMC > SMC.					

methodology is to maximize the utilization of all available information, which is achieved by combining partially model-based and partially model-free designs, and hence improve the FLC performance.

Table 8.1 summarizes the comparisons between all the control methods proposed and more points are addressed as the following.

(i) The SMC and ISMC use discontinuous control laws to achieve the robustness with respecting to system uncertainties. However, in practical applications, the SMC and ISMC suffer from the following disadvantages. First, the SMC and ISMC could be vulnerable to measurement noise since the control signals depend on the sign of the sliding surface, which is very close to zero and depends on the measured states. Second, the SMC and ISMC may employ unnecessarily large control signals to overcome the parametric uncertainties. Third, the SMC and ISMC could be vulnerable to exceptional disturbances which can drive the system be away from the sliding surface. The system performance is hardly predictable when the system is not

Table 8.2: Comparisons between LQR and LMI based linear control designs.

	LQR	LMI
Model	Linearized	Nonlinear
Nonlinearity and Uncertainties	Ignored	Considered
Feature	Optimal	Robust

on the specified sliding surface, especially the SMC.

(ii) The FLC offers a practical solution for controlling the 2WMR, although the design is lack of stability proof. By incorporating heuristic knowledge in the design, the FLC is much more user friendly than the SMC and ISMC. Through experimental testings, the FLC was proved to be effective for setpoint control and can provide satisfactory performance even the system is in presence of exceptional disturbances.

In particular, comparisons between the LQR and LMI based linear control designs are given in Table 8.2.

Comparisons between the SMC and ISMC are given in Table 8.3. The computing of the integral sliding surface is more complex than the linear sliding surface. In simulations, both SMC and ISMC can provide satisfactory performances. In real time implementation, ISMC can provide a better performance for setpoint control task. The main reason is that, in ISMC, the wheel position error is directly used for feedback, while in SMC, the convergence of the wheel position error depends on the convergence of the sliding surface and other three states.

Comparisons between the FLCs designed in Chapter 6 and Chapter 7 are presented in Table 8.4. Compared with the FLC proposed in Chapter 6, the design of FLC with ILT in Chapter 7 uses fewer fuzzy rules and has fewer parameters to be determined, which implies a simpler design. Furthermore, the FLC with ILT requires less model information that the values of the system parameters are unknown. However, by using the ILT, repetitive testing need to be con-

Table 8.3: Comparisons between the SMC and ISMC.

	SMC	ISMC
Sliding surface	Linear	Nonlinear
Reaching phase	Yes	No
Control Law	Strictly derived and fixed	Flexible in nominal controller design
Knowledge of initial states	Note required	Required

Table 8.4: Comparisons between the FLCs proposed.

	FLC+LQR	FLC+ILT
No. of fuzzy rules	16	10
No. of parameters	12	9
Parameter tuning	LQR	ILT
Verification	Experiment	Simulation

ducted. In each trial, the system response should start at the same initial states, which might be difficult to guarantee in practice.

8.2   Suggestions for Future Work

This section provides potential future directions of research in continuation of this work.

1. Chapter 3, the LQR based linear control is designed according to a linearized model of the 2WMR and the weighting matrices Q and R are chosen based on human experience. Thus the linear controller only gives an optimal solution subjected to the nominal linearized model and the LQR performance index. In future work, we could utilize the freedom in choosing the weighting matrices Q and R to achieve an optimal solution subjected to the nonlinear plant and a separately defined performance index instead of the LQR performance index. Meanwhile, the weighting matrices Q and R can be selected in a systematic way.

2. In Chapter 4, for system with unmatched uncertainties, LMI method is adopted in the sliding surface design, thus yielding a robust control system. An alternative possible approach to deal with the unmatched uncertainties is to minimize the unmatched uncertainties directly by selecting the the sliding surface coefficients appropriately, which could be considered as a future work.

3. In Chapter 5, the ISMC design offers one extra degree of freedom to incorporate a nominal controller and a linear controller is adopted. It would be interesting to investigate the ISMC design by incorporating the developed FLC or other advanced control methods.

4. In Chapter 7, iterative learning method is adopted for tuning the FLC output parameters. The proposed ILT method belongs to off-line learning methods. In future work, online learning based tuning method can be explored.

5. In this thesis, the developed 2WMR platform functions well for verification of the proposed control methods. However, due to the limited time and budget for building the prototype, both the mechanical and electrical designs of the prototype are not perfect. Some of the future works can focus on improving the hardware design. For example, a remote control block can be added to make the operation be more user friendly; safety protections can be considered in both the electrical and mechanical designs to make the operation of the robot be safer and avoid possible damage from collision. Furthermore, it would be interesting to explore different applications of the 2WMR.

6. This thesis presents control system design for an underactuated 2WMR. The developed methods are directly applicable to a 2-D unicycle system with lateral stability guaranteed, and theoretically extendable to a 3-D unicycle system. However, the modeling and behaviors of 3-D unicycle is much more complicated than the 2WMR or 2-D unicycle. The development and control of a 3-D unicycle can be considered in future work.

Bibliography

[1] P. K. W. Abeygunawardhana and T. Murakami, "Vibration suppression of two-wheel mobile manipulator using resonance-ratio-control-based null-space control", *IEEE Trans. Ind. Electron.*, Vol. 57, No. 12, pp. 4137-4146, Dec. 2010.

[2] N. P. I. Aneke, "Control of underactuated mechanical systems", Ph.D. dissertation, TU Eindhoven, Eindhoven, The Netherlands, 2003.

[3] H. Ashrafiuon and R. S. Erwin, "Sliding mode control of underactuated multibody systems and its application to shape change control", *Int. J. of Control*, Vol. 81, No. 12, pp. 1849-1858, Dec. 2008.

[4] K. J. Astrom and K. Furuta, "Swing up a pendulum by energy control", *Automatica*, Vol. 36, No. 2, pp. 287-295, Feb. 2000.

[5] L. Astudillo, O. Castillo, L. T. Aguilar and R. Martí nez-Soto, "Hybrid control for an autonomous wheeled mobile robot under perturbed torques", *in Proceedings of the 12th IFSA World Congress*, pp. 594-603, 2007.

[6] V. Azhmyakov, "On the set-valued approach to optimal control of sliding mode processes", *Journal of The Franklin Institute-Engineering and Applied Mathematics*, Vol. 349, No. 4, pp. 1323-1336, 2012.

[7] M. Basin and P. Rodriguez-Ramirez, "Sliding mode controller design for linear systems with unmeasured states", *J. of The Franklin Institute-Engineering and Applied Mathematics*, Vol. 349, No. 4, pp. 1337-1349, 2012.

[8] M. Basin, P. Rodriguez-Ramirez, A. Ferrara and D. Calderon-Alvarez, "Sliding mode optimal control for linear systems", *J. of The Franklin Institute-Engineering and Applied Mathematics*, Vol. 349, No. 4, pp. 1350-1363, 2012.

[9] O. Begovich, E. N. Sanchez and M. Maldonado, "TakagiCSugeno Fuzzy Scheme for Real-Time Trajectory Tracking of an Underactuated Robot", *IEEE Trans. Control Sys. Tech.*, Vol. 10, No. 1, pp. 14-20, Jan. 2002.

[10] W.-J. Cao and J.-X. Xu, "Nonlinear integral-type sliding surface for both matched and unmatched uncertain systems", *IEEE Trans. Autom. Control*, Vol. 49, No. 8, pp. 1355-1360, Aug., 2004.

[11] F. Castanos and L. Fridman, "Analysis and Design of Integral Sliding Manifolds for Systems With Unmatched Perturbations", *IEEE Trans. On Autom. Control*, Vol. 51, No. 5, pp. 853-858, May 2006.

[12] C.-H. Chiu, "The design and implementation of a wheeled inverted pendulum using an adaptive output recurrent cerebellar model articulation controller", *IEEE Trans. Ind. Electron.*, Vol. 57, No. 5, pp. 1814-1822, May 2010.

[13] C.-H. Chiu and C.-C. Chang, "Design and Development of Mamdani-Like Fuzzy Control Algorithm for a Wheeled Human-Conveyance Vehicle Control", *IEEE Trans. Ind. Electron.*, Vol. 59, No. 12, pp. 4774-4783, Dec. 2012.

[14] C.-H. Chiu, Y.-W. Lin and C.-H. Lin, "Real-time control of a wheeled inverted pendulum based on an intelligent model free controller", *Mechatronics*, Vol. 21, pp. 523-533, 2011.

[15] D. Chwa, "Nonlinear tracking control of 3-D overhead cranes against the initial swing angle and the variation of payload weight", *IEEE Trans. Control Sys. Tech.*, Vol. 17, pp. 876-883, 2009.

[16] V. Derhami, V. J. Majd and M. N. Ahmadabadi, "Exploration and exploitation balance management in fuzzy reinforcement learning", *Fuzzy Sets and Systems*, Vol. 161, pp. 578-595, 2010.

[17] J. Dong, Y. Wang and G.-H. Yang, "H_∞ and mixed H_2/H_∞ control of discrete-time T-S fuzzy systems with local nonlinear models", *Fuzzy Sets and Systems*, Vol. 164, pp. 1-24, 2011.

[18] C. Edwards and S. K. Spurgeon, "Sliding mode control: theory and applications", *Taylor and Francis*, 1998.

[19] M. I. El-Hawwary, A. L. Elshafei, H. M. Emara and H. A. A. Fattah, "Adaptive fuzzy control of the inverted pendulum problem", *IEEE Trans. Control Sys. Tech.*, Vol. 14, No. 6, November 2006, pp. 1135-1144.

[20] J. G. Elliot and R. F. Gans, "Closed-loop control of an underactuated sheet registration device using feedback linearization and gain scheduling", *IEEE Trans. Control Sys. Tech.*, Vol. 16, No. 4, pp. 589-599, July 2008.

[21] Y. Fang, B. Ma, P. Wang and X. Zhang, "A motion planning-based adaptive control method for an underactuated crane system", *IEEE Trans. Control Syst. Tech.*, Vol. 20, No. 1, pp. 241-248, Jan. 2012.

[22] Y. Fang, W. Dixon, D. Dawson and E. Zergeroglu, "Nonlinear coupling control laws for an underactuated overhead crane system", *IEEE/ASME Trans. Mechatron.*, Vol. 8, No. 3, pp. 418-423, Sep. 2003.

[23] I. Fantoni and R. Lozano, "Nonlinear control for underactuated mechanical systems", *Spring*, 2002.

[24] L. Freidovich, A. Shiriaev, F. Gordillo, F. Gó mez-Estern and J. Aracil, "Partial-energy-shaping control for orbital stabilization of high-frequency oscillations of the Furuta pendulum", *IEEE Trans. Control Sys. Tech.*, Vol. 17, pp. 853-858, 2009.

[25] J. Ghommam, F. Mnif, A. Benali and N. Derbel, "Asymptotic Backstepping Stabilization of an Underactuated Surface Vessel", *IEEE Trans. Control Sys. Tech.*, Vol. 14, No. 6, pp. 1150-1157, Nov. 2006.

[26] F. Grasser, A. D'Arrigo, S. Colombi and A. C. Rufer, "JOE: a mobile, inverted pendulum", *IEEE Trans. Ind. Electron.*, Vol. 49, No. 1, pp. 107-114, Feb. 2002.

[27] Z. Q. Guo, J.-X. Xu and T. H. Lee, "A gain-scheduling optimal fuzzy logic controller design for unicycle", *in Proc. of IEEE/ASME International Conference on Advanced Intelligent Mechatronics (AIM2009)*, pp. 1423-1428, 2009.

[28] C.-H. Huang, W.-J. Wang and C.-H. Chiu, "Design and implementation of fuzzy control on a two-wheel inverted pendulum", *IEEE Trans. On Ind. Electron.*, Vol. 58, No. 7, pp. 2988-3001, July 2011.

[29] J. Huang, Z.-H. Guan, T. Matsuno, T. Fukuda and K. Sekiyama, "Sliding-mode velocity control of mobile-wheeled inverted-pendulum systems", *IEEE Trans. Robotics*, Vol. 26, No. 4, pp. 750-758, 2010.

[30] C.-L. Hwang, H.-M. Wu and C.-L. Shih, "Fuzzy sliding-mode underactuated control for autonomous dynamic balance of an electrical bicycle", *IEEE Trans. Control Syst. Technol.*, Vol. 17, No. 3, pp. 658-670, May 2009.

[31] C. A. Ibanez, O. G. Frias and M.S. Castanon, "Lyapunov-based controller for the inverted pendulum cart system" *Nonlinear Dynamics*, Vol. 40, No. 4, pp. 367-374, June, 2005.

[32] C. A. Ibanez and O. G. Frias, "Controlling the inverted pendulum by means of a nested saturation function", *Nonlinear Dynamics*, Vol. 53, No. 4, pp. 273-280, Sept., 2008.

[33] S. Islam and X. P. Liu, "Robust sliding mode control for robot manipulators", *IEEE Trans. On Ind. Electron.*, Vol. 58, No. 6, pp. 2444-2453, June 2011.

[34] S. Jung and S. S. Kim, "Control experiment of a wheel-driven mobile inverted pendulum using neural network", IEEE Trans. Control Syst. Technol., Vol. 16, No. 2, pp. 297-303, Mar. 2008.

[35] H. K. Khalil, "Nonlinear systems", Third edition, Englewood Cliffs, NJ: Prentice Hall, 2002.

[36] S. Kurode, P. Trivedi, B. Bandyopadhyay and P. S. Gandhi, "Second order sliding mode control for a class of underactuated systems", *in Proc. of the 12th IEEE Int. Workshop on Variable Structure Systems (VSS12)*, pp. 458-462, 2012.

[37] Z. Li and J. Luo, "Adaptive robust dynamic balance and motion controls of mobile wheeled inverted pendulums", *IEEE Trans. Control Sys. Tech.*, Vol. 17, No. 1, pp. 233-241, Jan. 2009.

[38] Z. Li and C. Xu, "Adaptive fuzzy logic control of dynamic balance and motion for wheeled inverted pendulums", *Fuzzy Sets and Systems*, Vol. 160, pp. 1787-1803, 2009.

[39] Y.-W. Liang, S.-D. Xu, D.-C. Liaw and C.-C. Chen, "A study of T-S model-based SMC scheme with application to robot control," *IEEE Trans. Ind. Electron.*, Vol. 55, No. 11, pp. 3964-3971, Nov. 2008.

[40] S. C. Lin and C. C. Tsai, "Development of a self-balancing human transportation vehicle for the teaching of feedback control", IEEE Trans. Education, Vol. 52, No. 1, pp. 157-168, Feb. 2009.

[41] A. F. Loza, M. Jimenez-Lizarraga and L. Fridman, "Robust output nash strategies based on sliding mode observation in a two-player dfferential game", *Journal of The Franklin Institute-Engineering and Applied Mathematics*, Vol. 349, No. 4, pp. 1416-1429, 2012.

[42] R. Martí nez-Soto, O. Castillo and L. T. Aguilar, "Optimization of interval type-2 fuzzy logic controllers for a perturbed autonomous wheeled mobile robot using genetic algorithms", *Information Sciences*, Vol. 179, pp. 2158-2174, 2009.

[43] B. Mirkin, P.-O. Gutman and Y. Shtessel, "Coordinated decentralized sliding mode MRAC with control cost optimization for a class of nonlinear systems", *Journal of The Franklin Institute-Engineering and Applied Mathematics*, Vol. 349, No. 4, pp. 1364-1379, 2012.

[44] M. Nie and W. W. Tan, "Stable adaptive fuzzy PD plus PI controller for nonlinear uncertain systems", *Fuzzy Sets and Systems*, Vol. 179, pp. 1-18, 2011.

[45] R. Olfati-Saber, "Nonlinear control of underactuated mechanical systems with application to robotics and aerospace vehicles, *MIT PhD Thesis*, Feb. 2001.

[46] T. R. Oliveira, A. J. Peixoto and L. Hsu, "Global real-time optimization by output-feedback extremum-seeking control with sliding modes", *Journal of The Franklin Institute-Engineering and Applied Mathematics*, Vol. 349, No. 4, pp. 1397-1415, 2012.

[47] P. Oryschuk, A. Salerno, A. M. Al-Husseini and J. Angeles, "Experimental validation of an underactuated two-wheeled mobile robot", *IEEE/ASME Trans. Mechatronics*, vol. 14, no. 2, pp. 252-257, April 2009.

[48] M.-S. Park and D. Chwa, "Swing-up and stabilization control of inverted-pendulum systems via coupled sliding-mode control Method", *IEEE Trans. Ind. Electron.*, Vol. 56, No. 9, pp. 3541-3555, Sept. 2009.

[49] M.-S. Park and D. Chwa, "Orbital stabilization of inverted-pendulum systems via coupled sliding-mode control", *IEEE Trans. Ind. Electron.*, Vol. 56, No. 9, pp. 3556-3570, April, 2009.

[50] K. Pathak, J. Franch and S.K. Agrawal, "Velocity and position control of a wheeled inverted pendulum by partial feedback linearization", *IEEE Trans. Robot.*, Vol. 21, No. 3, pp. 505-513, 2005.

[51] K. Y. Pettersen, F. Mazenc and H. Nijmeijer, "Global uniform asymptotic stabilization of an underactuated surface vessel: experimental results", *IEEE Trans. Control Sys. Tech.*, Vol. 12, No. 6, pp 891-903, Nov. 2004.

[52] A. Polyakov, "Minimization of disturbances effects in time delay predictor-based sliding mode control systems", *Journal of The Franklin Institute-Engineering and Applied Mathematics*, Vol. 349, No. 4, pp. 1380-1396, 2012.

[53] Z. H. Qu, "Robust control of nonlinear uncertain systems", *John-Wiley and Sons*, New York, 1998.

[54] M. T. Ravichandran and A. D. Mahindrakar, "Robust stabilization of a class of underactuated mechanical systems using time scaling and Lyapunov redesign", *IEEE Trans. Ind. Electron.*, Vol. 58, No. 9, pp. 2444-2453, Sept. 2011.

[55] T. J. Ren, T. C. Chen and C. J. Chen, "Motion control for a two-wheeled vehicle using a self-tuning PID controller", *Control Eng. Practice*, Vol. 16, No. 3, pp. 365-375, Mar. 2008.

[56] M. Reyhanoglu, A. Schaft, N.H. McClamroch, I. Kolmanovsky, "Dynamics and control of a class of underactuated mechanical systems", *IEEE Trans. Autom. Control*, Vol. 44, No. 9, pp. 1663-1671, Sept. 1999.

[57] S. Riachy, Y. Orlov, T. Floquet, R. Santiesteban and J. Richard, "Second order sliding mode control of underactuated mechanical systems I: Local stabilization with application to an inverted pendulum", *Int. J. of Robust Nonlinear Control*, Vol. 18, No. 4/5, pp. 529-543, May 2007.

[58] X. Ruan, J. Chen, J. Cai and L. Dai, "Balancing control of two-wheeled upstanding robot using adaptive fuzzy control method", *IEEE Conf. on Intelligent Computing and Intelligent Systems*, Vol. 2, pp. 95-98, 2009.

[59] K. Sakurama, S. Hara and K. Nakano, "Swing-up and stabilization of a cart-pendulum system via energy control and controlled Lagrangian methods, *Elect. Eng. Jpn.*, Vol. 160, No. 5, pp. 24-30, May 2007.

[60] A. Salerno and J. Angeles, "A new family of Two Wheeled Mobile Robot: Modeling and Controllability", *IEEE Trans. Robotics*, Vol. 23. No. 1, pp. 169-173, Feb. 2007.

[61] R. Santiesteban, T. Floquet, Y. Orlov, S. Riachy and J. Richard, "Second-order sliding mode control of underactuated mechanical systems II: Orbital stabilization of an inverted

pendulum with application to swing up/balancing control", *International Journal of Robust Nonlinear Control*, Vol. 18, No. (4/5), pp. 544-556, 2007.

[62] S. Y. Seo, S. H. Kim, S.-H. Lee, S. H. Han and H. S. Kim, "Simulation of attitude control of a wheeled inverted pendulum", *in Proc. of the Int. Conf. on Control, Automation and Systems*, pp. 2264-2269, COEX, Seoul, Korea, 2007.

[63] J. J. Slotine and W. Li, "Applied nonlinear Control", *Englewood Cliffs, NJ: Prentice-Hall*, 1991.

[64] J. Solis and A. Takanishi, "Development of a wheeled inverted pendulum robot and a pilot experiment with master students", *in Proc. of the 7th Int. Symposium on Mechatronics and its Applications (ISMA10)*, pp. 1-6, 2010.

[65] J. Solis, R. Nakadate, T. Yamamoto and A. Takanishi, "Introduction of Mechatronics to Undergraduate Students Based on Robotic Platforms for Education Purposes", *in Proc. of the 18th IEEE Int. Symposium on Robot and Human Interactive Communication Toyama*, pp. 693-698, 2009.

[66] M. W. Spong, "Energy based control of a class of underactuated mechanical systems", *IFAC World Congress*, July 1996.

[67] Z. Sun, S. S. Ge and T. H. Lee, "Stabilization of underactuated mechanical systems: A nonregular backstepping approach", *Int. J. Control*, Vol. 74, No. 11, pp. 1045-1051, June 2001. *International Journal of Robust Nonlinear Control*, Vol. 18, No. (4/5), pp. 544-556, 2007.

[68] T. Takei, R. Imamura and S. Yuta, "Baggage transportation and navigation by a wheeled inverted pendulum mobile robot", *IEEE Trans. On Ind. Electron.*, Vol. 56, No. 10, pp. 3985-3994, Oct. 2009.

[69] C. W. Tao, J. S. Taur and Y. C. Chen, "Design of a parallel distributed fuzzy LQR controller for the twin rotor multi-input multi-output system", *Fuzzy Sets and Systems*, Vol. 161, pp. 2081-2103, 2010.

[70] C. W. Tao, J. S. Taur, C. M. Wang and U. S. Chen, "Fuzzy hierarchical swing-up and sliding position controller for the inverted pendulum-cart system", *Fuzzy Sets and Systems*, Vol. 159, pp. 2763-2784, 2008.

[71] C.-C. Tsai, H.-C. Huang and S.-C. Lin, "Adaptive neural network control of a self-balancing two-wheeled scooter," *IEEE Trans. Ind. Electron.*, Vol. 57, No. 4, pp. 1420-1428, April, 2010.

[72] V. I. Utkin, "On compensation of the forced term of motion in variable structure control systems", *Eng. Cybern.*, No. 4, pp. 169-173, 1965.

[73] V. I. Utkin, "Variable structure systems with sliding modes", *IEEE Trans. Auto. Control*, Vol. 22, No. 2, pp. 212-222, 1977.

[74] V. I. Utkin, "Sliding modes and their application in variable structure systems", *Imported Publications, Incorporated*, 1978.

[75] V. I. Utkin, "Sliding Modes in Control and Optimization", *Springer-Verlag*, 1992.

[76] V. I. Utkin and J. Shi, "Integral sliding mode in systems operating under uncertainty conditions", *Proc. of the 35th IEEE Conf. on Decision and Control*, pp. 4591-4596, 1996.

[77] J.-X. Xu, "A quasi-optimal sliding mode control scheme based on control Lyapunov function", *Journal of The Franklin Institute-Engineering and Applied Mathematics*, Vol. 349, No. 4 , pp. 1445-1458, 2012.

[78] J.-X. Xu, Z.-Q. Guo and T.H. Lee, "Synthesized design of a fuzzy logic controller for an underactuated unicycle", *Fuzzy Sets and Systems*, http://dx.doi.org/10.1016/j.fss.2012.04.004, 2012.

[79] J.-X. Xu, C.-C. Hang and C. Liu, "Parallel structure and tuning of a fuzzy PID controller", *Automatica*, Vol. 36, No. 5, pp. 673-684, 2000.

[80] J.-X. Xu, D.Q. Huang and S. Pindi, "Optimal tuning of PID parameters using iterative learning approach", *SICE J. Control, Measurement, and System Integration*, Vol. 1, No. 2, pp. 143-154, 2008.

[81] R. Xu and U. Ozguner, "Sliding mode control of a class of underactuated systems", *Automatica*, Vol. 44, pp. 233-241, 2008.

[82] K. D. Young, "Variable structure control for robotics and aerospace applications", *Elsevier Science Inc.*, New York, USA, 1993.

[83] K. D. Young and U. Ozguner, "Lecture notes in control and information sciences 247, Variable structure systems, sliding mode and nonlinear control", *Springer-Verlag*, Vol. 51, London, 1999.

[84] K. D. Young, V. I. Utkin and U. Ozguner, "A control engineers guide to sliding mode control", *IEEE Trans. on Control Sys. Tech.*, Vol. 7, No. 3, pp. 328-342, 1999.

[85] K. D. Young, "Asymptotic stability of model reference systems with variable structure control", *IEEE Trans. Auto. Control*, Vol. 22, No. 4, pp. 279-281, 1977.

[86] K. D. Young, P. V. Kokotovic and V. Utkin, "A singular perturbation analysis of high-gain feedback systems", *IEEE Trans. Auto. Control*, Vol. 22, No. 6, pp. 931-938, 1977.

[87] K. D. Young, "Design of variable structure model following control systems", *IEEE Trans. Auto. Control*, Vol. 23, No. 4, pp. 1079-1085, 1978.

[88] X. Yu and O. Kaynak, "Sliding-Mode Control With Soft Computing: A Survey", *IEEE Trans. Ind. Electron.*, Vol. 56, No. 9, pp. 3275-3285, Sept. 2009.

[89] L. A. Zadeh, "The concept of a linguistic variable and its application to approximate reasoning", Inf. Sci., Vol. 8, pp. 199-249, 1975.

Appendix A

Mathematic Derivations

A.1   Derivation of the 2WMR Dynamic Equations

The mathematical model of the 2WMR system shown in Fig. 2.3 is derived using a Euler–Lagrange formulation. We first present the kinetic and potential energies used to compute the Lagrangian function [23]. The potential energy of the wheel is

$$V_{wheel} = m_w g x \sin \varphi$$

and the kinetic energy of the wheel is

$$T_{wheel} = \frac{1}{2} m_w \dot{x}^2 + \frac{1}{2} I_w \dot{\phi}^2 = (\frac{1}{2} m_w r^2 + \frac{1}{2} I_w) \dot{\phi}^2.$$

We define x_p as the horizontal position and y_p as the vertical position of the centroid of the pendulum. We then have

$$x_p = x \cos \varphi + l \sin \theta, \quad y_p = x \sin \varphi + l \cos \theta.$$

The potential energy for the pendulum is

$$V_{pendulum} = m_p g y_p = m_p g (x \sin \varphi + l \cos \theta)$$

and the kinetic energy is

$$T_{pendulum} = \frac{1}{2} m_p (\dot{x}_p^2 + \dot{y}_p^2) + \frac{1}{2} I_p \dot{\theta}^2 = \frac{1}{2} m_p \left[\dot{x}^2 + l^2 \dot{\theta}^2 + 2 \dot{x} \dot{\theta} l \cos(\theta + \varphi) \right] + \frac{1}{2} I_p \dot{\theta}^2.$$

Therefore, the Lagrangian function of the 2WMR is given by

$$
\begin{aligned}
\mathcal{L} &= T_{wheel} + T_{pendulum} - V_{wheel} - V_{pendulum} \\
&= (\frac{1}{2}m_w r^2 + \frac{1}{2}I_w)\dot{\phi}^2 + \frac{1}{2}m_p\left[\dot{x}^2 + l^2\dot{\theta}^2 + 2\dot{x}\dot{\theta}l\cos(\theta+\varphi)\right] + \frac{1}{2}I_p\dot{\theta}^2 \\
&\quad - m_w gx\sin\varphi - m_p g(x\sin\varphi + l\cos\theta).
\end{aligned}
$$

The equations of motion for the 2WMR are then given by the Euler–Lagrange equations

$$
\frac{d}{dt}\left(\frac{\partial\mathcal{L}}{\partial\dot{\phi}}\right) - \frac{\partial\mathcal{L}}{\partial\phi} = \tau + \tau_f - rf_r, \tag{A.1}
$$

$$
\frac{d}{dt}\left(\frac{\partial\mathcal{L}}{\partial\dot{\theta}}\right) - \frac{\partial\mathcal{L}}{\partial\theta} = -\tau - \tau_f. \tag{A.2}
$$

The terms on the right-hand side of the equations represent torques applied externally to the system. For torques acting on the wheel on the right-hand side of (A.1), τ is the torque generated by the driving motor, τ_f represents the torque resulted by the joint friction and rf_r is the torque due to ground friction f_r. The torques acting on the pendulum shown in (A.2) are the reaction torques.

In equation (A.1),

$$
\frac{\partial\mathcal{L}}{\partial\phi} = 0,
$$

and

$$
\begin{aligned}
\frac{\partial\mathcal{L}}{\partial\dot{\phi}} &= \frac{\partial}{\partial\dot{\phi}}\left[(\frac{1}{2}m_w r^2 + \frac{1}{2}I_w)\dot{\phi}^2 + m_p\dot{x}\dot{\theta}l\cos(\theta+\varphi) + \frac{1}{2}m_p\dot{x}^2\right] \\
&= (m_w r^2 + I_w + m_p r^2)\dot{\phi} + m_p r\dot{\theta}\cos(\theta+\varphi)
\end{aligned}
$$

and thus

$$
\frac{d}{dt}\left(\frac{\partial\mathcal{L}}{\partial\dot{\phi}}\right) - \frac{\partial\mathcal{L}}{\partial\phi} = (m_w r^2 + m_p r^2 + I_w)\ddot{\phi} - m_p rl\sin(\theta+\varphi)\dot{\theta}^2 + m_p rl\cos(\theta+\varphi)\ddot{\theta}.
$$

Recall that $x = r\phi$, so we have

$$
\frac{d}{dt}\left(\frac{\partial\mathcal{L}}{\partial\dot{\phi}}\right) - \frac{\partial\mathcal{L}}{\partial\phi} = (m_w r + m_p r + \frac{I_w}{r})\ddot{x} - m_p rl\sin(\theta+\varphi)\dot{\theta}^2 + m_p rl\cos(\theta+\varphi)\ddot{\theta}.
$$

Substituting the above result in (A.1) and dividing both sides of the equation by r, we have

$$a\ddot{x} + b\ddot{\theta} - m_p l \sin(\theta + \varphi)\dot{\theta}^2 + \sin\varphi(m_p + m_w)g = \frac{1}{r}(\tau + \tau_f - rf_r), \qquad (A.3)$$

where $a = m_w + m_p + I_w/r^2$ and $b = m_p l \cos(\theta + \varphi)$.

In equation (A.2),

$$\frac{\partial\mathscr{L}}{\partial\theta} = m_p l g sin\theta - m_p l \dot{x}\dot{\theta}\sin(\theta + \varphi)$$

and

$$\begin{aligned}
\frac{\partial\mathscr{L}}{\partial\dot{\theta}} &= \frac{\partial}{\partial\dot{\theta}}\left\{\frac{1}{2}m_p\left[l^2\dot{\theta}^2 + 2\dot{x}\dot{\theta}l\cos(\theta + \varphi)\right] + \frac{1}{2}I_p\dot{\theta}^2\right\} \\
&= (I_p + m_p l^2)\dot{\theta} + m_p l\dot{x}\cos(\theta + \varphi),
\end{aligned}$$

and thus

$$\frac{d}{dt}\left(\frac{\partial\mathscr{L}}{\partial\dot{\theta}}\right) - \frac{\partial\mathscr{L}}{\partial\theta} = (I_p + m_p l^2)\ddot{\theta} + m_p l\cos(\theta + \varphi)\ddot{x} - m_p l g \sin\theta.$$

Substituting the above result in (A.2), we have

$$b\ddot{x} + c\ddot{\theta} - m_p l g \sin\theta = -\tau - \tau_f, \qquad (A.4)$$

where $c = I_p + m_p l^2$.

The dynamic behavior of the 2WMR system described by (A.3) and (A.4) is given by (2.1) and (2.2).

A.2   Model of General Underactuated System

Consider a multibody mechanical system with $n + m$ rigid body degree of freedom (DOF) and n actuators. Partitioning the generalized coordinate vector $\mathbf{x}$ into n actuated, $\mathbf{x}_a$, and m underactuated coordinates, $\mathbf{x}_u$, the motion equations of the system can be written as

$$\begin{bmatrix} M_{11} & M_{12} \\ M_{12}^T & M_{22} \end{bmatrix}\begin{bmatrix} \ddot{\mathbf{x}}_a \\ \ddot{\mathbf{x}}_u \end{bmatrix} = \begin{bmatrix} \eta_m + \mathbf{d}_m + \mathbf{u} \\ \eta_{uu} + \mathbf{d}_{uu} \end{bmatrix}$$

where $M_{11} \in \mathbb{R}^{n \times n}$, $M_{12} \in \mathbb{R}^{n \times m}$, $M_{22} \in \mathbb{R}^{m \times m}$.

Premultiplying the inverse of the inertia matrix to the above equation yields

$$
\begin{bmatrix} \ddot{\mathbf{x}}_a \\ \ddot{\mathbf{x}}_u \end{bmatrix} = \begin{bmatrix} \overline{M}_{11} & \overline{M}_{12} \\ \overline{M}_{12}^T & \overline{M}_{22} \end{bmatrix} \begin{bmatrix} \eta_m + \mathbf{d}_m + \mathbf{u} \\ \eta_{uu} + \mathbf{d}_{uu} \end{bmatrix}
$$

where

$$
\overline{M}_{11} = (M_{11} - M_{12} M_{22}^{-1} M_{12}^T)^{-1}
$$

$$
\overline{M}_{12} = -(M_{11} - M_{12} M_{22}^{-1} M_{12}^T)^{-1} M_{12} M_{22}^{-1}
$$

$$
\overline{M}_{22} = (M_{22} - M_{12}^T M_{11}^{-1} M_{12})^{-1}
$$

and $\overline{M}_{11} \in \mathbb{R}^{n \times n}$, $\overline{M}_{12} \in \mathbb{R}^{n \times m}$, $\overline{M}_{22} \in \mathbb{R}^{m \times m}$.

$$
\begin{bmatrix} \ddot{\mathbf{x}}_a \\ \ddot{\mathbf{x}}_u \end{bmatrix} = \begin{bmatrix} \overline{M}_{11} \\ \overline{M}_{12}^T \end{bmatrix} (\eta_m + \mathbf{d}_m + \mathbf{u}) + \begin{bmatrix} \overline{M}_{12} \\ \overline{M}_{22} \end{bmatrix} (\eta_{uu} + \mathbf{d}_{uu})
$$

Define

$$
M_1 = \begin{bmatrix} \overline{M}_{11} \\ \overline{M}_{12}^T \end{bmatrix}, \ M_2 = \begin{bmatrix} \overline{M}_{12} \\ \overline{M}_{22} \end{bmatrix}
$$

where $M_1 \in \mathbb{R}^{(m+n) \times n}$, $M_2 \in \mathbb{R}^{(n+m) \times m}$.

The full state expression consists of a class of a second-order nonlinear systems in the following form

$$
\dot{x}_1 = x_2
$$

$$
\dot{x}_2 = \eta_{u1} + \mathbf{g}_1 (\eta_m + \mathbf{d}_m + \mathbf{u}) + d_{u1}
$$

$$
\dot{x}_3 = x_4
$$

$$
\dot{x}_4 = \eta_{u2} + \mathbf{g}_2 (\eta_m + \mathbf{d}_m + \mathbf{u}) + d_{u2}
$$

$$
\cdots
$$

$$
\dot{x}_{2n+2m-1} = x_{2n+2m}
$$

$$
\dot{x}_{2n+2m} = \eta_{u(m+n)} + \mathbf{g}_{n+m} (\eta_m + \mathbf{d}_m + \mathbf{u}) + d_{u(n+m)}
$$

$$
y = [x_1, x_3, \cdots, x_{2n+2m-1}]^T
$$

with $g_i = M_1(i)$, $\eta_{ui} = M_2(i)\eta_{uu}$, $d_i = M_2(i)\mathbf{d}_{uu}$. $M_1(i)$, $M_2(i)$ are the *ith* row vector of M_1, M_2.

Therefore the state-space model of the underactuated system can be expressed as

$$\dot{\mathbf{x}} = \eta_u + G(\eta_m + \mathbf{d}_m + \mathbf{u}) + \mathbf{d}_u$$

with

$$\eta_u = [x_2, \ \eta_{u1}, \ x_4, \ \eta_{u2}, \ \cdots, \ x_{2n+2m}, \ \eta_{u(m+n)}]^T,$$

$$G = [\mathbf{0}, \ \mathbf{g}_1^T, \ \mathbf{0}, \ \mathbf{g}_2^T, \ \cdots, \ \mathbf{0}, \ \mathbf{g}_{m+n}^T]^T,$$

$$\mathbf{d}_u = [0, \ d_{u1}, \ 0, \ d_{u2}, \ \cdots, \ 0, \ d_{u(m+n)}]^T.$$

A.3   Analysis of Feedback Control for Stabilization of the Linearized 2WMR model

For velocity control of the 2WMR, the position of the wheel is not a concern. Thus, only three states $x_2 = \dot{x}$, $x_3 = \theta$, $x_4 = \dot{\theta}$ are used to described the 2WMR. The linearized 2WMR model is as

$$\begin{bmatrix} \dot{x}_2 \\ \dot{x}_3 \\ \dot{x}_4 \end{bmatrix} = \underbrace{\begin{bmatrix} 0 & a_{23} & 0 \\ 0 & 0 & 1 \\ 0 & a_{43} & 0 \end{bmatrix}}_{A_0} \begin{bmatrix} x_2 \\ x_3 \\ x_4 \end{bmatrix} + \underbrace{\begin{bmatrix} g_{10} \\ 0 \\ g_{20} \end{bmatrix}}_{\mathbf{g}_0} u. \tag{A.5}$$

with

$$a_{23} = -\frac{b_0 m_p l g}{ac - b_0{}^2},$$

$$a_{43} = \frac{a m_p l g}{ac - b_0{}^2},$$

$$g_{10} = \frac{1}{r}\frac{c}{ac - b_0{}^2} + \frac{b_0}{ac - b_0{}^2},$$

$$g_{20} = \frac{1}{r}\frac{-b_0}{ac - b_0{}^2} + \frac{-a}{ac - b_0{}^2},$$

and $b_0 = m_p l \cos\varphi$.

The linear feedback control law is $u = -\mathbf{kx}$ with $\mathbf{k} = [k_2,\ k_3,\ k_4]$ and $\mathbf{x} = [x_2,\ x_3,\ x_4]^T$. We denote the closed-loop system matrix by A_c. We have

$$A_c = A_0 - \mathbf{g}_0\mathbf{k} = \begin{bmatrix} -g_{10}k_2 & a_{23} - g_{10}k_3 & -g_{10}k_4 \\ 0 & 0 & 1 \\ -g_{20}k_2 & a_{43} - g_{20}k_3 & -g_{20}k_4 \end{bmatrix}.$$

The characteristic equation of A_c is

$$|\lambda I - A_c| = \lambda^3 + (g_{10}k_2 + g_{20}k_4)\lambda^2 + (g_{20}k_3 - a_{43})\lambda + k_2(a_{23}g_{20} - a_{43}g_{10}) = 0.$$

To ensure local stability around the desired equilibrium point, A_c should be a Hurwitz matrix. Applying the Routh criterion, we obtain the following necessary conditions for selection of feedback gains:

$$g_{10}k_2 + g_{20}k_4 > 0, \tag{A.6}$$

$$g_{20}k_3 - a_{43} > 0, \tag{A.7}$$

$$k_2(a_{23}g_{20} - a_{43}g_{10}) > 0. \tag{A.8}$$

Note that a, b_0, $c > 0$ and $ac - b_0^2 = (m_w + I_w/r^2)(I_p + m_p l^2) + I_p m_p + (m_p l \sin \varphi)^2 > 0$, and thus we have g_{10}, $a_{43} > 0$ and g_{20}, $a_{23} < 0$. It follows from (A.7) that $k_3 < a_{43}/g_{20} < 0$. Since $a_{23}g_{20} - a_{43}g_{10} = -m_p l g/[r(ac - b_0^2)] < 0$, we have $k_2 < 0$ from (A.8) and $k_4 < -k_2 g_{10}/g_{20} < 0$ from (A.6). Finally, we conclude that all the feedback gains must be negative.

A.4   Analysis of Feedback Control for Stabilization of the Augmented Linearized 2WMR Model

By introducing the state $E_I = \int_0^t (\dot{x} - v_r) d\tau$, which is the integration of the wheel velocity error, we have the augmented linearized 2WMR model as

$$
\begin{bmatrix} \dot{E}_I \\ \dot{e}_2 \\ \dot{e}_3 \\ \dot{e}_4 \end{bmatrix} = \underbrace{\begin{bmatrix} 0 & 1 & 0 & 0 \\ 0 & 0 & a_{23} & 0 \\ 0 & 0 & 0 & 1 \\ 0 & 0 & a_{43} & 0 \end{bmatrix}}_{A_0} \begin{bmatrix} E_I \\ e_2 \\ e_3 \\ e_4 \end{bmatrix} + \underbrace{\begin{bmatrix} 0 \\ g_{10} \\ 0 \\ g_{20} \end{bmatrix}}_{g_0} u.
\tag{A.9}
$$

The linear feedback control law is $u = -\mathbf{k}e$ with $\mathbf{k} = [k_1, k_2, k_3, k_4]$ and $\mathbf{e} = [E_I, e_2, e_3, e_4]^T$.

The closed-loop system matrix

$$
A_c = A_0 - \mathbf{g}_0 \mathbf{k} = \begin{bmatrix} 0 & 1 & 0 & 0 \\ -g_{10}k_1 & -g_{10}k_2 & a_{23} - g_{10}k_3 & -g_{10}k_4 \\ 0 & 0 & 0 & 1 \\ -g_{20}k_1 & -g_{20}k_2 & a_{43} - g_{20}k_3 & -g_{20}k_4 \end{bmatrix}
$$

should be a Hurwitz matrix. The characteristic equation of A_c is

$$
|\lambda I - A_c| = \lambda [\lambda^3 + (g_{10}k_2 + g_{20}k_4)\lambda^2 + (g_{20}k_3 - a_{43})\lambda + k_2(a_{23}g_{20} - a_{43}g_{10})]
$$

$$
+ g_{10}k_2 \lambda^2 + k_1(a_{23}g_{20} - a_{43}g_{10}) = 0.
$$

To ensure local stability around the desired equilibrium point, we have the following necessary conditions for selection of feedback gains:

$$
g_{10}k_2 + g_{20}k_4 > 0,
\tag{A.10}
$$

$$
g_{20}k_3 - a_{43} + g_{10}k_1 > 0,
\tag{A.11}
$$

$$
k_2(a_{23}g_{20} - a_{43}g_{10}) > 0,
\tag{A.12}
$$

$$
k_1(a_{23}g_{20} - a_{43}g_{10}) > 0.
\tag{A.13}
$$

Since $a_{23}g_{20} - a_{43}g_{10} < 0$, we have $k_2 < 0$ from (A.12) and $k_1 < 0$ from (A.13). Thus, we have $k_3 < a_{43} - g_{10}k_1/g_{20} < 0$ from (A.11) and $k_4 < -g_{10}k_2/g_{20} < 0$ from (A.10). Finally, we conclude that all the feedback gains must be negative.

Author's Publications

The author has contributed to the following publications:

Journal Papers

[1] Jian-Xin Xu, Zhao-Qin Guo and Tong Heng Lee, "Synthesized Design of a Fuzzy Logic Controller for an Underactuated Unicycle", *Fuzzy Sets and Systems*, Vol. 207, pp 77-93, November, 2012

[2] Jian-Xin Xu, Zhao-Qin Guo and Tong Heng Lee, "Design and Implementation of a Takagi-Sugeno Type Fuzzy Logic Controller On a Two-Wheeled Mobile Robot", *IEEE Transactions on Industrial Electronics*, Accepted, 2012.

[3] Jian-Xin Xu, Zhao-Qin Guo and Tong Heng Lee, "On Integral Sliding Mode Control for a Unicycle", *International Journal of Vehicle Design*, Accepted, 2012.

[4] Zhao-Qin Guo, Jian-Xin Xu and Tong Heng Lee, "Design and Implementation of a New Sliding Mode Controller on an Underactuated Wheeled Inverted Pendulum", *Journal of The Franklin Institute*, Accepted, 2013.

[5] Jian-Xin Xu, Zhao-Qin Guo and Tong Heng Lee, "Integral Sliding Mode Control Design and Implementation for an Underactuated Two-Wheeled Mobile Robot", *IEEE Transactions on Industrial Electronics*, Revised, 2013.

Conference Papers

[1] Zhao-Qin Guo, Jian-Xin Xu, and Tong Heng Lee, "A Gain-Scheduling Optimal Fuzzy Logic Controller Design for Unicycle," *In Proceedings of the 2009 IEEE/ASME International Conference on Advanced Intelligent Mechatronics* (AIM2009), pp 1423-1428, Suntec Convention and Exhibition Center, Singapore, July, 2009.

[2] Jian-Xin Xu, Zhao-Qin Guo, and Tong Heng Lee, "A Sliding Mode Control Scheme for an Underactuated Unicycle," *In Proceedings of the 2009 IEEE International Conference on Control and Automation* (ICCA2009), pp 897-902, Christchurch, New Zealand, November, 2009.

[3] Jian-Xin Xu, Zhao-Qin Guo, and Tong Heng Lee, "A Synthesized Integral Sliding Mode Controller for an Underactuated Unicycle," *In Proceedings of the 11th International Workshop on Variable Structure System* (VSS'10), pp 352-357, Mexico City, Mexico, June, 2010.

[4] Jian-Xin Xu, Zhao-Qin Guo, and Tong Heng Lee, "An Integral Sliding Mode Control Design for a Class of Underactuated Motion Systems,"*In Proceedings of the 2010 IEEE International Conference on Industrial Electronics* (IECON2010), pp 2385-2390, Phoenix, AZ, USA, November, 2010.

[5] Jian-Xin Xu, Jun Leng Lim, Abdullah Al Mamun, Zhao-Qin Guo, Tong Heng Lee, "An Optimal Linear Controller Design for an Underactuated Unicycle," *In Proceedings of the 2011 IEEE International Conference on Industrial Electronics* (IECON2011), pp 4266 -4271, Melbourne, Australia, November, 2011.

[6] Jian-Xin Xu, Zhao-Qin Guo, and Tong Heng Lee, "An Optimal Fuzzy Logic Controller for an Underactuated Unicycle," *In Proceedings of the 2011 IEEE International Conference on Industrial Electronics* (IECON2011), pp 2335-2340, Melbourne, Australia, November, 2011.

[7] Jian-Xin Xu, X.-L. Niu and Zhao-Qin Guo, "Sliding Mode Control Design for a Carangiform Robotic Fish", *In Proceedings of the 12th IEEE International Workshop on Variable Structure System* (VSS'12), pp 308-313, Mumbai, India, January, 2012.

[8] Jian-Xin Xu, Zhao-Qin Guo, and Tong Heng Lee, "Sliding Mode Controller Design for Underactuated Systems", *In Proceedings of the 12th IEEE International Workshop on Variable Structure System* (VSS'12), pp 385-390, Mumbai, India, January, 2012.